Al-Farabi Kazakh National University

UDC: 539.17:524.3

KHASSANOV MANAS

Generation and propagation of gamma rays in the magnetosphere of neutron stars

6D060500 - Nuclear Physics

Thesis is submitted in fulfillment of the requirements for the degree of Doctor of Philosophy (PhD)

Scientific advisers:
Doctor of Phys.-Math. Sci.,
prof. Abishev Medeu
PhD, prof. Claudio Spitalleri

Republic of Kazakhstan
Almaty, 2019

CONTENTS

NORMATIVE REFERENCES

The Law of the Republic of Kazakhstan dated 18 February 2011 No. 407 IV;

SOSE RK 5.04.034-2011: State obligatory standards of education of the Republic of Kazakhstan. Postgraduate study. Doctoral. General provisions(changes dated 23 August 2012 No.1080);

Rules of awarding scientific degrees dated 31 March 2011 No. 127;

Interstate standards: State standard 7.32-2001 (changes dated 2006);

State Standard No. 7.1-2003. Bibliography record. Bibliographic description. General requirements and rules.

ABBREVATIONS

IR	Infrared radiation.
NS	Neutron star.
SN	Supernovae.
IM	Interstellar medium.
EF	Electromagnetic field
SGR	Soft gamma repeator.
QED	Quantum electrodynamics.
GRB	Gamma ray burst.
ENDF	Evaluated Nuclear Data File
CRAM	Chebyshev rational approximation method.

INTRODUCTION

General description of work.

The dissertation is devoted to the generation of gamma on the surface of a neutron star and the propagation of radiation in its magnetosphere. We considered the generation of gamma quanta by the Pb-Bi cycle under the neutron flux generated in the nonequilibrium crust of a neutron star. The propagation of gamma radiation in the magnetosphere of a neutron star is calculated using nonlinear electrodynamics.

Assessment of current state of the studied scientific topic.

In the classical field of gamma astronomy, the atmosphere is opaque, so observations are possible only from space using satellites. Due to specialized satellites — Cos B (operating in 1975-1982), the Compton gamma observatory (AGILE (Astro-rivelatore Gamma a Immagini, LEggero — Lightweight space telescope for imaging in the gamma range, 2007), EGRET tool - Energetic Gamma Ray Experiment Telescope — Telescope for an experiment in the field of hard gamma radiation, 1991-2000) , Space Observatory named after. E. Fermi (since 2008) — a diffuse background, point and extended sources of gamma radiation were discovered. Almost all galactic radiation sources belong to neutron stars, black holes, and also to compact objects inside the galaxy. It is also necessary to say that these emissions are associated with galaxies with an active core in which supermassive black holes are located. An isotropic diffuse background in observations is generated by sources in distant galaxies. Dense molecular clouds appear to be extended sources.

A neutron star is one of the possible results of the evolution of massive stars. These compact objects are not only has an interesting astrophysical manifestations, but also of great interest for fundamental physics. Three Nobel Prizes have already been awarded for neutron star research (for the discovery of radio pulsars, for the discovery of a double pulsar and the verification of general relativity, as well as for the development of X-ray astronomy).

Currently, only 25 neutron stars have been detected in the optical and near-IR ranges, about a hundred in the gamma range and about two hundred in the X-ray range, compared with about 2,000 neutron stars in the radio range.

As a result, the available data do not yet allow us to draw certain conclusions about the mechanism of pulsar radiation in the gamma ranges. Therefore, obtaining new data on NS radiation in these ranges is very important[1-5].

The processes associated with the formation, evolution and transformation of neutron stars into a black hole are the most powerful explosive processes in the gamma-ray bursts, Kilonova stars , Hypernova, and Universe: Supernovae. To study the properties and characteristics of matter in a special ray even in extreme conditions, we can observe these listed astronomical objects which is located at cosmological distances. With the rapid development of technology over the past decades, the volume of observational materials has also increased significantly. However, a detailed understanding of the nature and mechanism of stellar explosions and gamma-ray bursts has not yet been obtained.

It is believed that the brightness of type 1a (SN 1a) at the maximum is constant, as a result of which they are perfectly suitable for the role of distance indicators in the Universe[6]. As a result of the explosion of SN 1a, the white dwarf turns into a neutron star. But due to some problems in explaining the observational data, research is needed aimed at identifying the mechanism of explosion of (SN 1a), generating and propagating radiation at the initial and final moments of the explosion, and determining the structure of magnetic fields in gamma-ray burst jets. These questions can be answered by computer simulations of the processes occurring in the depths and on the surface of a neutron star, the mechanisms of generation and propagation of radiation in the NS magnetosphere, as well as high-precision measurements of the spectrum, intensity and polarization of star radiation. Unfortunately, polarization observations of SN 1a, especially in the early stages of shell expansion, and the intrinsic and early optical radiation of gamma-ray bursts are few [7]. The polarization of intrinsic optical radiation from gamma-ray bursts has not yet been recorded; there are only a few measurements of after glow polarization.

Neutron stars have no internal resources to make up for the energy that is lost by various types of radiation and over the course of millions of years it slowly fades away, turning into a dead object. However, if accretion occurs on the surface of a neutron star, it will restore its energy[8].

Accretion causes complex magneto hydrodynamic and nuclear processes both on the surface and inside a neutron star. Accretion launches a chain of nuclear reactions that serve as an efficient source of energy[9]. In this case, the neutron star's crust become non-stable, which leads to the appearance of nonequilibrium processes such as the expansion of the crust, star tremors on the surface of a neutron star, and neutron diffusion processes into the inner layers. However, when accretion ends, the neutron star will again begin to lose energy. Using sensitive X-ray telescopes and special observation methods, we can detect the signatures of these processes: the temperature of a neutron star rises during accretion episodes, but then gradually decreases[9]. In particular, Creation of the detailed "cooling curve" of a neutron star can give a unique information of its crust, which is one of the main tasks of studying a neutron star[10,11].

In recent years, theoretical studies of fast processes in astrophysical objects (explosions of new and supernovae, the propagation of shock waves, etc.) have been intensively conducted. Therefore, detailed calculations of the s-process and r-process under various conditions are becoming increasingly relevant, and reliable data are needed on the values of $< v\sigma >_T$ in a wide range of values of A and Z, in particular, for radioactive and excited nuclei [133].

Nowadays, the available data do not yet allow us to draw certain conclusions about the mechanism of pulsar radiation in the gamma ranges, so for this reason theoretical studies of nuclear reactions occurring at these objects are intensively carried out. The cyclic nuclear reaction Pb-Bi, first considered back by D.D. Clayton, plays an important role in explaining the nucleosynthesis of heavy elements, explosions of novae and supernovae. Therefore, detailed calculations related to the nuclear reaction of Pb-Bi cycle and all its sub-cycles, as well as calculations of the

intensity of gamma radiation by Pb-Bi cycle, are relevant today in explaining the mechanism of pulsed radiation in the gamma ranges Super strong magnetic fields of some neutron stars of the so-called magnetars can lead to nonlinear quantum electrodynamic effects (such as vacuum polarization), which are important for irradiative processes. Therefore, all these various properties of a neutron star are of great interest for theoretical astrophysics of non-ideal plasma physics and nuclear physics.

The aims of the thesis is to study the mechanisms of generation and propagation of gamma radiation in nonequilibrium processes on the crust and in the magnetosphere of the NS.

Research tasks. In order to achieve the aim the following tasks were set:

–Simulation of the cyclic reactions Pb-Bi.

–Determination of radiation intensity by Pb-Bi cycle.

–Determination of the relative delay time of the two normal modes of gamma radiation passing through the magnetosphere of a neutron star.

Research object.

Crust and magnetosphere of neutron stars.

Research subjects.

Generation of gamma rays by Pb-Bi cyclic reaction in the crust of neutron stars and propagation of it in the magnetosphere.

Research methods.

Analytical and numerical methods, computer simulation .

Main statements submitted for the defense.

–Pb-Bi cycle has additional subcycles in the neutron flux range $10^{13} - 10^{18}$ $\mathrm{neutron/cm^2}$; therefore, the complete Pb-Bi cycle in the indicated neutron flux range contains Tl206, Pb206-Pb209, Bi209-Bi210, Po210-Po211.

–The intensity of the gamma radiation of the complete Pb-Bi cycle, which takes place on the surface of the neutron star under flux of interstellar matter, is of the order of 10^{18} photon/$\mathrm{cm^2}$ sec.

–Gamma radiation passed through magnetic field of neutron star splits into the two normal modes, which are delayed with respect to each other by 10^{-8} sec.

Scientific novelty. The following results have been obtained for the first time within this dissertation:

–Isotopic composition and Pb-Bi complete cycle was determined.

–The intensity of the gamma radiation of the Pb-Bi cycle on the surface of the ns was calculated.

–The dependence the relative time delay between two normal modes from the gamma radiation passed through magnetic field of neutron star was calculated.

Scientific and practical value of the thesis.

Determination of the Pb-Bi cyclic reactions parameters give us possibility to define several problems of the elements abundance due the stellar nucleosynthesis and clarify genesis of the gamma ray bursts.

Definition of the gamma rays propagation details through dipolar and quadrupolar magnetosphere of a neutron stars gives us alternative method of measuring parameters of the magnetic field of NS.

Reliability of the obtained results.

Reliability of the obtained results confirmed by the publications in peer reviewed scientific journals and by participation in the international conferences.

Correlation of the work with other research projects.

The work has been carried out within the plans of the research projects of Ministry of Education and Science of the republic of Kazakhstan "Motion of rotating extended bodies in gravitational fields" (2015-2017), "Numerical study of the dynamics of test bodies in the field of extended bodies with an internal structure in general relativity (2018-2020)".

Personal contribution of the author.

With a scientific supervisors, author took part in setting the task and he proposed to consider an extended Pb-Bi cyclic reaction. He developed software package "IBIS" to work with ENDF files and to calculate the energy release during cyclic reaction. Author also wrote a code using "Mathematica" to calculate time delay of the electromagnetic pulse.

The thesis approbation.

The results of the work were presented and discussed at the following conferences:

–International Conference "Proceedings of the Fourteenth Marcel Grossmann Meeting on Recent Developments in Theoretical and Experimental General Relativity, Astrophysics, and Relativistic Field Theories"(Rome, Italy, July 2018).

–Scientific Conference dedicated to the 80th anniversary of Academician of the NAS RK Abdildin M.M. Abdildin readings: Actual Problems of Modern Physics. – Almaty, 2018.

–International Scientific Conference of Students and Young Scientists « Farabi alemi». – Almaty, 2016.

–International Scientific Conference of Students and Young Scientists «Farabi alemi». – Almaty, 2017.

–International Scientific forum «Nuclear science and technologies». – Almaty, 2017.

Publications.

9 publications (4 papers, 5 abstracts) were made based on the result of the study, among them 1 paper in journal indexed in Scopus (impact factor - **5.231**), 3 paper in journals recommended by CCES MES RK.

1. Abishev M.E., Toktarbay S., Beissen N.A., Belissarova F.B., Khassanov M.K., Kudussov A.S., Abylayeva A.Zh. Effect of nonlinear electrodynamics of vacuum in the magnetic quadruple field of a pulsar // Monthly Notices of the Royal Astronomical Society. – 2018. – Vol. 481, Issue 1. – P. 36-43.

2. Abishev M.E., Toktarbay S., Khassanov M.K., Abylayeva A.Zh. Propagation of a electromagnetic radiation in the strong magnetic quadrupole and

gravitational field // Recent Contributions to Physics(Rec. Contr. Phys.).– 2018. – Vol.66, No.3. – P.4-11.

3. Абишев М.Е., Хасанов М.К., Утепова Д.С., Айтасов Т. Моделирование взаимодействия тепловых нейтронов с каталитическим составом (Pb, Bi, Po) с безграничной среде // Reports of NAS RK. – 2016. – Vol. 3, No. 307. – P. 5-9.

4. Абишев М.Е., Хасанов М.К. Расчет количества тепла испускаемая каталитическим составом (Pb, Bi, Po) в программном комплексе "IBUS" // News of the NAS of the RK, physico-mathematical series. – 2017. – Vol. 3, No. 313. – P. 53-56.

5. Abishev M.E., Toktarbay S., Amankhan T., Abylayeva A.Zh., Khassanov M.K. Effects Of Nonlinear Electrodynamics Of Vacuum In The Strong Magnetic Field Of A NS // Proceedings of the Fourteenth Marcel Grossmann Meeting on Recent Developments in Theoretical and Experimental General Relativity, Astrophysics, and Relativistic Field Theories. –Singapore: World Scientific Publishing, 2018. – P. 4379-4384.

6. Abishev M.E., Toktarbay S., Beissen N.A., Belissarova F.B., Khassanov M.K., Kudussov A.S., Abylayeva A.Zh. Effect of nonlinear electrodynamics of vacuum in the magnetic quadruple field of a pulsar // Materials of the International Scientific Conference dedicated to the 80th anniversary of Academician of the NAS RK Abdildin M.M. Abdildin readings: Actual Problems of Modern Physics. – Almaty, 2018. – P. 73–79.

7. Хасанов М.К., Айтасов Т., Джанибеков А. Моделирование взаимодействия тепловых нейтронов с каталитическим составом (Pb,Bi,Po) в безграничной среде // International Scientific Conference of Students and Young Scientists « Farabi alemi». – Almaty, 2016. – P. 85.

8. Хасанов М.К. О программном комплексе "IBUS" // International Scientific Conference of Students and Young Scientists «Farabi alemi». – Almaty, 2017. – P. 111.

9. Абишев М., Кенжебаев Н., Хасанов М., Джанибеков А. Расчет изотопного состава каталитического материала при облучении реакторными нейтронами // International Scientific forum «Nuclear science and technologies». – Almaty, 2017. – P. 93.

The structure and volume of the thesis

The thesis consists of an introduction, two chapters, conclusion and list of references of 149 titles. The total volume of work is 100 pages including 20 figures.

GENERATION GAMMA QUANTA IN THE NEUTRON STARS

1.1 Literature review

The phenomenon of Gamma-Ray Burst (GRB) being mysterious at the time of discovery in 1973 in a seminal article [111], nowadays is widely accepted by astrophysical community to be of the cosmological origin. Its early guesses are based on explosions in the active galactic nuclei which was proposed in [112]. The focus on mechanism of GRB formation, in particular, occurring in the vicinity of a collapsing object due to neutrino-antineutrino annihilation was studied in [113]. Another models of the energetic gamma emission during collapses and supernova explosions were studied in [114]; there scientists considered the reactions with heavy nuclei. An interesting scenario of a so-called "starquake" followed by explosions and emissions from a non-equilibrium layer in the crust of a neutron star, accompanied by gamma radiation due to fission of super-heavy nuclei, was proposed in [114] as an alternative model of the galactic origin of the GRB. There were more than hundred models proposed in few years after the announcement in order to solve a puzzle of GRBs [115].

Despite the fact of several hundred pulsars detection in hard X-ray and gamma-ray domain, together with their temporal and spectral parameters measured with good accuracy, there is still not complete data on the polarization properties of such an interesting objects. Very few space experiments have been launched for investigating the polarization in hard radiation [86].

One of the examples of the linear polarization is its discovery for GRB 021206 was reported in [116]. The successful interpretation was given using a synchrotron radiation for electrons moving with relativistic speed in a strong magnetic field. Data on polarization were obtained by space experiment Reuven Ramaly High Energy Solar Spectroscopic Imager (RHESSI) – the high-energy solar spectrograph. The space observatory consists of nine large-volume coaxial germanium detectors (300 cm^3) with high spectral resolution for studying the X-ray and gamma radiation of the Sun in the energy range of 3 keV-17 MeV. RHESSI has a high angular resolution (2 from the arc) with a large field of view of 1°; however, flat focal detectors are not shielded and open to the entire sky. Due to this constructional feature of the detectors RHESSI frequently registers GRB in its focal plane, although the probability of their falling into the field for constructing an image is small. As a results of such observations we have spectra of high-resolution, arrival time and energy of every individual photon. Being not optimized for gamma-ray polarimetry, RHESSI, nonetheless is suitable for measuring polarization and its design makes it the most sensitive among modern instruments for astrophysical measurements of the polarization of gamma radiation [116].

Obtained data in [116] were analyzed in [117] where it was concluded that they did not give the slightest hint of registering a polarized signal.

It is well known that some gamma-ray pulsars are characterized by magnetic fields near critical B value, but there exist so-called "magnetars" which could have even higher magnetic field to reach about 10^{15} G. In such objects in the vicinity of strongly magnetized neutron star there are favorable conditions for non-linear electrodynamic effects, in particular, vacuum birefringence [62,82,108]. This effect may have different

manifestations. One of them dramatically increases the linear polarization of the thermal radiation of the isolated neutron stars [109], from a level of a few per cent up to even 100 per cent, depending on the viewing geometry and the surface emission mechanism. Currently, this vacuum non-linear electrodynamics prediction can be tested by measurement of a polarization degree of isolated neutron star thermal emission.

Pioneering observations [110] of optical polarization from a thermally emitting isolated neutron star RX J1856.5-3754 shown that a linear polarization degree of this star thermal emission is 16.43+5.26 per cent [86].

Outside of a neutron star, due to the presence of a very strong magnetic field, the magnetosphere is formed, the radius of which can reach several star radii. This magnetosphere is usually transparent for the low-frequency part of the electromagnetic spectrum.It can only be guaranteed that the magnetospheres of neutron stars are transparent in the region of x-ray and gamma radiation.

The gravitational field of a neutron star is created by its substance, as well as a magnetic dipole field with charged particles in the magnetosphere. Since the energy density of the substance of compact neutron stars ~ $10^{36}\,erg/cm^3$ is more than six orders of magnitude greater than the maximum energy density of the magnetic field, even in the case of a magnetar, the matter makes the main contribution to the gravitational field. Assuming that it is spherically symmetric distributed, the Schwarzschild metric (see chapter 2.4) can be used as the metric tensor of pseudo-Riemannian space-time [73]:

In theoretical works [82,86,95,96] the effects of nonlinear electrodynamics were predicted when measuring the degree of polarization of thermal radiation of an isolated neutron star. In [82] non-linearity is limited to considering the case of dipole magnetic moment. However, for a neutron star with a strong magnetic field where B reaches 10^{15} G, it is also necessary to consider the effects caused by quadrupole magnetic moment.

Despite the fact that the numerous observations have been conducted for more than 30 years and there are various attempts to build a theoretical model, to date there is no reliable model for the formation of the observed radiation, nor for the day of the GRB energy source. Although long GRB are most likely of cosmological origin, it is possible that short GRB have a different origin (possibly even galactic) and are associated with giant outbreaks of [119].

There are experimental evidences that the solar system formed partly as a product of supernova explosion, where elements obtained in the r-process mixed with the initial gas-dust medium; the latter fact being examined by the isotopic composition of ancient meteorites. It was claimed [132] that shock wave from the supernova explosion initiated gravitational compression, which further led to the formation of the solar system[132].

Reasonably the most comprehensive analysis on GRB nature can be given through observations in the entire electromagnetic spectrum.

In recent years, theoreticaland numerical studies of fast processes in astrophysical objects, e.g., explosions of new and supernovae, the propagation of shock waves, etc., have been intensively conducted. Therefore, detailed calculations of the r-process under various conditions are becoming increasingly relevant, and reliable data are needed on

the values of $v\sigma_T$ in a wide range of values of A and Z, in particular, for radioactive and excited nuclei [133].

Recently, theLaser Interferometer Gravitational-Wave Observatory (LIGO) collaboration recorded a powerful gravitational wave signal, followed by a kilonova burst, manifested in the form of a gamma-ray burst and persisting for several days in the visible part of the spectrum caused by radioactive processes. An arrival time of the gamma-ray signal from GRB 170817A is delayed only by 2 seconds from the arrival of gravitational wave signal, and their location on the sky is overlapping, giving us a first time ever opportunity for detecting the signal from single object in the entire electromagnetic spectra but also non-electromagnetic counterpart.

The observational data show that an explosion of coalescing stars results with isotropic expansion having initial temperature of about 4300 degrees Celsius, moving with ballistic non-relativistic velocity 0.2–0.3 of the speed of light, which further will decay and expanding shell will cool on a timescale of days. It is was calculated that the sphere consisted of a newly formed chemical elements, of which only Strontium was about five masses of the Earth. For the first time, unequivocal evidence has been obtained of the occurrence of the r-process during the coalescence of neutron stars, in which heavy elements such as gold, lead, uranium and others are formed. Moreover, this is the first empirical evidence that neutron stars are indeed made up of neutrons.

Now it has been proven that this event acts as a reactor in which heavy elements are synthesized [135].

In the outer crust of neutron stars, atomic nuclei are completely ionized everywhere. The electrons in this layer are highly degenerate and free. As mentioned, the outer shell can be divided into two parts, the outer layer and the inner layer. The total thickness of the outer shell reaches up to a couple of hundred meters. The thickness of the outer layer is only a few meters where the electrons are not very degenerate. The pressure in the outer shell is created by degenerate electrons which at a density $\rho \geq 10^6 g/cm^{-3}$, become relativistic and at densities $\rho \gg 10^6 g/cm^{-3}$ they are ultra relativistic. Also, at such kind of densities, the ions form a liquid whose properties are mainly determined by the Coulomb interaction between ions (Coulomb liquid)[13,14,15].

With increasing pressure, beta capture by nuclei in the layer becomes ergetically beneficial. This is due to a strong increase in the Fermi energy of electrons, which leads to the enrichment of nuclei by neutrons. The boundary between the outer and inner shell of a neutron star appears when the density reaches $\rho = \rho_{drip}$ and, accordingly, free neutrons appea.

Also, In [141], three objects HD187861, HD196944, and HD224959 were analyzed. These objects are the so-called AGB stars. Their analysis showed that these stars are highly enriched in lead than any other element heavier than iron. Consequentially, this gives us the assertion that in a binary system consisting of a neutron star and an AGB, like the above, when expanding the star and filling the rosh cavity in the accreting substance, lead isotopes will prevail.

An accretion stream contributes significantly to the development of a neutron star. The substance from the accretion disk falls on the surface of a neutron star and

spreads uniformly over it. The newly income substance from accretion disk, increasing gravitational pressure, contributes to the compression of matter in the crust, pushing it into a star. In this case, the accretion process turns the crust of neutron star from the equilibrium state, as a result the crust of the neutron star becomes non-equilibrium. The nuclear composition of deviated from equilibrium crust is very different from equilibrium crust of the neutron stars [39,144]. This is primarily due to the presence of a significant amount of free neutrons in the crust of the neutron star. These free neutrons can diffuse under the influence of the concentration gradient and gravity [40]. The neutron concentration gradient can change sign in the nonequilibrium crust, and, in particular, at the outer boundary it is always directed outward (or equal to zero), since there are no free neutrons outside. whereas, the force of gravity acting on free neutrons is always directed inside the star.

Also, processes occurring on the upper layers of the inner cortex, which is described in detail in [140], can be sources of free neutrons. The inner layers of the outer crust of a neutron star atomic nuclei forms a super dense crystalline structure where nonlinear interactions can occur. The reason for this is the very small lattice parameter. This small parameter is much smaller than the size of the electron orbits in the atom. In crystals with such properties, excited states of nuclei appear due to electron capture. Captured nuclei in such crystals can exist for a long time. In [142], the authors draw attention to the fact that if the density of the number of such excited nuclei increases, then nonlinear interaction arises. These nonlinear interactions result in mode generation and induced radiation in the crystal. The consequence of these emissions may be the appearance of free neutrons. These free neutrons are literally knocked out from nuclei of supersaturated neutrons and a concentration gradient of free neutrons appears, then due to the presence of a concentration gradient they can be transferred to the upper layers of the outer crust of a neutron star, thereby forming a free neutron flux [140].

1.2 The structure of neutron stars.

After two years of neutron detecting, neutron stars were theoretically predicted by Walter Bade and Frits Zweki as the most possible result of supernova explosions. Walter Bade and Frits Zwiky proposed the term "supernovae" and they also suggested that these objects can be an important source of cosmic rays in galactic. Outstanding Soviet physicist Landau also considered objects in the universe where density of matter is so dense that atomic nuclei form a giant nucleus. He also calculated that the mass of these objects should exceed 1.6 of solar mass[12].

A neutron star was first discovered after 43 years of its prediction by Jocelyn Bell and Antony Hewish. Today, neutron stars can be observed in all ranges of electromagnetic radiation, however, most of them (around 2000) are observed in the form of a radio pulsar. About two hundred observed neutron stars enter into binary systems, where a neutron star absorbs its nearby stars, forming an accretion disk and manifests itself as x-ray radiation. Also, flashes due to explosive thermonuclear burning of accreted matter sometimes appear in the outer layers of these neutron stars. Also, some of these systems can form x-ray transitions when alternations

between periods of active accretion(may lasts days or weeks) and with a periods of calm (may lasts months or sometimes years). Also, more than a hundred isolated neutron stars were detected in the X-ray range of radiation [12,13].

Due to the fact that the density of a neutron star is very high, the general theory of relativity plays an important role. The structure of non-rotating neutron stars can be represented by Tolman-Oppenheimer which is the equation of the relativistic hydrostatic equilibrium of a spherically symmetric mass in the GR [12].

The structure of most neutron stars can be divided into two main regions - the core which can also be separated into the outer and inner and the shell. The neutron star shell is also can be divided into solid crust and liquid ocean (Coulomb liquid). Such a schematic representation of the structure of a neutron star is shown in figure 1. [13].

According to calculations, the density of the inner core in a neutron star reaches $\rho \geq 2\rho_0$, the radius of which can be a few km. However, not all neutron stars have an inner core, since for neutron stars with mass $M \geq 1.4{\sim}1.5M_s$ the density does not reach $2\rho_0$. The results of calculating the composition and properties of matter in the inner core of a neutron star strongly depend on the theoretical models being awarded that describe collective fundamental interactions. For this reason, the composition of the inner core of a neutron star remains a mystery to this day.

For most neutron stars, the outer core compose most of their masses. For this reason, it is believed that this is a superfluid neutron liquid with components of the superconducting proton, also muons and electrons. All these components degenerate violently. As for the thickness, it is usually equal to a few kilometers, while the density lies in the interval $0.5\rho_0 \leq \rho \leq 2\rho_0$.

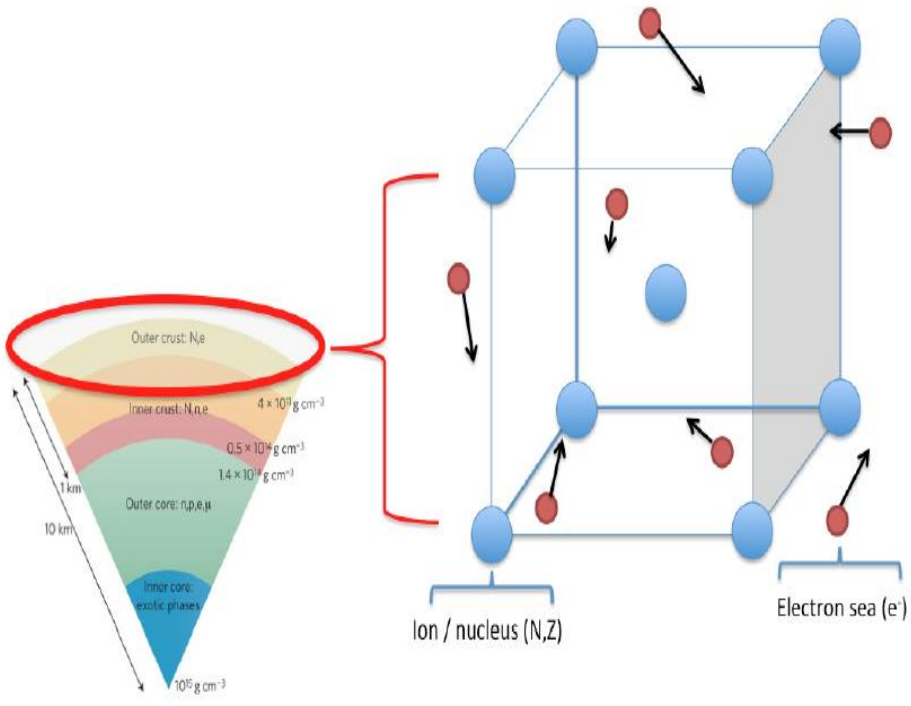

Figure 1 – Schematic structure of a neutron star.

The shells of most neutron stars can be divided into the ocean from the Coulomb liquid and into a solid crust that is divided into outer crust and inner crust. A plasma gas atmosphere may exist on the surface of the outer crust of a neutron star in some neutron stars, and there may be a liquid crystal mantle between the core and the crust. The inner crust of a neutron star consists of nuclei forming a solid crystal where there is an abundance of free neutrons and electrons. In the outer crust, free neutrons can decay.

The density of the inner crust varies from $\rho \approx (4-6) \times 10^{11} g/cm^{-3}$ to $\sim 5\rho_0$. The thickness can reach 2 kilometers. At a density of $\sim 5\rho_0$, the atomic nuclei of the inner crust make up a homogeneous mass. At equilibria of the inner crust, the equilibrium of beta decay and beta capture occurs, which leads to an interesting composition of the substance that cannot be obtained in laboratory conditions. In this case, the nuclei of a substance are redundant with respect to neutrons. These nuclei are in a liquid of neutrons and electrons. Such a state of matter is rather well described in [14]. In the inner crust, neutrons are in excess. Estimates made by special theoretical methods show that the critical superfluity temperature reaches 10^9 K degrees. This is an order of magnitude higher than the kinetic temperature of a substance in the inner crust. It should be noted here that the critical excess temperature is highly dependent on the density of the substance.

The heat capacity of the inner crust of a neutron star, depending on the case, can be determined by neutrons, electrons, atomic nuclei, and also by collective excitation vibrations - phonons. Degenerate neutrons determine the pressure in the inner crust of a neutron star. Atomic nuclei can become crucial in determining the specific heat if there is a redundancy of degenerate neutrons. However, these nuclei in the inner crust of a neutron star form a crystal lattice of the so-called Wigner crystal; therefore, to completely determine the specific heat, the phonon contribution to the specific heat must also be taken into account. If the temperature of the Coulomb crystal is lower than the Debye temperature, then the phonons are frozen and the electrons can become decisive in determining the heat capacity of the inner crust of a neutron star. In the opposite case, the electrons are relativistic and extremely degenerate; therefore, their contribution to the determination of the inner crust of a neutron star can be neglected [12,15,16].

There are theoretical predictions that between the core and the inner crust of a neutron star there should exist a so-called mantle which consists of exotic atomic nuclei. With an increase in the density in a neutron star, the shape of the atomic nuclei in the mantle can undergo changes due to Coulomb forces, since it is no longer profitable for them to take the spherical shape instead, they become close in shape to cylinders. Such a state of nuclei is also called the “spaghetti” phase. [14,17]. The mantle consisting of such nuclei will no longer be on the nodes of the crystal lattice, but will possess the properties of a liquid crystal. The mantle is not predicted by all theoretical models, but only by some of them. It exists, for example, in the FPS model, but in the modern SLY model there are no promises to the side of this statement.

In the outer crust of neutron stars, atomic nuclei are completely ionized everywhere. The electrons in this layer are highly degenerate and free. As mentioned, the outer shell can be divided into two parts, the outer layer and the inner layer. The total thickness of the outer shell reaches up to a couple of hundred meters. The thickness of the outer layer is only a few meters where the electrons are not very degenerate. The pressure in the outer shell is created by degenerate electrons which at a density $\rho \geq 10^6 g/cm^{-3}$, become relativistic and at densities $\rho \gg 10^6 g/cm^{-3}$ they are ultra relativistic. Also, at such kind of densities, the ions form a liquid whose properties are mainly determined by the Coulomb interaction between ions (Coulomb liquid).

With increasing pressure, beta capture by nuclei in the layer becomes ergetically beneficial. This is due to a strong increase in the Fermi energy of electrons, which leads to the enrichment of nuclei by neutrons. The boundary between the outer and inner shell of a neutron star appears when the density reaches $\rho = \rho_{drip}$ and, accordingly, free neutrons appear.

The outer boundary of the outer crust is usually located at the crystallization point of the Coulomb liquid, which the ocean of the neutron star consists of. The position of this point is determined by the density dependence of the melting point of the Coulomb crystal. As was said, the outer crust is a crystal lattice and its boundary is located at the crystallization point of the Coulomb liquid. This point is very important in that its position is found from the density dependence of melting in the so-called Coulomb crystal. If we disregard the interaction of electrons with ions and consider ions like classical particles and consider a model of a single-component Coulomb plasma, then crystallization of the crystal described above occurs at Γ = 175. However, the authors of [18] obtained the value Γ ~ 100-200, which corresponds to a more realistic picture. The parameter Γ determines the equation $\Gamma = (Ze)^2/ak_BT$ – is the Coulomb coupling parameter characterizing the ratio of the potential Coulomb energy of ions to their kinetic energy, n_i –volume concentration of ions, $a = (4\pi n_i/3)^{-1/3}$ ionic radius spheres, k_B Boltzmann constant.

Depending on the temperature gradient in a neutron star, which depends on age and how the neutron star was formed, the melting point for an ordinary shell is calculated at a density $\rho_m \sim 10^6 - 10^9\ g/cm^3$. The temperature gradient are also known as a thermal structure of neutron star. If a neutron star has an extremely strong magnetic field, that is, it is a magnetar, then it may not contain an atmosphere[19].

Based on the virial theorem, the upper numerical value varies is $B \sim 10^{18} - 10^{19}\ G$. Depending on the type of neutron star and its type, the magnetic fields on the surface of standard neutron stars are considered equal to $B \sim 10^8 - 10^{15}\ Gs$. Such values for magnetic field induction cannot be obtained in terrestrial conditions today. [20, 21, 22]: Inside the neutron star, due to the combustion process, the magnetic field also differs from the value on the surface. A magnetic field is also used to explain abnormal X-ray pulsars and soft gamma repetitions.

To date, there is an incredible amount of theoretical models for describing field generation. These models were proposed both for young neutron stars and for a supernova explosion. All these models take into account many factors such as

convection, thermomagnetic effects, differential rotation, magnetorotational instability, and so on. But it is important to note that all these models encounter specific difficulties when comparing with data on neutron stars. For example, according to the "α-Ω model", for a period of 30 ms, the pulsar's magnetic field is created by convection, then due to the existence of a differential toroidal magnetic field (this field can rotate) it acquires the values $B \sim 10^{16} G$ [23,24].

In [23], it is said that sources of a magnetic field can exist in a nucleus. In this case, superconductivity forms protons in the nucleus, which is why this field will be in the form of quantized magnetic tubes — Abrikosov's vortices. Their transverse dimensions will be microscopic values. Thus, the magnetic field of a neutron star is supported by electric currents which, for theoretical reasons, can flow in the star's core or in the inner crust, that is, where there is high electrical conductivity. It must also be said that there is an ohmic attenuation of the magnetic field in the nucleus of a neutron star. It may exceed the age of the universe.

Evolution makes changes in many physical processes that in most cases are interconnected, which leads to a change in the magnetic field of a neutron star [21]. We list only a few of them. Firstly, the ohmic field is subject to attenuation, secondly, during stellar impacts, the magnetic field lines can reconnect, and also due to the interconnectedness of the components of thermal conductivity, electrical conductivity and thermoelectric coefficients of the plasma from the magnetic field and temperature, a relationship is established between magnetic and thermal evolution. Separately, it should be noted accretion onto the surface of a neutron star, which also affects the magnetic field near the surface.

Due to the interaction of the Abrikosov vortices and the magnetic field with the matter of the neutron star's crust, changes in the evolution of the magnetic field can occur. It should also be noted about the existence of a superfluid neutron fluid in which Onsager-Feynman vortices exist, which in turn also affects the evolution of the magnetic field.

1.3 Outer crust of non-accreting neutron star in equilibrium state and its chemical composition.

It is known that the outer core of a neutron star consists of a homogeneous system of electrons, protons and neutrons with a relatively low density. Such a homogeneous system does not reunite in clusters. The reason for this lies in the fact that the range of nucleon – nucleon interaction is much smaller than the average internucleon separation. The electrons in the cortex are represented as a homogeneous relativistic Fermi gas and they are free. This circumstance stems from the low density in the cortex. as a result of the Coulomb interaction, the nuclei form a crystal lattice. The nuclei themselves are formed due to the grouping of nucleons. This circumstance follows from the energy gain for the system[119].

$$E(Z,A;n) = \frac{M(Z,A)}{A} + \frac{m_e^4}{8\pi^2 n}\left[x_F y_F\ (x_F^2+y_F^2) - ln(x_F+y_F)\right] - \frac{C_l z^2}{A^{4/3}} p_F \qquad (1.1)$$

The first term depends only on the mass per nucleon of the nucleus in the crystal lattice and is the contribution of the nuclei to the total energy. It is important to note here that it is absolutely independent of the baryon density of the system (A/V). The scaled Fermi momentum $x_F = p_F^e/m_e$ depends solely on the electron-baryon fraction Z / A: and the baryon density n. $y_F = \sqrt{1 + x_F^2}$. is the scaled Fermi energy x_F. The second term is the contribution of a free Fermi gas of electrons with mass m_e.

$$p_{\mathrm{F}}^{\mathrm{e}} = (3\pi^2 n_{\mathrm{e}})^{1/3} = (3\pi^2 n \frac{\mathrm{Z}}{\mathrm{A}})^{1/3} = (\frac{\mathrm{Z}}{\mathrm{A}})^{1/3} p_F \tag{1.2}$$

The last term is the contribution of the electrostatic lattice ($C_l = 3.40665 \times 10^{-3}$). It is also a function of the Fermi momentum $p_F = (3\pi^2 n)^{\frac{1}{3}}$. Of course, one cannot neglect this member, although his contribution is not large enough. Here we can draw an analogy with the Coulomb term in the liquid drop formula[125]. Now we consider a system where the pressure is determined mainly by degenerate electrons. In such a system, the pressure at T = 0 is determined as follows:

$$E(Z,A;n) = n^2\left(\frac{\partial \varepsilon}{\partial n}\right)_{T=0} = \frac{m_{\mathrm{e}}^4}{3\pi^2}(x_F^3 y_F - \frac{3}{8}[x_F y_F\ (x_F^2+y_F^2) - ln(x_F+y_F)] - \frac{nC_l z^2}{3A^{4/3}} p_F \tag{1.3}$$

To determine the composition of the outer crust of a non-accreting neutron star, it can be obtained by minimizing the chemical potential of the system under consideration. In this case, calculations must be carried out at a fixed pressure, and not at a fixed density.

$$\mu(Z,A;P) = \frac{M(Z,A)}{A} + \frac{Z}{A}\mu_e - \frac{4C_l z^2}{3A^{4/3}} p_F \tag{1.4}$$

The relation among the baryon density and the pressure is provided by the underlying crustal equation of state; see Eq. (1.3). where μ_e is the electronic chemical potential

To find the isotopic composition of the outer crust of a neutron star, the authors of [121] did the following: First, for a given nuclear particle (Z, A) and also for pressure P, we determined the baryon density of the system. This was done using the equation of state. The corresponding baryon density of the system is given by p_F and μ_e where $p_F -$ is the Fermi baryon momentum. $\mu_e -$ is the chemical potential. After scanning all the given tabular mass values, the chemical potential $\mu\ (A, Z; P)$ was calculated; Then, the authors of [121] selected a combination of the proton and nucleon numbers in such a way that they minimized the chemical potential $\mu\ (A, Z; P)$. At low densities, the authors neglected the electronic contribution to the

total energy, which will certainly affect the nuclear chemical composition of the neutron star's crust. Defined in this way, the preferred nucleus with the lowest mass per nucleon is Fe. It should be noted that during the calculation the pressure was kept constant. With a deepening in the crust of a neutron star, density and pressure increase. In this case, the electrons make a rather significant contribution to the total energy of the system. In this case, the energy advantageous is to reduce the fraction of electrons Z / A; in this case, it is necessary to increase neutron-proton asymmetry accordingly. However, an increase in the asymmetry leads to an increase in the mass per nucleon. The relationship between the electron contribution and the energy of nuclear symmetry, which strongly affects symmetric nuclei, determines the type of the most suitable nucleus. [121].

Summing up the work of the authors of [121], we can say that the outer crust of a neutron star consists of a crystalline nuclear lattice immersed in an electron gas. This electron gas, with an increase in pressure and density, favors a change in the nuclei in the direction of more rich with neutrons. It should be noted that if the core is in equilibrium, then there will be no free neutrons in the outer crust of the neutron star.

Numerical calculations made in the work [121] using neural networks make it possible to predict the chemical composition of the neutron star crust. Their basic idea is to view the modeling of $\delta_{LDM}(Z,N)$ in equation

$$M(Z,N) = M_{\text{LDM}}(Z,N) + \delta_{\text{LDM}}(Z,N) \tag{1.5}$$

The problem with the statistical approach is that there are two different interpretations of probability itself. The first one is that probability is a property of the physical world often and this interpretation is called "frequentist". Another interpretation is called "Baysian" and it is believed that probability arises from the uncertainty in our knowledge of the physical world [124]. Thus, in the "frequentist" interpretation, probability cannot be determined for a hypothesis or for a parameter. However, in a Bayesian context, this approach is natural. The authors of [121] used in their calculations an approach based on the Bayesian neural network (BNN) and it is called the "universal approximator". This universal approximator can approximate any real function of one or several variables[122,123]. The result of simulation work [121] is shown in Figure 2.

For illustration, the author considered a "canonical" $M_0 = 1.4M_s$ neutron star with a radius of $R_0 = 12.78$ km as predicted by a realistic equation of state [120]. These two quantities are sufficient to define the boundary conditions at the edge of the outer crust, namely, $M(R_0) = M_0$ and $P(R_0) = P_0 \approx 0$. Given P_0, the corresponding baryon density, energy density, and composition may be determined from the minimization of the chemical potential[121].

However, according to the author himself, the simulation results are very sensitive to nuclear masses in the 20 <Z <50 range.

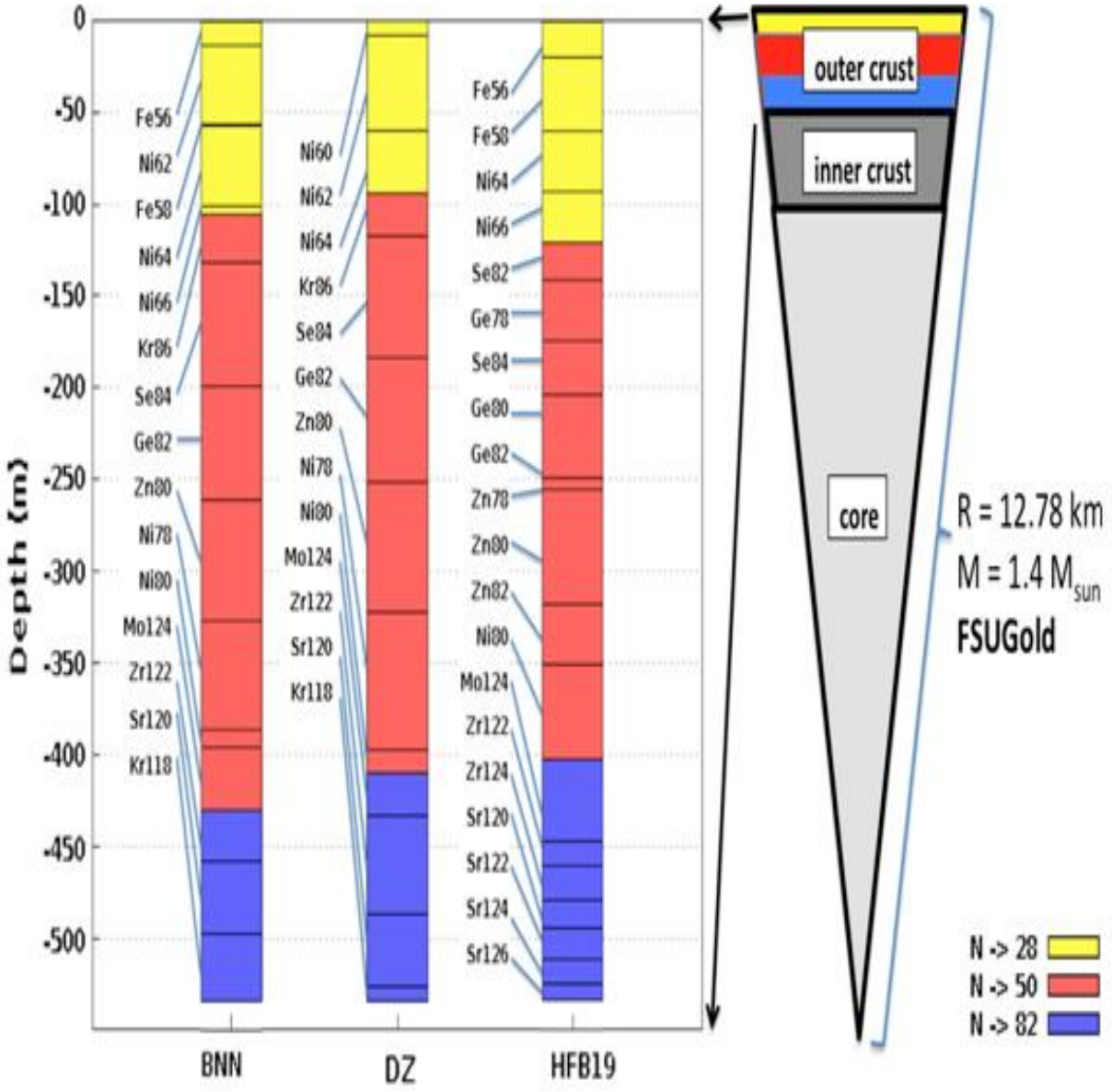

Figure 2 – Results of computer simulation using BNN approach from work [121].

1.4 Accretion of interstellar matter onto a single neutron star.

Nowadays, astronomers have discovered about 800 neutron stars. Of these, about 700 are radio pulsars, and the rest are x-ray sources. However, experts in astrophysics and astronomy science suggest that their number should actually exceed tens of millions. This circumstance is explained by the fact that during the evolution of the Galaxy a large number of stars, including massive ones, died. However, the number of detected neutron stars is much smaller, since there are huge difficulties in detecting them. If a neutron star is one component of a binary system, then due to gravitational forces, the mother pulls from an ordinary star to the surface of a neutron star, i.e. accretion. An example of such a binary system can be a neutron star and an AGB star. Accretions in such systems result in power radiation. Such emissions are usually detected using

space telescopes. Most neutron stars detected in the x-ray range form binary systems[5].

Theoretical studies show that a neutron star can be an isolated star resulting from the explosion of a single massive star, the so-called natural star death[24]. It should also be noted that the binary systems described above can decay as a result of which an isolated neutron star is also formed. Thus, during the explosion of a more massive star, about half of the entire mass of the system as a whole is lost (supernova explosion) forming two single stars. In this case, one of them will be a neutron star.

With a radius of 10 km, an isolated neutron star is difficult to detect; one could even say that it is impossible. Even if we assume that our single neutron star has a high temperature, it does not seem possible to detect thermal radiation from a distance of more than one kilo parsec today. However, the good news in this area is that astronomers have found an excellent method of detecting single neutron stars.

For a single neutron star, there are two stages of evolution which gives us the opportunity to deduct it. The first is the stage of ejections. The second is accretion. Let us consider each of them from the position of finding a neutron star. The stage of ejections takes a relatively short period of time in its evolutions, and therefore it is not so attractive for using it as a detection method, and at the stage of ejections a single neutron star manifests itself as a radio pulsar. But the stage of accretion of matter onto a neutron star can take quite a long time and from the point of view of observation it is the most suitable. The accretion of matter on the surface of a neutron star is interesting in that there are many different processes that carry certain information about the neutron star. However, accretion in most literature is regarded as a process occurring in binary systems and not in single stars. Therefore, the question arises of the origin of matter for accretions on a single neutron star. Everything is simple here, the answer is interstellar medium. The idea of accretion of interstellar matter onto neutron stars has been discussed for a long time by the scientific community. We know that during IM accretion, energy is released to the surface of a single neutron star, which we can detect using modern X-ray satellites, such as ROSAT. You can read more about this in the works of A. Treves and M. Colpy. Thus, in recent days, accretion onto a single neutron star has become popular in the society of astrophysicists [25].

Specifically bright sources of this kind should be observed when neutron stars goes through molecular clouds, since it is in them that the density of interstellar matter is greatest. In this case, the radiation power depends on the density of the medium and the speed of passage of a neutron star through it.

For example, if the speed of a neutron star relative to the surrounding matter is sufficiently small, about a few kilometers per second, and the cloud itself will have a high concentration (of the order of $10^2 - 10^4\ cm^{-3}$), then a so-called supercritical accretion mode may appear with the formation of emissions of the type jets, which are observed, for example, in the object SS 433 and in some young stars[26].

The classical theory of accretion is rooted in the 30s and 40s [27]. Accretion on single NS began to be considered at the very beginning of the 70s [28], when it became clear that accreting on the source of neutron stars are X-ray radiation.

Although accretion, as we have found, occurs both in binary systems and on single stars, their physics is quite different from each other, so far no accretion to individual objects exists orbital momentum. It should also be noted that the rate of accretion is several orders of magnitude lower when it comes to accretions on a single star [29]. For calculations in astrophysics, the key role is played by finding the accretion rate.

As we know, the rate of accretion of Bondi is given by equality[30]

$$\dot{M} \cong \pi R^2 \rho_\infty \vartheta_\infty \tag{1.6}$$

Modern works are aimed at taking into account various effects that can change (usually reduce) the rate of accretion compared to the classic Bondi results.

$$\dot{M} = \sigma \rho_\infty \vartheta_\infty \tag{1.7}$$

Let us to define the cross section σ. The radius of gravity capture is equal to[31] (in the case of spherical accretion):

$$R_G = 2GM / \mathrm{c}_s^2 \tag{1.8}$$

where c_s is the speed of sound in the IM.

There is a strong dependence between temperature and accretion rate.

$$\dot{M} \propto T_\infty^{-3/2} \tag{1.9}$$

Heating cannot stop accretion [32], however, its rate can noticeably decrease. In the case of cylindrical accretion ($\vartheta_\infty > c_s$), the formula for the radius of gravity capture changes:

$$R_G = 2GM / \left(c_s^2 + \vartheta_\infty^2\right) \tag{1.10}$$

And thus, for the rate of accretion, we have:

$$\dot{M} = k\pi \frac{\left(2GM\right)^2}{\left(c_s^2 + \vartheta_\infty^2\right)^{3/2}} \rho_\infty \tag{1.11}$$

The proportionality coefficient k, depends on the speed of the NS. Roughly we can put it equal to one. There are no exact analytical solutions in this case[31].

Also, the accretion rate depends on the magnetic field of a neutron star. For example, in [33], a numerical simulation of spherical and cylindrical accretion onto a neutron

star is considered. As calculations for spherically symmetric accretion show, the accretion rate decreases. If you compare with the results of Bondi (classical results), then it is less than about 2 times. The dependence of the rate of accretion onto a magnetic dipole on the magnetic field and magnetic permeability of the medium is established in formula (1.12):

$$\dot{M}_{dip} \propto \eta_m^{0.38} \ , \ \dot{M}_{dip} \propto \left(\dot{M}_B / \mu^2 \right) \tag{1.12}$$

where M_B is the Bondi accretion rate, η_m is the magnetic permeability.

As calculations show, if a neutron star has a magnetic field and accretion is cylindrical, then the rate accretion decreases several times compared with the case when the neutron star does not have a magnetic field [31]. Formula, (1.13) shows this dependence:

$$\dot{M} \propto B^{-1.3} \tag{1.13}$$

Thus, modern studies show that the rate of Bondi accretion is the upper limit, rarely realized in nature.

1.5 The diffusion of neutrons in the nonequilibrium crust of neutron stars.

The crust of neutron stars is of great interest, since it is in it that the processes that determine the evolution of x-ray radiation in the post-accretion period occur. The crust is traditionally divided into two parts: external ($\rho < \rho_{drip} \approx 4 \cdot 10^{11}\ g/cm^3$) - until the appearance of free neutrons, where the ionic crystal lattice is immersed in a sea of degenerate relativistic electrons and internal ($\rho \leq 2 \cdot 10^{14}\ g/cm^3$ is the nuclear density), where neutrons unbound in atomic nuclei are formed (the separation energy of part of the neutrons becomes negative) and a free neutron gas is formed. With the exception of the outer layer, the matter of a neutron star is relatively cold, in the sense that the characteristic Fermi energies of a degenerate substance are much higher than the characteristic thermal energies $k_B T$ [34], nevertheless $T \simeq 10^8\ K$ [35]. If the substance during the earlier hot stage $T \simeq 10^{11}\ K$ [36] had sufficient time to achieve nuclear equilibrium, we can assume that the matter in the crust is in the ground state. However, the accretion flux makes a significant contribution to the evolution of a neutron star. The matter from the accretion disk hits the neutron star and spreads uniformly on the surface. Within an hour, the arrivals of hydrogen and helium due to 3α reactions, CNO cycle, αp-processes, rp-processes burn up to heavy elements with Z up to 48 [37, 38], creating the initial composition of the hard crust. The equilibrium of compact objects is achieved due to the pressure of degenerate matter, which increases with the compaction of the object. The newly arrived substance, increasing gravitational pressure, contributes to the compression of matter in the crust, pushing it into the star. The pressure and density in the element of the accreted substance gradually increase,

and nuclear reactions begin that heat up the crust and make a significant contribution to the thermal x-ray radiation of a compact object. The substance in the accreted crust does not heat up above 10^9 K, which prevents the Coulomb barriers from being overcome. As a result, the composition of the crust of an accreting neutron star differs significantly from the equilibrium crust.

Thus, due to accretions, the neutron star is a binary system or a single star independently, the composition of the crust differs from the equilibrium one.

With a deviation from equilibrium, the nuclear composition of the substance in the layer of the crust of a neutron star is very different from the equilibrium. This is primarily due to the existance of a significant number of free neutrons. The nuclei apparently form a crystal lattice[39]; therefore, they can be considered immobile. While, neutrons are free and can diffuse under the influence of a gravity and gradient of concentration. The neutron concentration gradient can change sign in the nonequilibrium layer, and, in particular, at the outer boundary it is always directed outward (or equal to zero), since there are no free neutrons outside $\rho < 10^{10}\mu_e\ g/cm^3$. The force of gravity acting on neutrons is always directed inside the star. In a nonequilibrium layer of the crust, pressure is determined mainly by electrons. The ratio of the relativistic pressure of degenerate electrons P_e and neutrons in the no relativistic degeneracy P_n approximation is

$$\frac{P_n}{P_B} = \frac{5.3\cdot 10^9 \rho_n^{5/3}}{1.2\cdot 10^{15}\left(\rho/\mu_B\right)^{4/3}} = 2.8\cdot 10^{-5}\rho^{1/3}\frac{x_n^{5/3}}{\left(1-x_n\right)^{4/3}} \qquad (1.14)$$

For the maximum accepted value of the weight concentration of neutrons $x_n = 0.5$, $\mu_e = 4(1 - x_n)$ for nuclei with $Q_n = 0$ at the inner boundary of the nonequilibrium layer at a density, we have $\rho_2 \approx 3 \cdot 10^{11}\mu_e\ g/cm^3$ we have $(P_n/P_e)_{max} \approx 0{,}3$.On average, the role of gravity in neutron diffusion is predominant, especially at the outer boundary, where the neutron pressure is negligible. At the same time, in the dense regions of the nonequilibrium layer, a large neutron density gradient may appear, the effect of which on diffusion may be important.

From the calculated point of view, the inclusion of the term with $\frac{dn}{dr}$ in the diffusion equation increases its order and significantly complicates the solution. There are also fundamental difficulties associated with the need to specify additional boundary conditions at the layer boundary. This requires knowledge of the physical conditions outside the nonequilibrium layer and the study of reactions with neutrons occurring outside it. All this would greatly complicate the task, at the same time, to obtain semi-quantitative results on the evolution of the layer and the luminosity of a neutron star, it is enough to take into account in the diffusion equation only the main term determined by gravity. Such a solution was obtained in [40]. The problem was solved in a plane approximation under conditions of static equilibrium defined by the equations

$$P = \frac{GM_0 M}{4\pi R_0^4} \ , \ r = \int_P^{P_2} \frac{R_0^2 dp}{\rho G M_0} \ , \ r << R_0 \, ; \tag{1.15}$$

here M is the mass of the nonequilibrium layer lying over a given radius r, counted from the lower boundary of the layer, where $P = P_2$. The atomic weight and charge of nuclei depend on the Fermi energy of electrons, and therefore, on the density of electrons. In the process of diffusion, a redistribution of matter in the layer occurs, neutrons escape into the core of the star, as a result of which the density and chemical composition of the substance in the layer change. With a decrease in the electron density and Fermi energy, the nucleus is able to emit an electron, and then, due to the presence of free neutrons, capture about four neutrons in order to arrive at a state with $Q_n = 0$. In this case, the internal energy of the nucleus partially turns into heat. Thus, when the density of matter decreases during the diffusion of neutrons into the star, the nuclear chemical energy of the nuclei and neutrons is released. The transformation of nuclei must be considered in the diffusion equation, since part of the neutrons joins or detaches from the nuclei, and in the equation determining the energy balance in a nonequilibrium layer. considering the transformation of nuclei, the diffusion equation can be easily obtained in the approximation when the reactions of neutrons with nuclei occur much faster than the diffusion process. This condition is always take place with great accuracy.

The diffusion equation was also derived in the work[40]. For this, it was assumed that in the layer of a unit area of thickness dr there are

$$\xi = n_n dr + \left(\frac{A dN_A}{4\pi R_0^2} \right) \tag{1.16}$$

nucleons. $dN_A -$ the number of nucleus in the layer dr.

During diffusion, both n_n and A change, but N_A does not depend on time. The change in the number of nucleons in a given layer over time dt is equal to the difference of diffusion neutron fluxes J_n (1 / cm^2 sec) at the boundaries of the dr layer during time dt. Thus

$$\xi\left(t + dt\right) - \xi(\mathrm{t}) = \left[J_n\left(N_A + dN_A\right) - J_n\left(N_A\right) \right] dt \tag{1.17}$$

Expanding in dt and dN_A in (1.16) and (1.17) and dividing by $dN_A dt$, we obtain the diffusion equation

$$\frac{\partial}{\partial t}\left(n_n \frac{dr}{dN_A} + \frac{A}{4\pi R_0^2} \right) = \frac{\partial J_n}{\partial N_A} \tag{1.18}$$

with boundary condition $J_n(t,N)=0$. The flux J_n is defined in a system associated with nuclei, and is positive if neutrons diffuse into the star.

In the process of neutron diffusion, heat is released, which is transferred to the outside by heat conduction and radiated, and partially transferred inward and heats the star. Generally speaking, it is necessary to solve the heat equation taking into account the energy sources in the star.

According to the calculations performed in [40], neutrons primarily leave the upper layers of the nonequilibrium region. When neutrons become negligible, the density change will cease. A decrease in the number of neutrons due to diffusion leads to a decrease in pressure P. Since P is determined by electrons, the number of which only increases due to β decays, the layer must expand to maintain equilibrium. At the same time, internal stresses increase in the hard crust.

Thus, due to the process of neutron diffusion, the core composition of the crust varies greatly, as mentioned earlier, due to the fact that by decreasing the electron density and Fermi energy, the nucleus is able to emit an electron, and then, due to the presence of free neutrons, capture about four neutrons in order to arrive to the state with $Q_n = 0$, the released heat is transferred to the outside by heat conduction and radiated, and partially transferred to the inside and heats the star. Further in the next subsection, we consider a chain of nuclear reactions, namely, the Pb-Bi cycle and its energy contribution to the heating of a neutron star at various values of the neutron flux.

1.6 «Isotopes Burn Up Software» and its test.

In Nuclear Physics, there are often problems where the property of a system depends on the concentration of the isotopic composition of the system, which can vary on time. Calculations of this kind are performed using burnup calculation codes. An important part of the burnup calculation is the solution of the burnup equations, which describe the rates at which the concentrations of various nuclides change. Burnup equations form a first-order linear differential system of equations that can be written

$$\frac{d}{dt}N_i(t)=\lambda_i N_i(t)-\sigma_i\varphi N_i(t)+\sum_{i\neq j}\lambda_j N_j(t)P_{j\to i}+\sum_{i\neq j}\sigma_i\varphi N_i(t)Q_{j\to i} \qquad (1.19)$$

where first term on the right side of the equation describes out coming concentration of i - isotopes due to radioactive decay of these isotopes; second term describes out coming concentration of i - isotopes due to radioactive capture of these isotopes; third term is a concentration of incoming isotopes due to radioactive decay of j - isotopes; fourth term is a concentration of incoming isotopes due to radioactive capture of j - isotopes.

Further we consider the burnup system under the assumption that these coefficients describing out coming and in coming are fixed constants for each isotope.

The burnup equations can then be written in matrix notation as

$$\frac{d}{dt}\boldsymbol{N}(t) = \boldsymbol{A}\boldsymbol{N}(t) \tag{1.20}$$

Where $\boldsymbol{N}(t) \in \mathrm{R}^{\mathrm{n}}$ = nuclide concentration vector, which is can change in time. $\boldsymbol{A} \in \mathrm{R}^{\mathrm{n}\times\mathrm{n}}$ = burnup matrix containing the decay and transmutation coefficients of the nuclides under consideration which is not changes in a time.

$$\mathbf{A} = \begin{pmatrix} -\lambda_1 - F\sigma_1 & \lambda_2 P_{2\to1} + Q_{2\to1} F\sigma_{2\to1} & \cdots & \lambda_n P_{n\to1} + Q_{n\to1} F\sigma_{n\to1} \\ \lambda_1 P_{1\to2} + Q_{1\to2} F\sigma_{1\to2} & -\lambda_2 - F\sigma_2 & \cdots & \lambda_n P_{n\to2} + Q_{n\to2} F\sigma_{n\to2} \\ \vdots & \vdots & \ddots & \vdots \\ \lambda_1 P_{1\to n} + Q_{1\to n} F\sigma_{1\to n} & \lambda_2 P_{2\to n} + Q_{2\to n} F\sigma_{2\to n} & \cdots & -\lambda_n - F\sigma_n \end{pmatrix} \tag{1.21}$$

Equation above can be formally solved by the matrix exponential method yielding the simple solution

$$\boldsymbol{N}(t) = \boldsymbol{N}(0)\exp(\boldsymbol{A}t) \tag{1.22}$$

where the exponential of the matrix $\boldsymbol{A}t$ is defined as the power series expression

$$e^{\mathbf{A}t} = \sum_{k=0}^{\infty} \frac{1}{k!}(\mathbf{A}t)^k \tag{1.23}$$

with the additional definition $\boldsymbol{A}^0 = \boldsymbol{I}$.

There are numerous algorithms for computing the matrix exponential such as Pade approximation and Chebyshev rational approximation method(CRAM). Let's consider on each method in more detail.

In solving the burnup equations with the matrix exponential method, it is beneficial to estimate the character of the matrix eigenvalues, e.g., whether they are real-valued or complex-valued, and, in the latter case, the magnitude of the eigenvalues' imaginary parts.

It is known that the general solution of system (1.20) is a linear combination of functions of the form

$$t^k e^{\alpha t}\cos(\omega t)\mathbf{a}, t^l e^{\alpha t}\sin(\omega t)\mathbf{b}; \mathbf{a}, \mathbf{b} \in R^n \tag{1.24}$$

where $\lambda = \alpha + \mathrm{i}\omega$ runs through all the eigenvalues of $\mathbf{A}$ with $\omega \geq 0$ and $k, l \leq m(\lambda) - 1$, where $m(\lambda)$ denotes the algebraic multiplicity of eigenvalue[126]. If all eigenvalues of the burnup matrix are real, the concentration of each nuclide is a linear combination of functions of the form $f(t) = t^k e^{\alpha t}$. In this case the eigenvalue determines the rate of exponential growth or decay of the function f. On the other

hand, an eigenvalue with a nonzero imaginary part ω indicates that the solution has an oscillating component with period $T = 2\pi\omega$.

The theorem in [126, P. 165] therefore gives a useful characterization of the real parts of the burnup eigenvalues. The real parts of the eigenvalues of the burnup matrix must therefore all be nonpositive. A purely imaginary eigenvalue would correspond to a nondamped oscillation, which is physically unrealistic in the context of burnup calculation. It can thus be deduced that the real parts of the nonzero eigenvalues of the burnup matrix are always negative.

The characterization of the imaginary parts of the burnup eigenvalues is more difficult. If the burnup chain does not contain any closed cycles—i.e., no paths from any vertex back to itself exist in the burnup matrix—the matrix can be permuted into a triangular form. In this case the eigenvalues are the diagonal elements, and hence, all are real-valued and negative. The nonreal eigenvalues result from closed transition cycles occurring in the burnup chain. However, not all closed transition cycles induce nonreal eigenvalues, and in practice only a fraction of the eigenvalues of the burnup matrix have nonzero imaginary parts.

A suitable mathematical method for establishing a link between the structure and eigenvalues of a matrix is the computation of the strongly connected components of the graph of the matrix. A strongly connected component is defined as a set of vertices such that there exists a path from each vertex to every other vertex. If all of the strongly connected components of a matrix are sorted topologically, the corresponding systems of differential equations can be solved independently in this order. The different cyclic components of a burnup chain can therefore be studied conveniently by calculating its strongly connected components. If the burnup matrix does not contain any closed cycles, the size of every strongly connected component is one, and the solution of system (1.20) can be calculated by solving n ordinary linear differential equations. The nonreal eigenvalues can therefore be identified with certain cyclic parts in the burnup transition chain.

In [127] have computed the eigenvalues for a wide range of burnup matrices, and based on experiments, it seems that they are generally confined to a region near the negative real axis. Based on observations it appears that a prerequisite for a nonreal eigenvalue is that the majority of the reactions involved in a closed cycle have transition rates that are of the same order. In this scenario the slowest reactions appear to have the most significance for the period of the oscillation. This seems reasonable from a physical standpoint, as well. The cycle that is most likely to induce oscillations appears to consist of an alpha decay followed by successive (n,$\boldsymbol{\gamma}$) and β^- reactions. An example of this kind of loop is the transition cycle resulting from the alpha decay of Cm242. The decay constant of this reaction is of order 10^{-8}1/s (half-life 162 days), and in a thermal reactor operating at full power, the corresponding cycle typically induces three pairs of complex eigenvalues with imaginary parts of order $\leq 10^{-8}$ [127].

The most obvious approach is to calculate the exponential directly from the definition (1.23) using a truncated Taylor series. This approximation is naturally most accurate near the origin, so it is ill-suited for burnup calculations, where the matrix

norm $\|\boldsymbol{A}t\|$ can become arbitrarily large. In some cases even increasing the number of terms does not improve the approximation because of the accuracy limitations in the computer arithmetic's. The accuracy of the series method can be improved by using the method of scaling and squaring, which is based on the identity

$$e^{\mathbf{A}t} = (e^{\mathbf{A}t/m})^m \tag{1.25}$$

where m can be taken as a power of two, $m = 2^k$, so that the norm $\|\boldsymbol{A}t/m\|$ becomes sufficiently small. The truncated series is then calculated for the scaled matrix, and the result is squared by repeated multiplications. The accuracy of this technique may be compromised, if the elements of $e^{\boldsymbol{A}t}$ grow before they decay, as t increases. Numerical problems are faced when this so-called "hump" is located between t/m and t [128].

The most well-established method for calculating the matrix exponential is probably the rational Pade approximation with scaling and squaring. For example, the matrix exponential function *expm* in MATLAB is based on this approach. Although this method generally outperforms the truncated Taylor series approach, it shares the requirement of $\|\boldsymbol{A}t\|$ remaining relatively small [128]. Accordingly, numerical problems are faced when $\|\boldsymbol{A}t\| \gg 1$ and t$\sim 10^6$s, both of which are plausible values in the context of burnup calculation. The rational Pade approximation gives as

$$N_{pq}(x) = \sum_{k=0}^{p} \frac{(p+q-k)!\,p!}{(p+q)!k!(p-k)!}(x)^k \tag{1.26}$$

$$D_{pq}(x) = \sum_{k=0}^{p} \frac{(p+q-k)!\,p!}{(p+q)!k!(q-k)!}(-x)^k \tag{1.27}$$

$$exp(\mathbf{A}\Delta t) \approx \frac{N_{pq}(\mathbf{A}\Delta t)}{D_{pq}(\mathbf{A}\Delta t)} \tag{1.28}$$

Another approach to rational approximation is to calculate the best approximation on some subset of the complex plane. This approach was made famous by Cody, Meinardus, and Varga [129] in 1969 in the context of rational approximation of e^{-x} in [0,∞]. Let $\pi_{k,l}$ denote the collection of all real rational functions $r_{k,l}$ of the form

$$p_{k,l} = \frac{p_k(x)}{p_l(x)} \tag{1.29}$$

where p_j is a polynomial of degree j or less.

It is known from approximation theory that there exists a unique $\overline{r_{k,l}} \in \pi_{k,l}$ such that

$$\sup_{-\infty < x \le 0} |\bar{r}_{k,l}(-x) - e^x| = \inf_{r_{k,l} \in \pi_{k,l}} \{\sup_{-\infty < x \le 0} |r_{k,l}(-x) - e^x|\} \tag{1.30}$$

Establishing this approximation for given k and l is not easy, but it can be done with the Remes algorithm or the Carathéodory-Fejér method. It has been shown that this Chebyshev rational approximation $\overline{r_{k,l}}$ converges approximately at the rate 9.3^{-k} [130]. The contour plot of $\left|e^z - \overline{r_{14,14}(-z)}\right|$ is shown in figure 3, from which it can be seen that this approximation is remarkably accurate in a wide region in the left complex plane. From a computational point of view, it is advantageous that the poles $\{\theta_1, \ldots \theta_k\}$ of the rational function $\overline{r_{k,l}}$ are distinct, so that it can be computed as a partial fraction expansion [131].

$$\bar{r}_{k,l}(z) = \alpha_0 + \sum_{i=0}^{k} \frac{\alpha_i}{z - \theta_i} \tag{1.31}$$

where α_0 is the limit of the function at infinity and the scalars α_i are the residues at the poles θ_i. Therefore, the values of α_i and θ_i depend on *k*. Equation (1.31) can be derived by noting that $\left|\overline{r_{k,k}} - \alpha_0\right| \in \pi_{k-1,k}$ for which the result readily follows from the residue theorem. It should be noted that the poles of $\overline{r_{k,k}}$ come in conjugate pairs, so that for a real-valued variable $x \in \mathrm{R}$, the computational cost can be reduced to half [127]:

$$\bar{r}_{k,k}(x) = \alpha_0 + \mathrm{Re}\sum_{i=1}^{k/2} \frac{\alpha_i}{x - \theta_i} \tag{1.32}$$

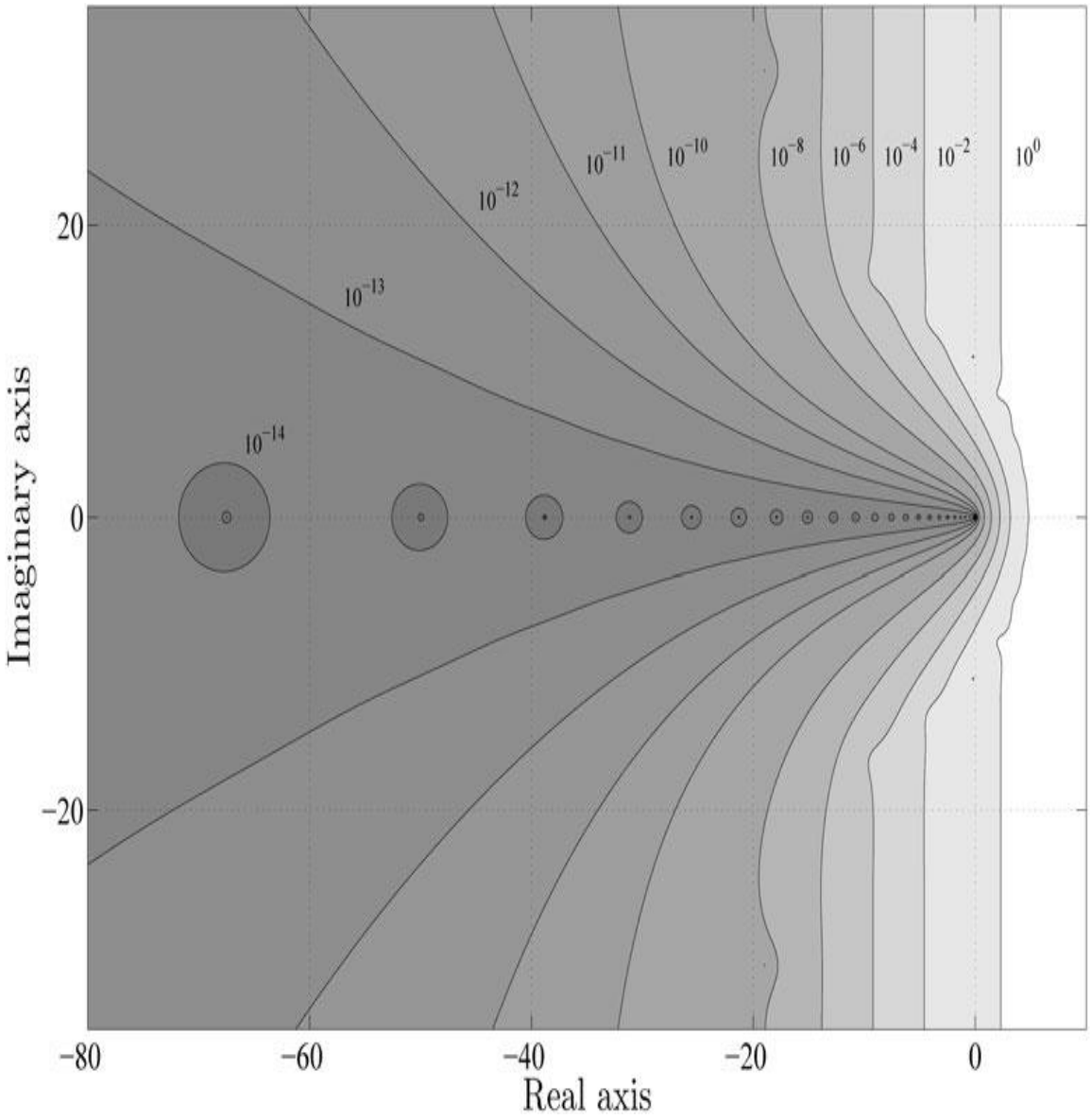

Figure 3 – Contour plot of $\left|e^{z} - \overline{r_{14,14}(-z)}\right|$ [127].

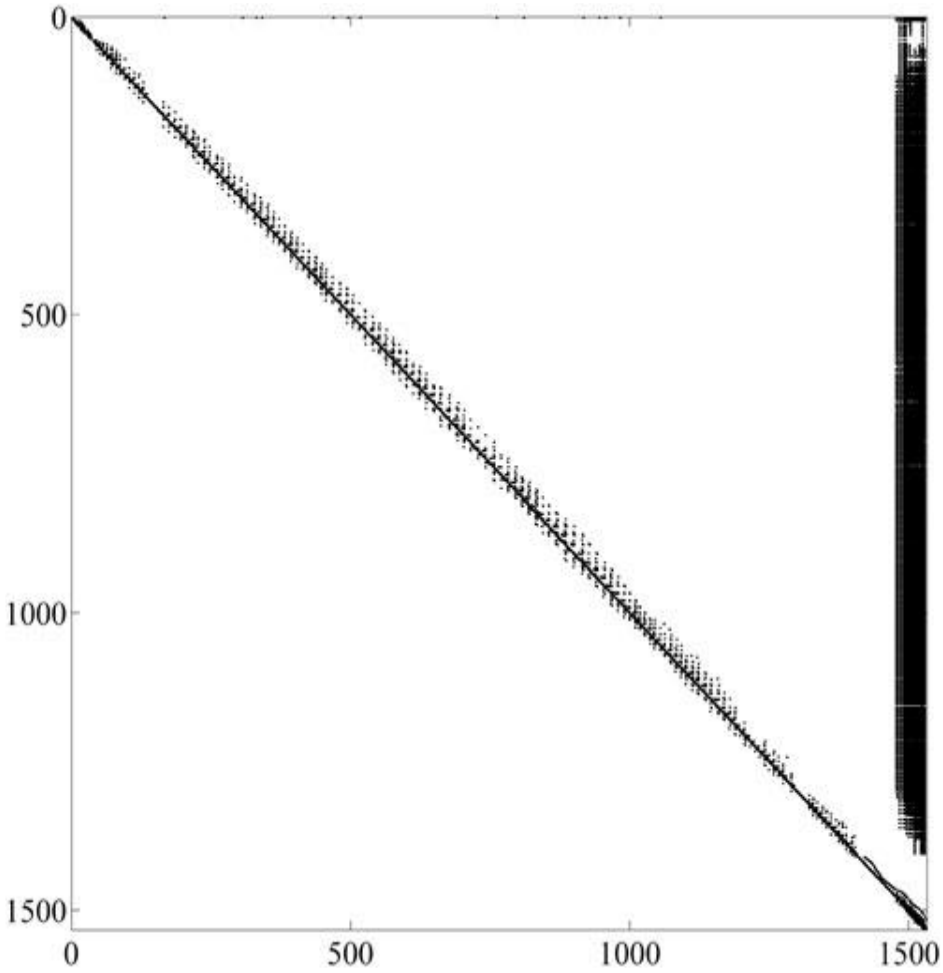

Figure 4 – The structure of the burnup matrix created for all isotopes existing in ENDF data bases.

Table 1 – PFD Coefficients for CRAM Approximation of Order 14[134]

Coefficient	Real Part	Imaginary Part
θ_1	$-8.897\,773\,186\,468\,8 \times 10^{0}$	$+1.663\,098\,261\,990\,2 \times 10^{1}$
θ_2	$-3.703\,275\,049\,423\,4 \times 10^{0}$	$+1.365\,637\,187\,148\,3 \times 10^{1}$
θ_3	$-0.208\,758\,638\,250\,1 \times 10^{0}$	$+1.099\,126\,056\,190\,1 \times 10^{1}$
θ_4	$+3.993\,369\,710\,578\,5 \times 10^{0}$	$+6.004\,831\,642\,235\,0 \times 10^{0}$
θ_5	$+5.089\,345\,060\,580\,6 \times 10^{0}$	$+3.588\,824\,029\,027\,0 \times 10^{0}$
θ_6	$+5.623\,142\,572\,745\,9 \times 10^{0}$	$+1.194\,069\,046\,343\,9 \times 10^{0}$
θ_7	$+2.269\,783\,829\,231\,1 \times 10^{0}$	$+8.461\,737\,973\,040\,2 \times 10^{0}$

α_1	$-7.154\,288\,063\,589\,0 \times 10^{-5}$	$+1.436\,104\,334\,954\,1 \times 10^{-4}$
α_2	$+9.439\,025\,310\,736\,1 \times 10^{-3}$	$-1.718\,479\,195\,848\,3 \times 10^{-2}$
α_3	$-3.763\,600\,387\,822\,6 \times 10^{-1}$	$+3.351\,834\,702\,945\,0 \times 10^{-1}$
α_4	$-2.349\,823\,209\,108\,2 \times 10^{1}$	$-5.808\,359\,129\,714\,2 \times 10^{0}$
α_5	$+4.693\,327\,448\,883\,1 \times 10^{1}$	$+4.564\,364\,976\,882\,7 \times 10^{1}$
α_6	$-2.787\,516\,194\,014\,5 \times 10^{1}$	$-1.021\,473\,399\,905\,6 \times 10^{2}$
α_7	$+4.807\,112\,098\,832\,5 \times 10^{0}$	$-1.320\,979\,383\,742\,8 \times 10^{0}$
α_0	$-7.154\,288\,063\,589\,0 \times 10^{-5}$	$+0.000\,000\,000\,000\,0 \times 10^{0}$

Table 1 – PFD Coefficients for CRAM Approximation of Order 16[134]

Coefficient	Real Part	Imaginary Part
θ_1	$-1.084\,391\,707\,869\,6 \times 10^{1}$	$+1.927\,744\,616\,718\,1 \times 10^{1}$
θ_2	$-5.264\,971\,343\,442\,6 \times 10^{0}$	$+1.622\,022\,147\,316\,7 \times 10^{1}$
θ_3	$+5.948\,152\,268\,951\,1 \times 10^{0}$	$+3.587\,457\,362\,018\,3 \times 10^{0}$
θ_4	$+3.509\,103\,608\,414\,9 \times 10^{0}$	$+8.436\,198\,985\,884\,3 \times 10^{0}$
θ_5	$+6.416\,177\,699\,099\,4 \times 10^{0}$	$+1.194\,122\,393\,370\,1 \times 10^{0}$
θ_6	$+1.419\,375\,897\,185\,6 \times 10^{0}$	$+1.092\,536\,348\,449\,6 \times 10^{1}$
θ_7	$+4.993\,174\,737\,717\,9 \times 10^{0}$	$+5.996\,881\,713\,603\,9 \times 10^{0}$
θ_8	$-1.413\,928\,462\,488\,8 \times 10^{0}$	$+1.349\,772\,569\,889\,2 \times 10^{1}$
α_1	$-5.090\,152\,186\,522\,4 \times 10^{-7}$	$-2.422\,001\,765\,285\,2 \times 10^{-5}$
α_2	$+2.115\,174\,218\,246\,6 \times 10^{-4}$	$+4.389\,296\,964\,738\,0 \times 10^{-3}$
α_3	$+1.133\,977\,517\,848\,3 \times 10^{2}$	$+1.019\,472\,170\,421\,5 \times 10^{2}$

α_4	$+1.505\,958\,527\,002\,3 \times 10^{1}$	$-5.751\,405\,277\,642\,1 \times 10^{0}$
α_5	$-6.450\,087\,802\,553\,9 \times 10^{1}$	$-2.245\,944\,076\,265\,2 \times 10^{2}$
α_6	$-1.479\,300\,711\,355\,7 \times 10^{0}$	$+1.768\,658\,832\,378\,2 \times 10^{0}$
α_7	$-6.251\,839\,246\,320\,7 \times 10^{1}$	$-1.119\,039\,109\,428\,3 \times 10^{1}$
α_8	$+4.102\,313\,683\,541\,0 \times 10^{-2}$	$-1.574\,346\,617\,345\,5 \times 10^{-1}$
α_0	$+2.124\,853\,710\,495\,2 \times 10^{-16}$	$+0.000\,000\,000\,000\,0 \times 10^{0}$

Based on the expressions above, we developed the «IBUS» software package (ISOTOPE BURNUP SOFTWARE)[44,46]. The «IBUS» software package has a fairly convenient interface which is shown in figure 5 and is intended for both the average user and users with programming experience (it has a built-in c-sharp language compiler and an editor for code). This software package is designed to solve the problems of determining the concentration of isotopes, as well as to determine the reaction products under the influence of thermal neutrons. As a nuclear database for determining the constants for each isotope such as reaction cross sections, half-life, etc., «IBUS» uses ENDF / BVII.1 database with total memory 2,37Gb.

There are also two modes for loading data from the ENDF/BVII database. The first mode is pointed mode, that is, when the user downloads data selectively for the declared isotopes. In this mode of operation, the program reacts very quickly and the calculation speed is quite good with a small number of isotopes since the calculation is carried out according to the Pade algorithm and the burnup matrix is not too large. The disadvantage of this mode is the neglect of possible reaction channels if they are not indicated or follow from the region of the considered isotopes [46].

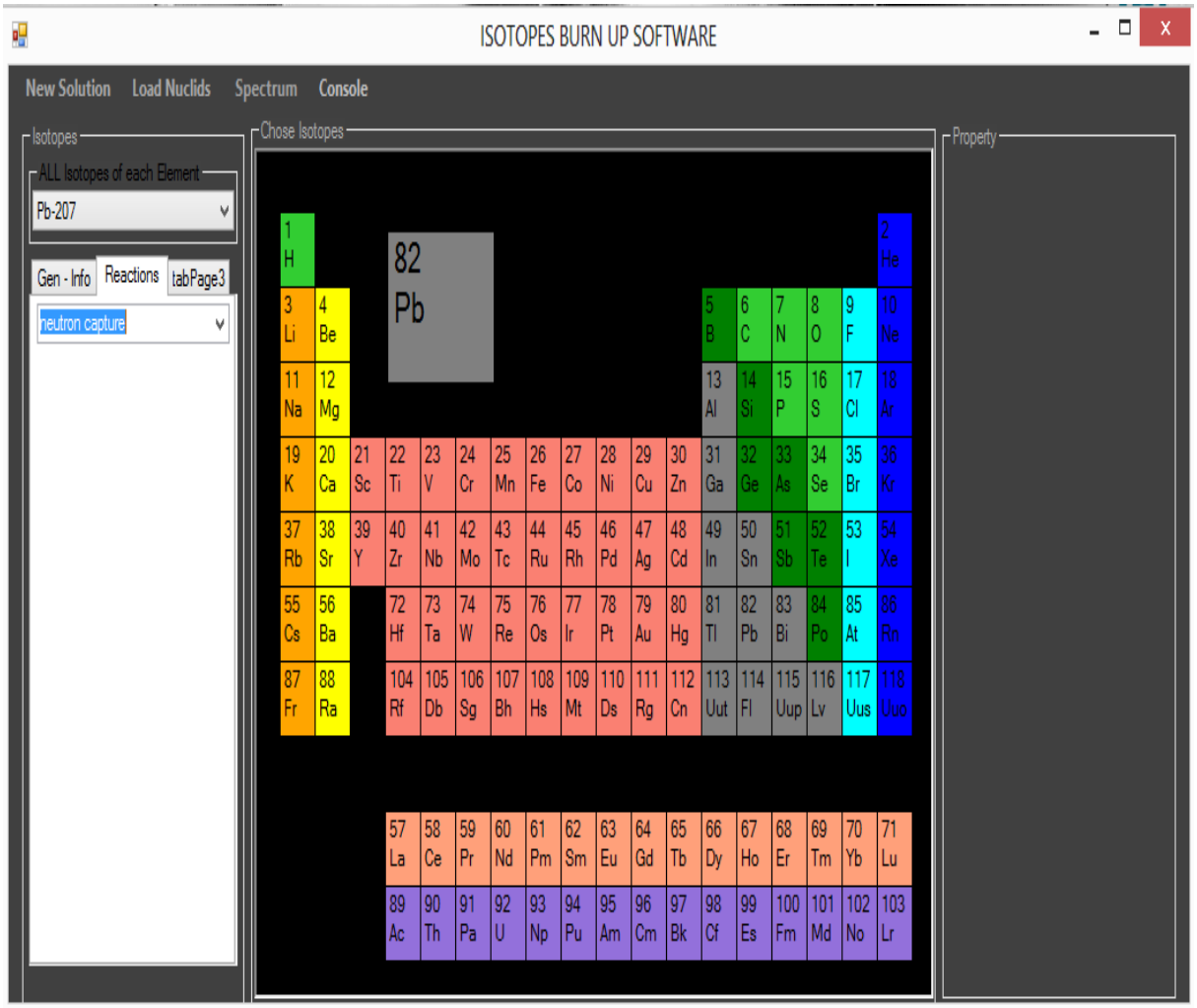

Figure 5 – Interface of the «IBUS» software package [44,46].

The second mode of operation is automatic. In this mode, the program loads all the specified parameters for the isotopes defined in the nuclear database. With this mode of operation, the program takes some time to complete the data download, and also automatically builds the burnup matrix for all isotopes in automatic mode, while it occupies almost the entire RAM of the computer. This mode is suitable for calculating with a small number of iterations. However, this mode takes into account all possible reaction channels from the database. In this mode, the program finds the exponent of the burnup matrix by the CRAM method [44,45].

Also, for optimization of calculation, both methods can be used at the same time i.e. combined. For this, it is necessary to consider the analytical channels of our interest or the necessary reaction channels and the associated isotopes. Then calculate in the first mode for a relatively short period of time. Then for the same period of time to calculate in the second mode. Analyzing the obtained calculation results, we can determine the most suitable mode of the two. For example, if the results are practically the same and there is no increase of the difference in time, then we can use first mode in our simulation for a long period of time. Otherwise, we need to re-analyze more thoroughly the isotopes and reaction channels that we did not take into account in the first case. Thus, the software package «IBUS» [43,46] also allows

sensitivity analysis. To do this, we need to load the reaction cross sections manually in the first mode without using the nuclear database. Changing them every time you start the program in both modes, you can analyze the sensitive reaction channel.

To test the «IBUS» software package[43,46], we performed the same calculations as in [41], without additional restrictions on the reaction channels as was done in [41].

The nucleosynthesis of heavy stable nuclei by successive captures of neutrons in a weak neutron flux (the s-process) is terminated at large atomic weight by alpha decay to isotopes of lead. Authors in [41] analyzed the details of this termination and calculate the abundances of lead and bismuth isotopes synthesized by the exposure of lighter nuclei to neutrons. They demonstrate that the results are nearly insensitive to the poorly known neutron-capture cross-section of Pb–208. The continuous distribution of integrated neutron exposures responsible for the observed abundances has an anomalously large high-exposure component. This result suggests that the bulk of the lead has been synthesized by special astrophysical circumstances rather than by a smooth extension of the circumstances attending the synthesis for $A < 200$[41].

To achieve the goals, authors in [41] is considered Pb-Bi cyclic reaction chain shown in figure 6.

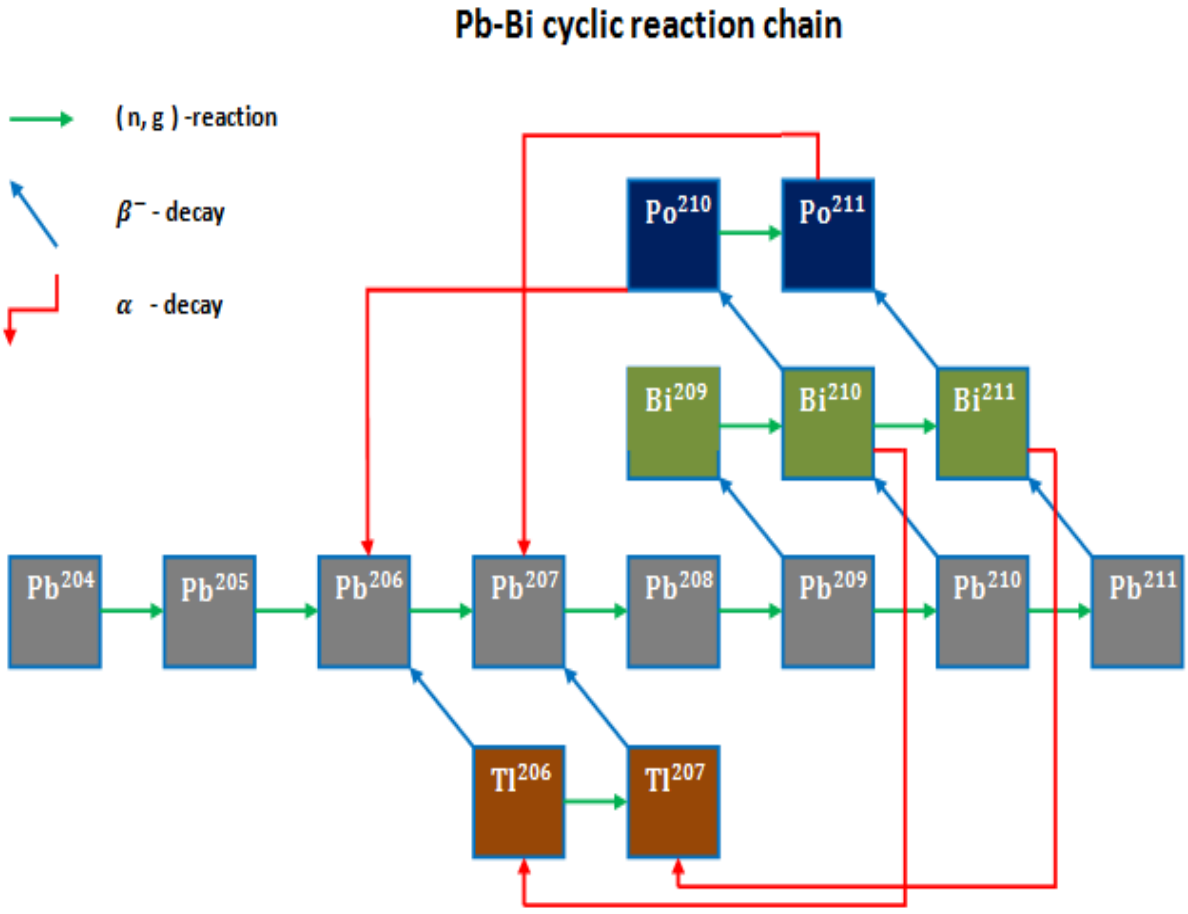

Figure 6 – Nuclear cyclic reaction chain Pb-Bi scheme.

In this chain the last stable isotope of the s-process is Bi-209. When it captures a neutron the region of unstable masses is entered, and the corresponding decay schemes are indicated in figure 7, which is adapted from the Nuclear Data Sheets (Gove 1965). The authors, making a theoretical analysis of the ground and isomeric states of the isotopes Pb-210, Bi-210 and Po-210, come to the conclusion that the neutron capture may be ignored in favor of the approximation that Bi-210

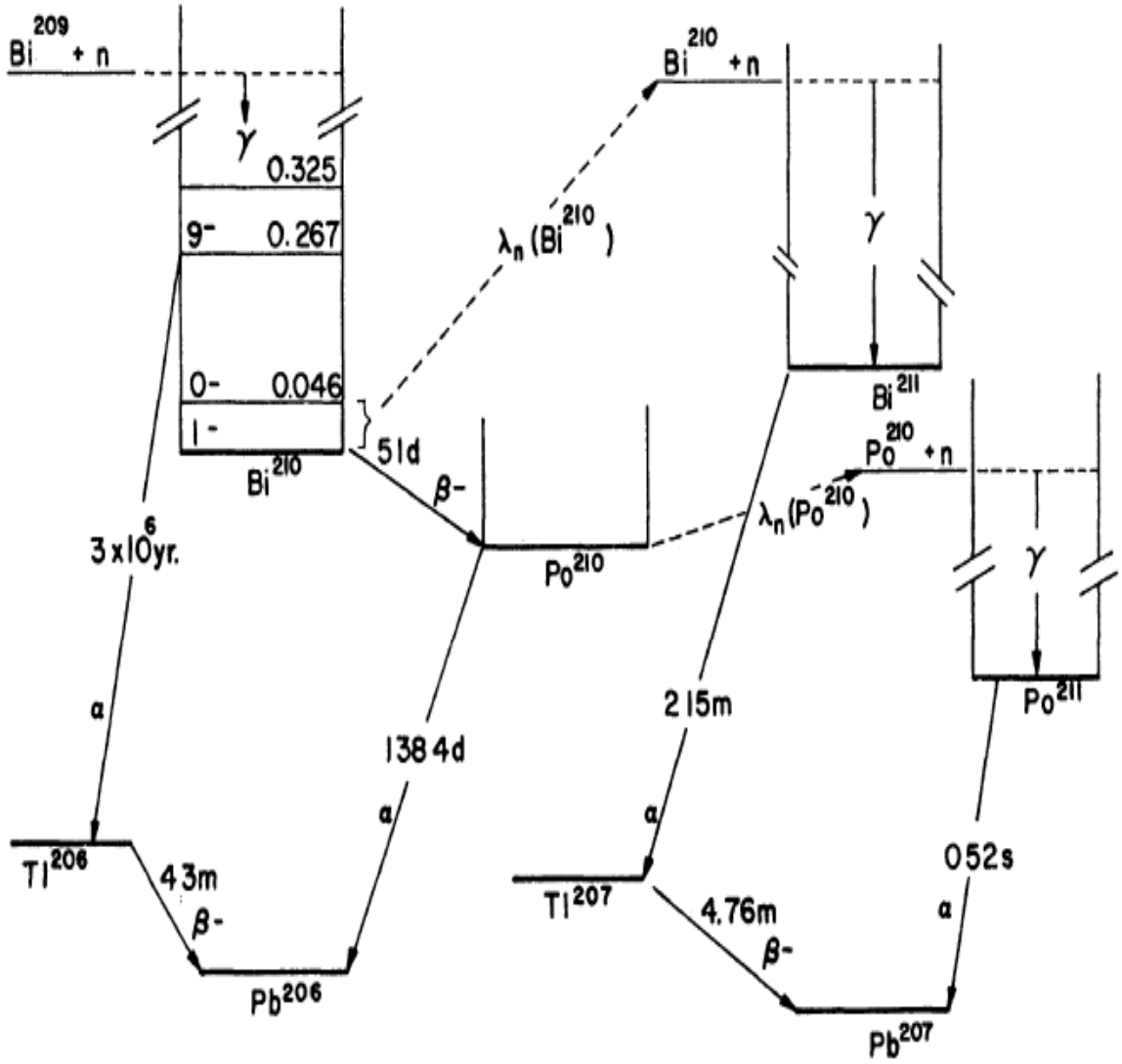

Figure 7 – Nuclear cyclic reaction chain Pb-Bi and its isotopes ground and existed state scheme(from Nuclear Data Sheets (Gove).

decays instantaneously to Po-210. Because the abundance of any nucleus in a chain is approximately proportional to the total lifetime of that nucleus, moreover, the abundance of Bi-210 may be taken to be zero at all times.

The situation is not so clear with regard to the fate of Po-210, however. Its alpha-decay half-life of 138 days cannot be shortened by decay of excited states because the excited states of Po-210 lie too high in excitation energy to compete

thermally. If the lifetime of Po-210 against neutron capture is comparable to 138 days, the chain may form some Po-211, which quickly decays to Pb-207. In such a case, moreover, the abundance of Po-210 in the chain will not be negligible, and its decay to Pb-206 after the event will have to be included as a contributor to the Pb-206 abundance. They(authors) regard this possibility unlikely, for reasons to be discussed shortly, but we include it in this general discussion to allow for astrophysical circumstances in which the lead isotopes may participate in a relatively rapid neutron-capture chain. The differential equations in this case are

$$\begin{aligned}
\frac{dPb^{206}}{dt} &= \lambda_{\alpha}\left(Po^{210}\right)Po^{210} - \lambda_{n}\left(206\right)Pb^{206} + \lambda_{n}\left(205\right)N_{205} \\
\frac{dPb^{207}}{dt} &= \lambda_{n}\left(206\right)Pb^{206} - \lambda_{n}\left(207\right)Pb^{207} + \lambda_{n}\left(Po^{210}\right)Po^{210} \\
\frac{dPb^{208}}{dt} &= \lambda_{n}\left(207\right)Pb^{207} - \lambda_{n}\left(208\right)Pb^{208} \\
\frac{dBi^{209}}{dt} &= \lambda_{n}\left(208\right)Pb^{208} - \lambda_{n}\left(209\right)Bi^{209} \\
\frac{dPo^{210}}{dt} &= \lambda_{n}\left(209\right)Bi^{209} - \lambda_{\alpha}\left(Po^{210}\right)Po^{210} - \lambda_{n}\left(Po^{210}\right)Po^{210}
\end{aligned} \tag{1.33}$$

The element abundances are represented by their chemical symbols except for the chain abundance at $A = 205$ which is represented simply by N_{205} showed that the evolution of the abundance distribution due to neutron captures could conveniently be followed in terms of an exposure parameter

$$\tau = \int n_n(t) v_T dt \tag{1.34}$$

where n_n is the free neutron density and $v_T = (2kT/m_n)^{1/2}$ is a characteristic thermal neutron velocity. For conceptual simplicity it can be chose to write the coupled differential equations as a matrix equation:

$$\frac{d\,\mathbf{X}}{d\,\tau} = \sum \mathbf{X} + \mathbf{b}\left(\tau\right) \tag{1.35}$$

where $\boldsymbol{X} = [Pb^{206}, Pb^{207}, Pb^{208}, Bi^{209}, Po^{210}]$ – vector of an abundance and $\boldsymbol{b}(\tau) = [\Psi_{205}, 0,0,0,0]$; $\Psi_{205} = \sigma_{205} N_{205}(\tau)$. $\boldsymbol{\Sigma}$ –is a matrix

$$\sum = \begin{pmatrix} -\sigma_{206} & 0 & 0 & 0 & \dfrac{\lambda_\alpha(210)}{\lambda_n(210)} \\ \sigma_{206} & -\sigma_{207} & 0 & 0 & 0 \\ 0 & \sigma_{207} & -\sigma_{208} & 0 & 0 \\ 0 & 0 & \sigma_{208} & -\sigma_{209} & 0 \\ 0 & 0 & 0 & \sigma_{209} & -\left(1+\dfrac{\lambda_\alpha(210)}{\lambda_n(210)}\sigma_{210}\right) \end{pmatrix} \tag{1.36}$$

The symbol σ_a represents the usual thermal average of the neutron capture cross section by the neutron velocity spectrum. The function $\Psi_{205} = \sigma_{205}N_{205}$ is a well-known function of τ, which depends on all previous sections in the chain and on the identity of the initial isotopes from which the entire chain is generated. The solutions of equation (1.33) in principle would be easily feasible if the matrix $\boldsymbol{\Sigma}$ had constant elements. Unfortunately, this is not so, and as a result of this, the general equation does not have analytical general solutions. The problem is not in cross sections, since they can be considered constant, even if the temperature of an astrophysical event can vary to some extent with time. The complexity is associated with the branching of $\lambda_\alpha(210)/\ \lambda_n(210)$ [41].

But since $\lambda_\alpha(210)$ is constant and equal to $138(\text{days})^{-1}$ while the flux during the s-process varies from $10^{10} - 10^{15}\text{neutron/cm}^2$, in the calculation, They(Authors) can neglect the probability of neutron capture by the isotope Po-210, assuming that all that is formed instantly undergoes alpha decay and turn into lead isotopes Po-206, thereby forming the Pb-Bi cycle [41]. This allowed the authors to reduce the number of differential equations. Given this, (1.35) can be written in the form of a matrix equation 4 by 4.

$$\frac{d}{d\tau}\begin{pmatrix} Pb^{206} \\ Pb^{207} \\ Pb^{208} \\ Bi^{209} \end{pmatrix} = \begin{pmatrix} -\sigma_{206} & 0 & 0 & \sigma_{209} \\ \sigma_{206} & -\sigma_{207} & 0 & 0 \\ 0 & \sigma_{207} & -\sigma_{208} & 0 \\ 0 & 0 & \sigma_{208} & -\sigma_{209} \end{pmatrix}\begin{pmatrix} Pb^{206} \\ Pb^{207} \\ Pb^{208} \\ Bi^{209} \end{pmatrix} + \begin{pmatrix} \psi_{205} \\ 0 \\ 0 \\ 0 \end{pmatrix} \tag{1.37}$$

Equation (1.37) is a linear matrix equation with constant coefficients and can be solved in essentially closed form. Following the notation of Clayton *el at.* (1961), Authors of [41] choose to work with the functions $\Psi_{\mathrm{A}}(\tau) = \sigma_{\mathrm{A}}\mathrm{N}(\tau)$.

In matrix and unit vector notification (1.37) can be written as

$$\frac{d\boldsymbol{\psi}}{d\tau} = \mathbf{M}\boldsymbol{\psi} + \mathbf{e}_1 \sigma_{205} \psi_{205} \tag{1.38}$$

where $\boldsymbol{\Psi}$ is the vector whose solution is sought, and Ψ_{205} is some known function of τ which acts as a source function for the solution. Inasmuch as the s-process can synthesize no lead with zero neutron flux, we have the boundary condition $\Psi(0) = 0$.

Now the matrix $\boldsymbol{M}$ can be written as the product of its eigenvector and eigenvalue matrices

$$\mathbf{M} = \mathbf{A}\boldsymbol{\Lambda}\mathrm{B} \tag{1.39}$$

where $\boldsymbol{A}$ is the matrix of column eigenvectors, $\boldsymbol{\Lambda}$ is the diagonal matrix of eigenvalues, and $\mathbf{B}$ is the matrix of row eigenvectors. The matrix $\boldsymbol{M}$ is singular, so one of the eigenvalues, which we choose to call the first, is zero; $\lambda_1 = \Lambda_{11} = 0$. For the measured values of the cross-sections the second eigenvalue λ_2 is a negative real number, whereas λ_3 and λ_4 are complex eigenvalues, conjugate to each other, with negative real parts. In principle two of the eigenvalues could be equal, in which case it might not be possible to obtain a diagonal $\boldsymbol{\Lambda}$. However, a slight adjustment of any of the cross-sections within their experimental errors would eliminate this problem.

From matrix theory we have that $\boldsymbol{AB} = \boldsymbol{BA} = \mathbf{I}$, where $\mathbf{I}$ is the identity matrix. There remains some arbitrariness in the normalization of $\boldsymbol{A}$ and $\boldsymbol{B}$, however, since we may right-multiply $\boldsymbol{A}$ by any diagonal matrix and left-multiply $\boldsymbol{B}$ by its inverse without altering any essential relation. For reasons of convenience to become apparent below, we have adopted the convention that $B_{1i} = 1$, and $\boldsymbol{A}$ will be adjusted accordingly. The cross-sections, and hence the eigenvalues and vectors, depend upon the temperature assumed for the s-process, and the reader is referred to Macklin and Gibbons. At that moment the value of σ_{208} been measured, but it is known to be a small number consistent with the value we have adopted here. The seriousness of the uncertainty in its value will be discussed later. The differential equation (1.37) may easily be solved with the aid of this decomposition of the matrix $\boldsymbol{M}$. If we multiply through on the left by $\boldsymbol{B}$ we obtain

$$\frac{d}{d\tau}(\mathbf{B}\boldsymbol{\psi}) = \boldsymbol{\Lambda}(\mathbf{B}\boldsymbol{\psi}) + (\mathbf{B}\mathbf{e}_1)\sigma_{205}\psi_{205} \tag{1.40}$$

Because $\boldsymbol{\Lambda}$ is diagonal this matrix equation can be written as four uncoupled equations, and since $(\boldsymbol{Be_1})_i = 1$, they are

$$\frac{d}{d\tau}(\mathbf{B}\boldsymbol{\psi})_i = \lambda_1(\mathbf{B}\boldsymbol{\psi})_i + \sigma_{205}\psi_{205} \tag{1.41}$$

These equations are solved with the aid of an integrating factor:

$$(\mathbf{B\Psi})_i = \sigma_{206} e^{-\lambda_i \tau} \int_0^{\tau} e^{-\lambda \tau'} \Psi_{205}(\tau') d\tau' \tag{1.42}$$

If recombine the matrix A Eigenvectors into vector and multiply on the left by A, we have

$$\Psi_A = \sigma_{206} \sum_{i=1}^{4} A_{iA} \sigma_{206} e^{-\lambda_i \tau} \int_0^{\tau} e^{-\lambda \tau'} \Psi_{205}(\tau') d\tau' \tag{1.43}$$

Thus the Ψ_A have been obtained in terms of τ and of the eigenvalues and vectors of their cross-section matrix. The source function Ψ_{205} is as yet unspecified, except that it must vanish for large τ since infinite neutron fluxes destroy all of the $A = 205$ nuclei. This source function depends upon the seed nuclei for the s-process capture chain and upon all of the cross-sections between the starting point of the chain and $A = 205$, as explained by Clayton. But the integral of equation (1.43) is clearly finite for all values of τ and approaches an asymptotic value for very large τ. However, for $i > 1, e^{\lambda_i \tau}$ will drop to zero for large τ inasmuch as those eigenvalues have negative real parts. Thus the asymptotic value of the integral is given by the $\lambda_1 = 0$ term:

$$\Psi_A(\infty) = \sigma_{206} A_{1A} \int_0^{\infty} \Psi_{205}(\tau) d\tau \tag{1.44}$$

If the Ψ function are defined as the σN product per initial seed nucleus, then

$$\int_0^{\infty} \Psi_{205}(\tau) d\tau = 1 \tag{1.45}$$

and the eigenvector A_{1A} gives the equilibrium abundance of each isotope. The four components of A_1 are equal because the equilibrium σN products must clearly be equal. For each A the equilibrium value of Ψ_A will be designated by $\Psi_A(\infty) = \Psi_T$ as in Clayton.

To calculate $\Psi_A(\tau)$ explicitly from equation (1.43) it is necessary to make a specific choice for $\Psi_{205}(\tau)$. Because the neutron-capture cross-sections are energy-dependent, Ψ_{205} depends upon the temperature assumed for the s-process. However, Seeger showed that the shape of the Ψ curves is nearly the same for all temperatures, so that scale changes in τ are adequate to transform from one temperature to another. Clayton has explained that point in more detail. As a result we may use the 30-keV cross-sections for $A \leq 205$ with the proviso that the r-scale be changed if the s-

process temperature differs significantly from 30 keV. The function $\Psi_{205}(\tau)$ also depends on the choice of seed nuclei for the s-process. We follow authors earlier work and that in choosing the iron-abundance peak as the seed from which the s-nuclei were generated. Clayton in has reviewed the reasons for this choice. Having made those choices it is possible to write an exact expression for $\Psi_{205}(\tau)$. The exact expression for Ψ_{205} may be analytically integrated in equation (1.43) to give the exact solutions for Ψ_A. The resulting series has such severe round-off error, however, that it very difficult to evaluate even with the aid of the best computers. We therefore abandon the exact solution in favor of an approximate solution of adequate accuracy.

Clayton showed in work that the function

$$\Psi_{205}(\tau) = \frac{\mu}{\Gamma(m)}(\mu\tau)^{m-1}e^{-\mu\tau} \tag{1.46}$$

closely approximates the exact solution has been shown in his previous work. For the 30-keV cross-sections the values of those parameters are $\mu = 22.544$ millibarns and m = 35.397. The approximation has small percentage error except for small values of τ, where it is much greater than the exact. The use of equation (1.46) as a generator of the Pb abundances is therefore restricted to those values of r for which equation (1.46) is a good approximation. Roughly speaking, equation (1.46) will be adequate for values of τ greater than one-half of that value τ_{205} (max) for which (1.46) has a maximum; that is, for

$$\tau > \frac{1}{2}\tau_{205}(\max) = \frac{1}{2}\frac{m-1}{\mu} = 0.75 \tag{1.47}$$

Substitution of equation (1.46) into equation (1.43) yields

$$\Psi_A(\tau) = \sigma_{205}\sum_1^4 A_{iA}e^{-\lambda_i\tau}\int_0^\tau \frac{\mu}{\Gamma(m)}(\mu\tau')^{m-1}e^{-(\mu+\lambda_i)\tau'}d\tau' \tag{1.48}$$

The integrals are incomplete gamma functions with complex arguments and can be evaluated by standard numerical technique [41].

The results of the simulation that have been made by the authors are illustrated on the follow figure 8 and on figure 9.

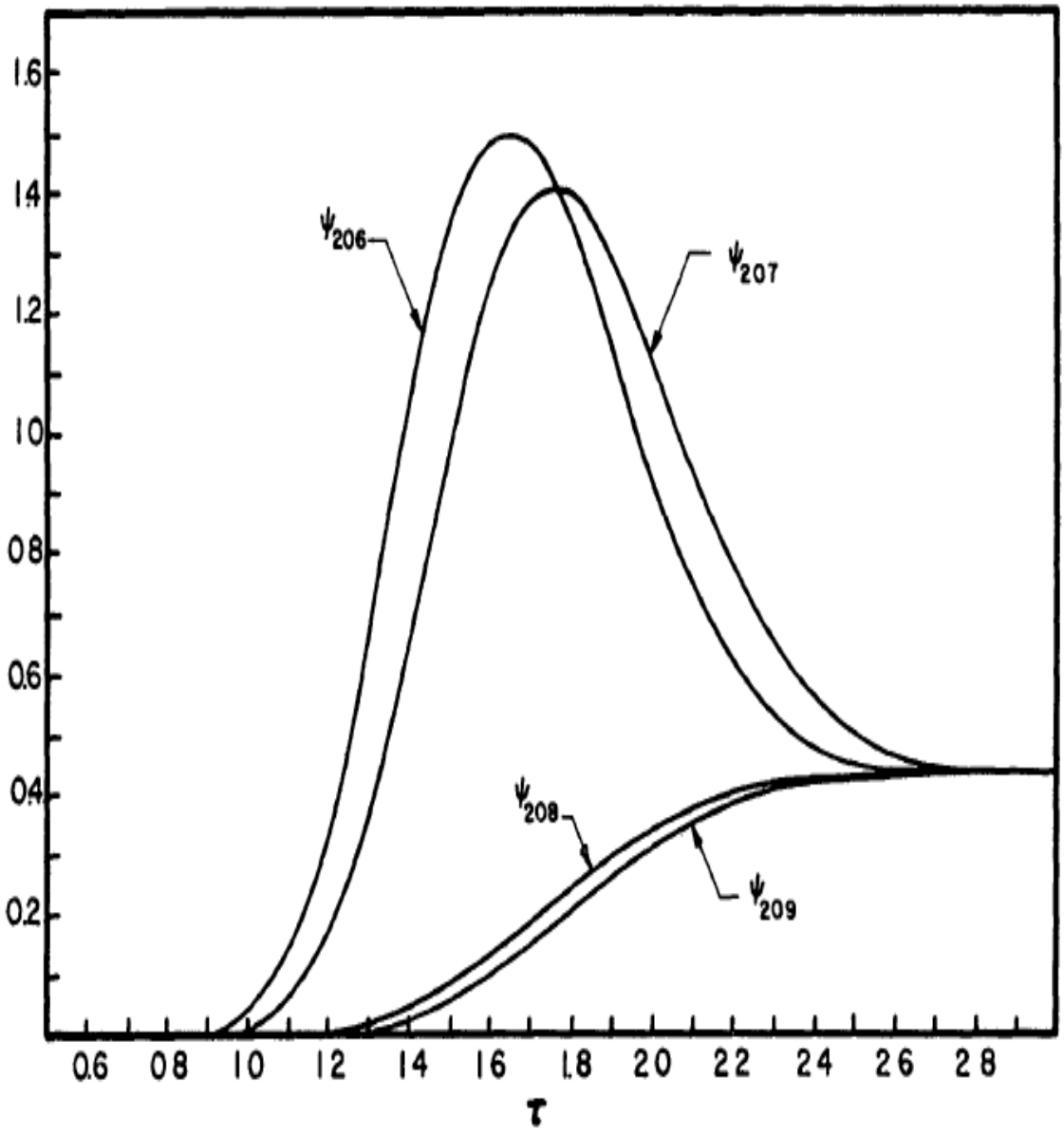

Figure 8 – The values of $\Psi_A = \sigma_A N_A$ in units of millibarn-atoms as a function of the parameter τ in units of 10^{15} neutrons cm^{-2} resulting from the irradiation of one Fe^{66} nucleus The cross-sections used are appropriate to kT = 30 keV; $\sigma_{204} = 9.6$, $\sigma_{207} = 8.7$, $\sigma_{208} = 0.5$ and $\sigma_{208} = 12.1$ in units of millibarns [41].

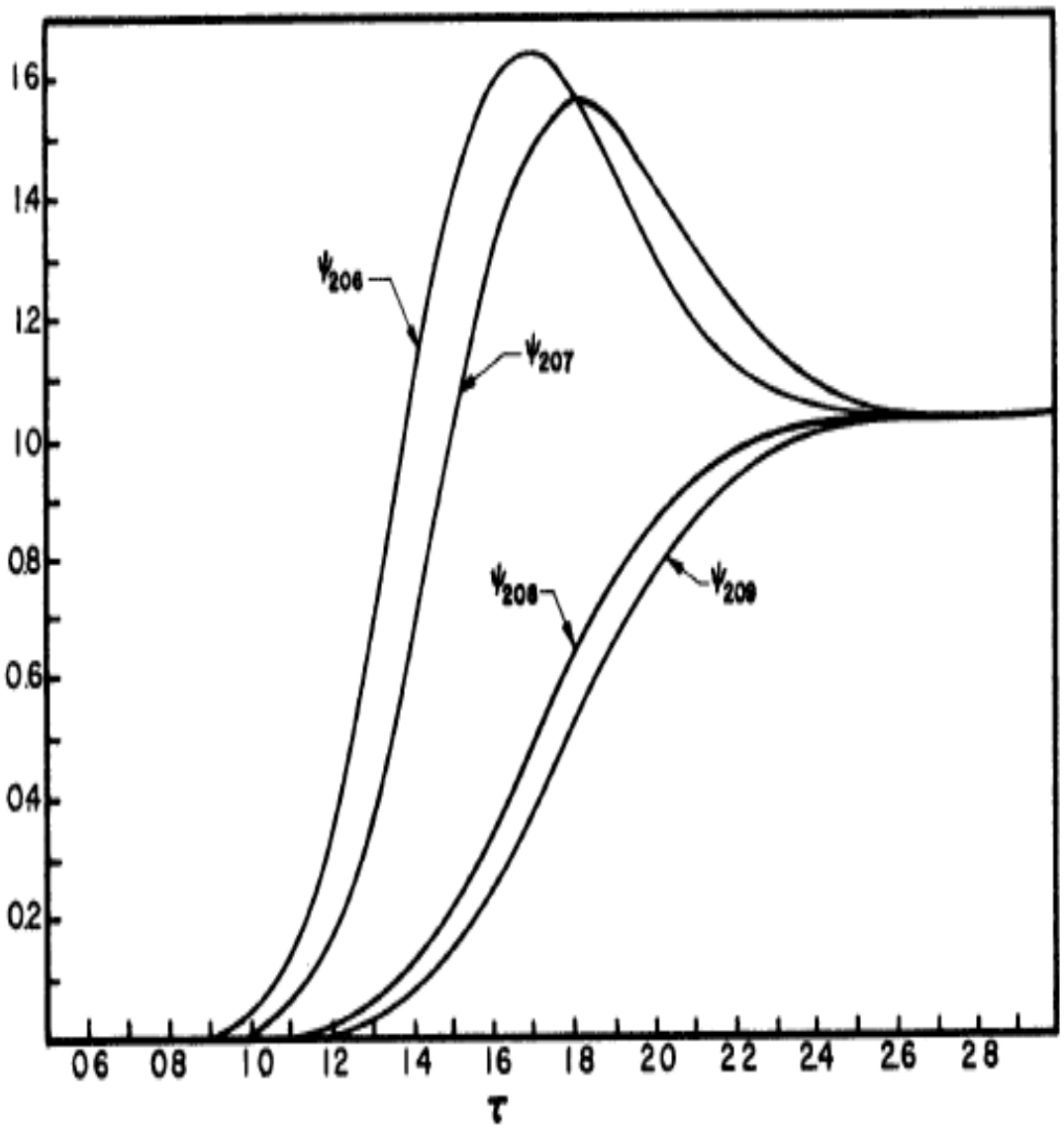

Figure 9 – This display of Ψ_A is identical to that of figure 8 except that the value of σ_{208} has been arbitrarily increased to 1.5mb for comparison [41].

Now having the results of [41] and having a complete picture of the calculation and analysis carried out in [41], we will carry out our own simulation using the IBUS(ISOTOPE BURNUP SOFTWARE) software package.

The difference between our calculations and those performed in [41] is that we do not approximate the Pb–209, Bi–210, and Po–210 isotopes by artificially closing a possible channel of neutron capture reactions. However, it is not possible to generate a burnup matrix for all isotopes from the nuclear database and perform calculations for a period of time of an astrophysical scale while maintaining the necessary accuracy of calculation from the point of view of calculation time. For this reason, we cannot use the automatic mode in the IBUS operation.

The most appropriate is to expand the range of considered isotopes artificially removed in [41], namely, to include the neutron capture reaction for beta and alpha

unstable isotopes Pb–209, Bi–210 and Po–210 and consider the accumulation of Bi–211, Po–211, Pb–210 and also of Po–210 itself, since it is considered in [41] that this isotope performs instant alpha decay. Our calculation results are presented in the figures below.

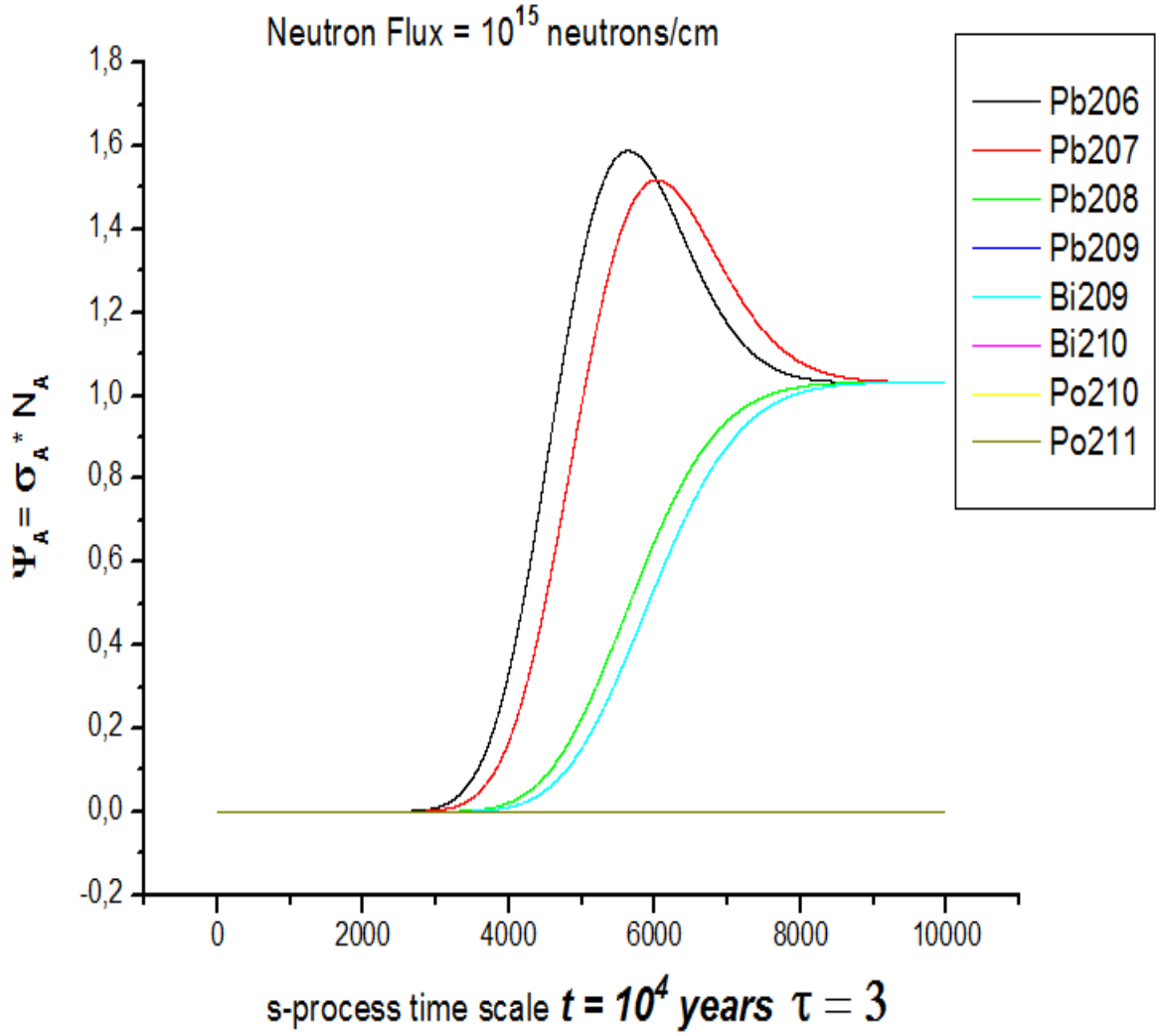

Figure 10 – «IBUS» simulation result. Dependence of Ψ_A on time(years) $\sigma_{208} = 1.5\text{mb}$.

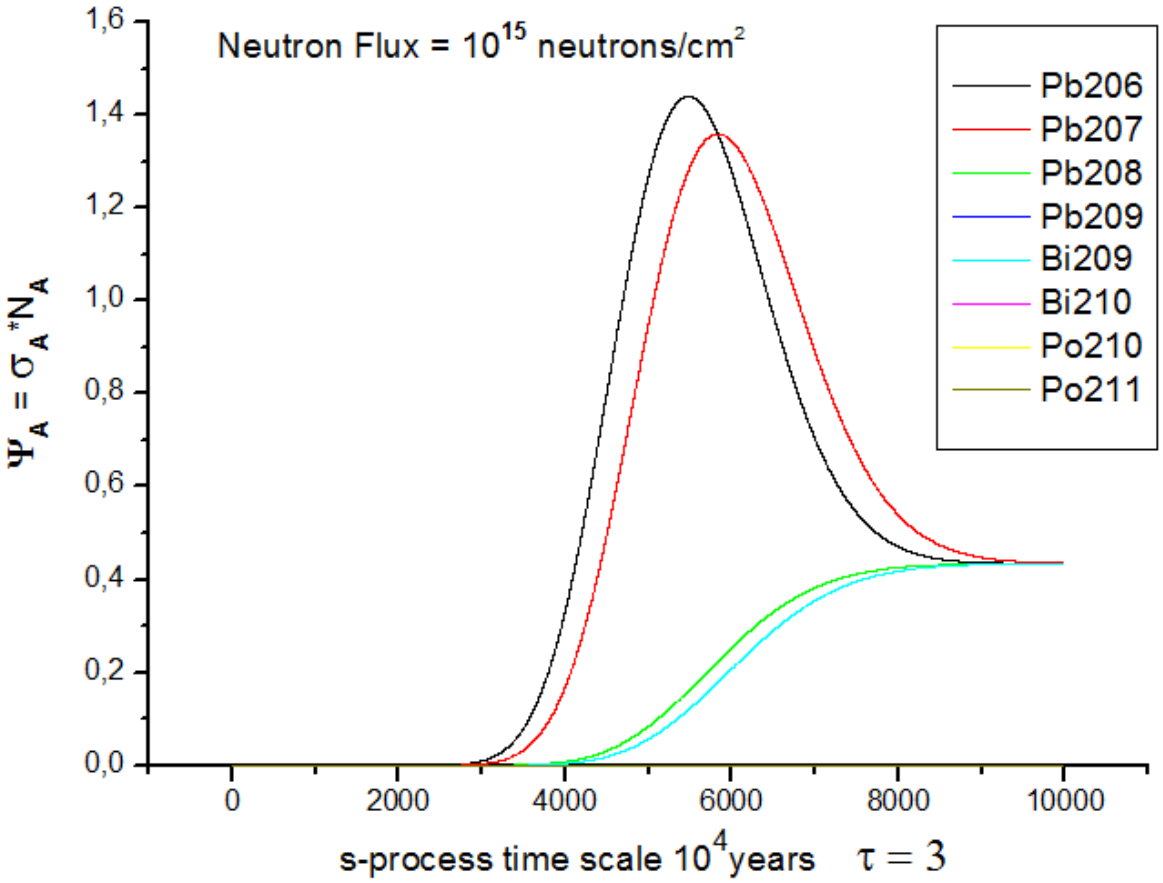

Figure 11 – «IBUS» simulation result. Dependence of Ψ_A on time(years) $\sigma_{204} = 9.6$, $\sigma_{207} = 8.7$, $\sigma_{208} = 0.5$ and $\sigma_{208} = 12.1$ in units of millibarns.

The results obtained by the IBUS software package [43,46] which is shown in figure 10 and figure 11 coincide with the results of work [41,42], with the exception that in our case a slight accumulation of the Po-210 isotope is observed. This circumstance is explained by the fact that in the work it was believed that the Po-210 isotope performs instant alpha decay. This circumstance is explained by the fact that in the work it was believed that the Po-210 isotope performs instant alpha decay. However, its half-life is 138 (days).

1.6 Numerical calculation of the intensity of cyclic reactions.

In the literature, an X-ray pulsar means a neutron star. However, this neutron star is not ordinary but has a strong magnetic field and rotates very quickly. It is not easy to detect such a neutron star if it is single. However, the so-called binary system is often found paired with an ordinary star. In such binary systems, a neutron star draws gas from its component onto itself. This process in astrophysics is known as accretion. In the process of accretion, the trapped gas acquires a high speed and begins to rotate around a neutron star, while the gas begins to compress and warm up. A so-called accretion disk is formed. Due to the fact that a neutron star has a sufficiently strong magnetic field, the gas penetrates a little into the magnetosphere of

a neutron star and slows down. However, the matter from the accretion disk is quite strongly ionized, therefore it cannot radially fall onto the surface of a neutron star, instead, it flows along magnetic lines to the poles of the neutron star, thereby forming an accretion flow of matter, which is shown in Figure 12. The substance is very hot and emits X-rays when incident on the magnetic poles of a neutron star and look like repeating signals with a period from thousandths of a second to several minutes[145,146,147,148].

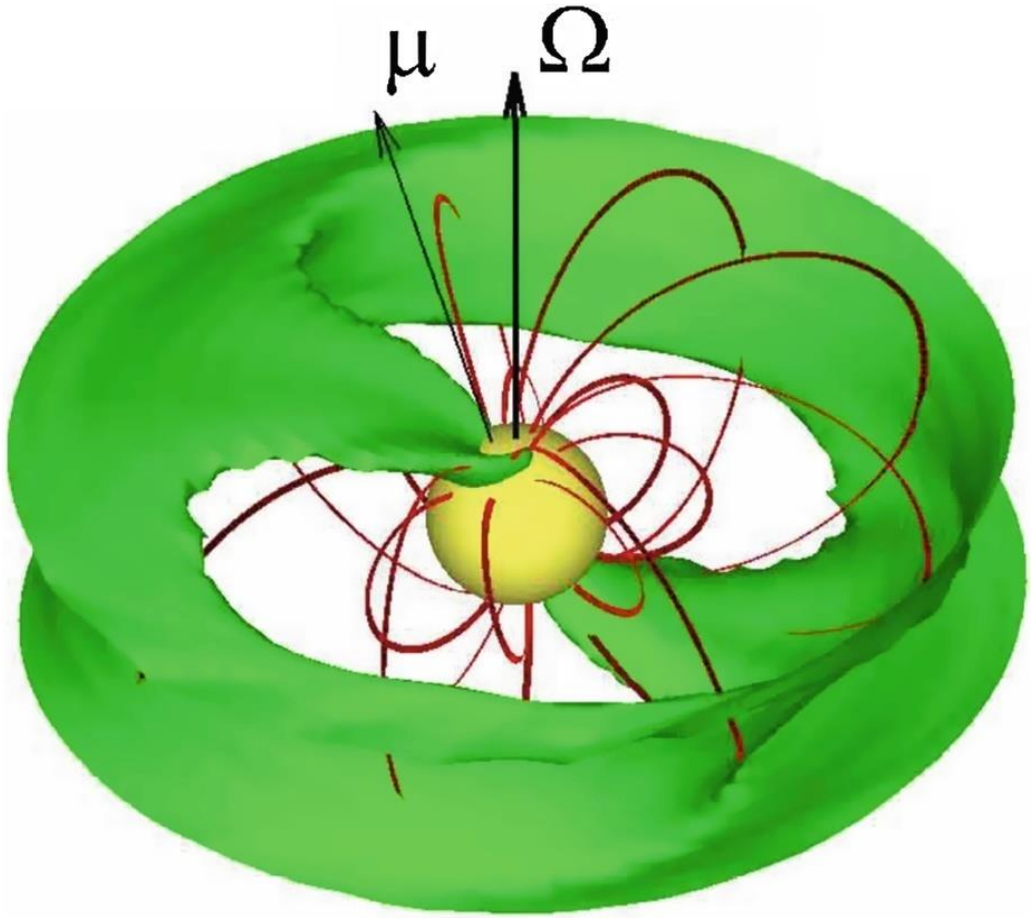

Figure 12 – the Accretion disk and the accretion flux that flows to the poles of a neutron star [143].

An accretion stream contributes significantly to the development of a neutron star. The substance from the accretion disk falls on the surface of a neutron star and spreads uniformly over it. The newly income substance from accretion disk, increasing gravitational pressure, contributes to the compression of matter in the crust, pushing it into a star. In this case, the accretion process turns the crust of neutron star from the equilibrium state, as a result the crust of the neutron star becomes non-equilibrium. The nuclear composition of deviated from equilibrium crust is very different from equilibrium crust of the neutron stars [39,144]. This is primarily due to the presence of a significant amount of free neutrons in the crust of the neutron star. These free neutrons can diffuse under the influence of the concentration gradient and gravity [40]. The neutron concentration gradient can

change sign in the nonequilibrium crust, and, in particular, at the outer boundary it is always directed outward (or equal to zero), since there are no free neutrons outside. whereas, the force of gravity acting on free neutrons is always directed inside the star.

It should also be noted that free neutrons can occur in the inner layers of the outer crust of a neutron star. In superdense crystalline structures of the outer crust of neutron stars, nonlinear interactions exist. This nonlinear interaction is associated with an extremely small lattice parameter which is much smaller than the size of electronic atomic orbits. Such crystals stimulate the formation of excited states of nuclei in electron capture reactions and support their long-term existence. It was shown that an increase in the density of the number of such nuclei and their nonlinear interactions lead to the generation of high modes and induced radiation in the crystal, which, in turn, can cause reactions with generation free neutrons from the nuclei [142]. These knocked-out neutrons become free and, due to the presence of a concentration gradient, can be transferred to the upper layers of the outer crust of a neutron star, thereby forming a free neutron flux [140].

When a substance in a binary system flows from an ordinary star to a neutron star, we are able to detect an X-ray pulsar. The component of a neutron star can be a giant or a supergiant, while the stellar wind of these stars that throws matter into space must be strong enough for the neutron star to be observable. Also in some cases, the component may be a small star, similar to the Sun, which filled its share of Roche. Recall that the Roche lobe is the region beyond which matter is no longer held by the gravity of these stars and is attracted by the gravity of a neutron star (see figure -13) [149].

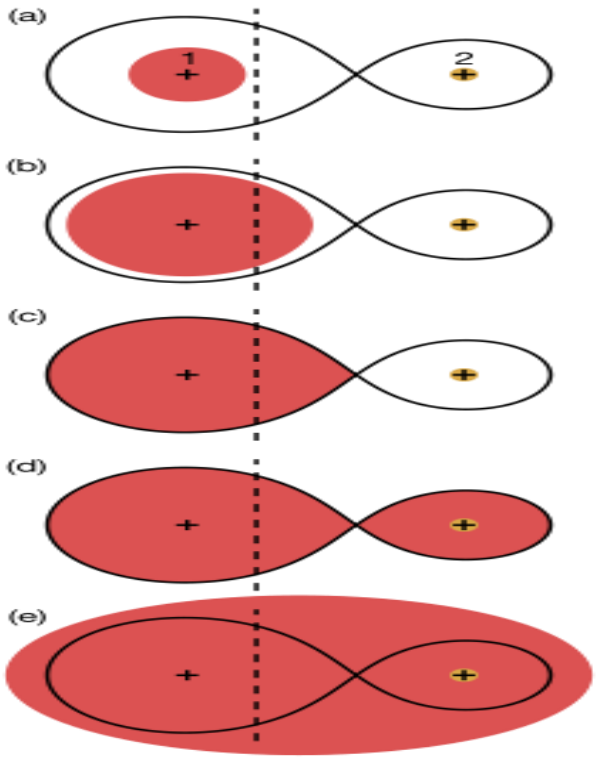

Figure 13 – Stages in the life of a binary system as a common envelope is formed. The black line is the Roche equipotential surface.

About half of the stable nuclei heavier than iron are believed to be synthesized during the late stages of evolution of stars with masses in the range 0.8±8 solar masses. These elements are then expelled into the interstellar medium by the stellar winds from the surface of the stars. These occurs when the star is in the "asymptotic giant branch" (AGB) phase of its life. Nuclei (mainly iron) deep inside the star slowly capture neutrons and progressively build up heavier elements (the "s-process"). The s-process accumulates synthesized material with atomic weight in Pb-Bi. region. Therefore, such stars will have large excesses of lead compared to other heavy elements.

The discovery of a large amount of lead with a low metal content in three stars (HD187861, HD196944, and HD224959) was reported in [141]. Their analysis showed that these stars are highly enriched in lead than any other element heavier than iron.

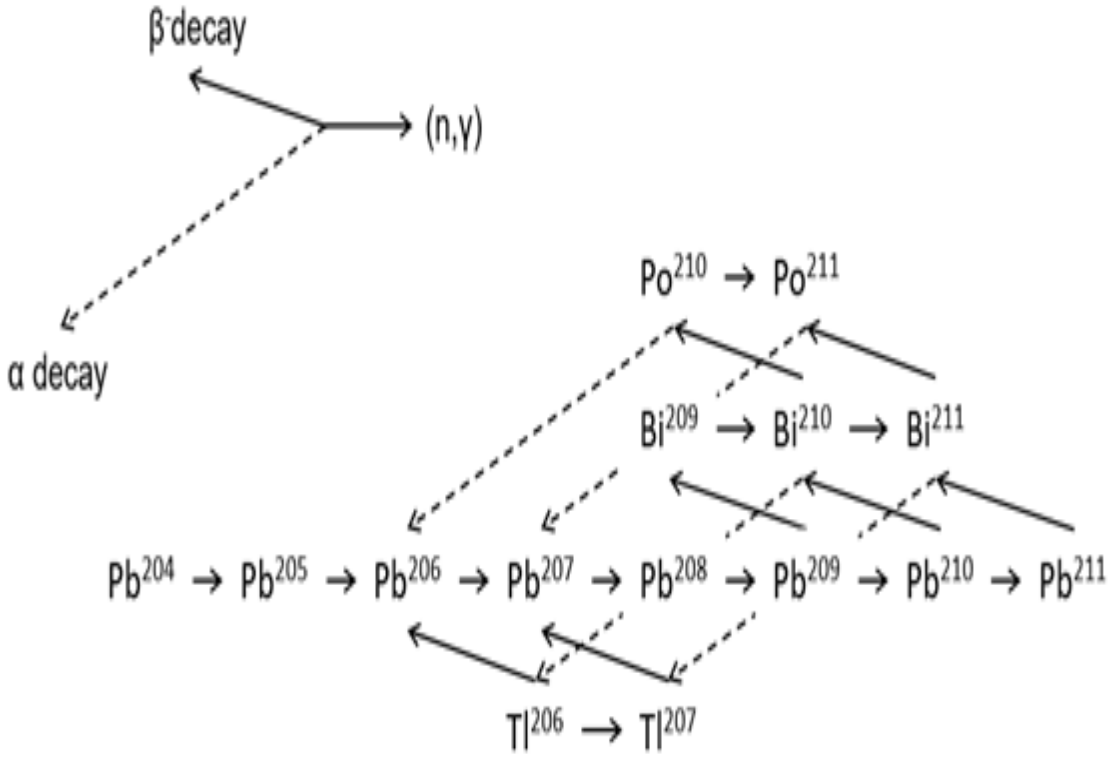

Figure 14 – An extended scheme of a cyclic nuclear reaction.

Thus, the synthesized lead inside the star's AGB during the expansion of the star fills the Roche lobe and by accretion is pulled by the gravity of the neutron star to its surface. A stream of compressed lead falling onto the surface of a neutron star takes its outer crust out of balance, thereby causing various processes that lead to the appearance of a significant amount of free neutrons on its surface, such as a star quake, neutron diffusion, etc. The isotopes of lead from the accretion due to the interaction with the free neutron flux triggers the cyclic nuclear reaction Pb-Bi.

To calculate the number of emitted gamma quanta in such a scenario, we considered all isotopes forming subcycles near the main Pb-Bi cycle [44]. See figure 14.

As can be seen from figure 14 along the lead isotopes between Pb-206 and Pb-211 as a result of interaction with neutrons, four cyclic reactions can occur, some of which at relatively small ($10^{10} - 10^{18}$ neutron/cm^2) is not realized since the beta and alpha decay times of unstable isotopes are much shorter than the average neutron absorption time.

However, in our calculations, we did not make a detailed analysis for each branch with the aim of simplifying and artificially stopping the formation of new isotopes. Instead, in the calculations carried out using the «IBUS» software package, we took into account each reaction channel and, through direct calculations, found out the possibility of the formation of one or another reaction channel for a specific neutron flux.

The calculation results showed that in the limit ($10^{13} - 10^{18}$ neutron/cm^2) of the neutron flux, only the first three cyclic reactions of the possible four shown in figure 15 are realized.

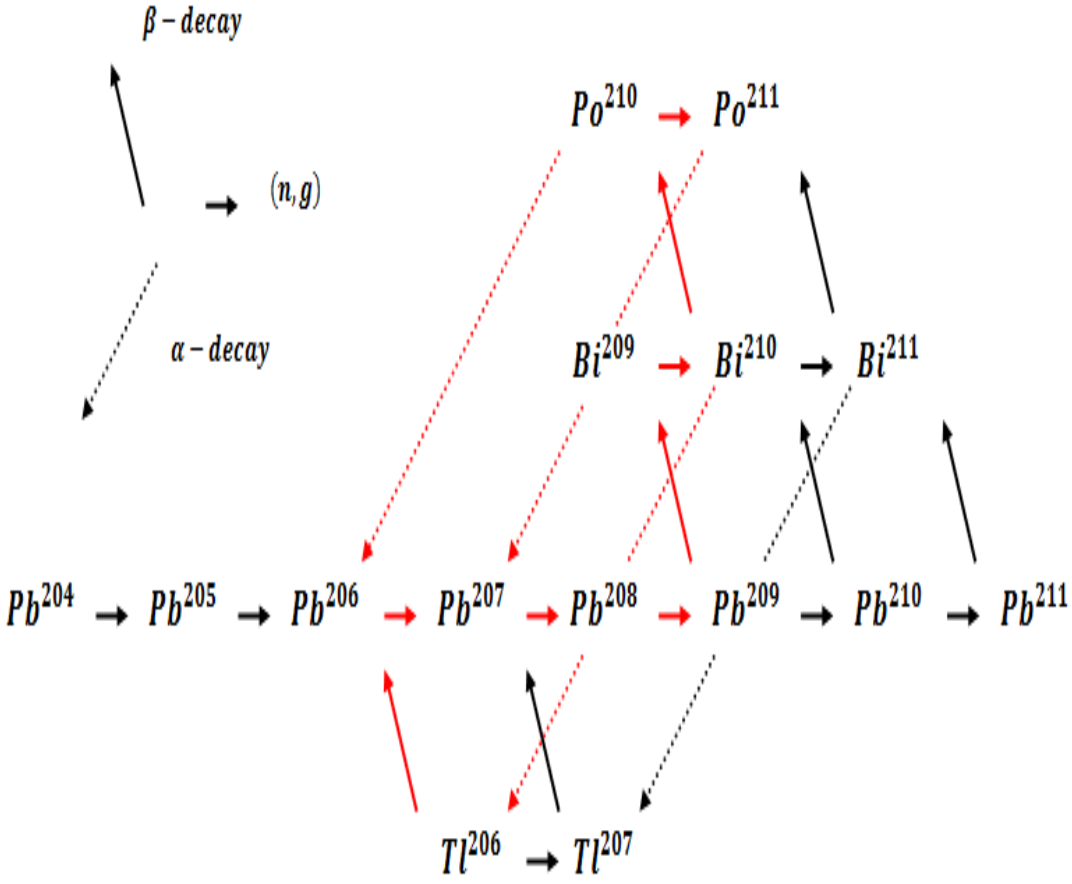

Figure 15 – three cyclic reactions of the possible four.

In modeling, we consider that the property of matter on the surface of a neutron star coincides with properties in terrestrial or laboratory conditions (that is, it is not superdense). We also consider that the initial isotopic composition of accreted lead is similar to the percentage of isotopes of natural lead [44].

The below figure 16 shows the result of the emission of the number of gamma quanta of (n,g) reaction by each isotope of cyclic Pb-Bi reactions resulting from accreted lead which is irradiated with neutrons ($10^{13} - 10^{18}$ neutron/cm^2) [45] .

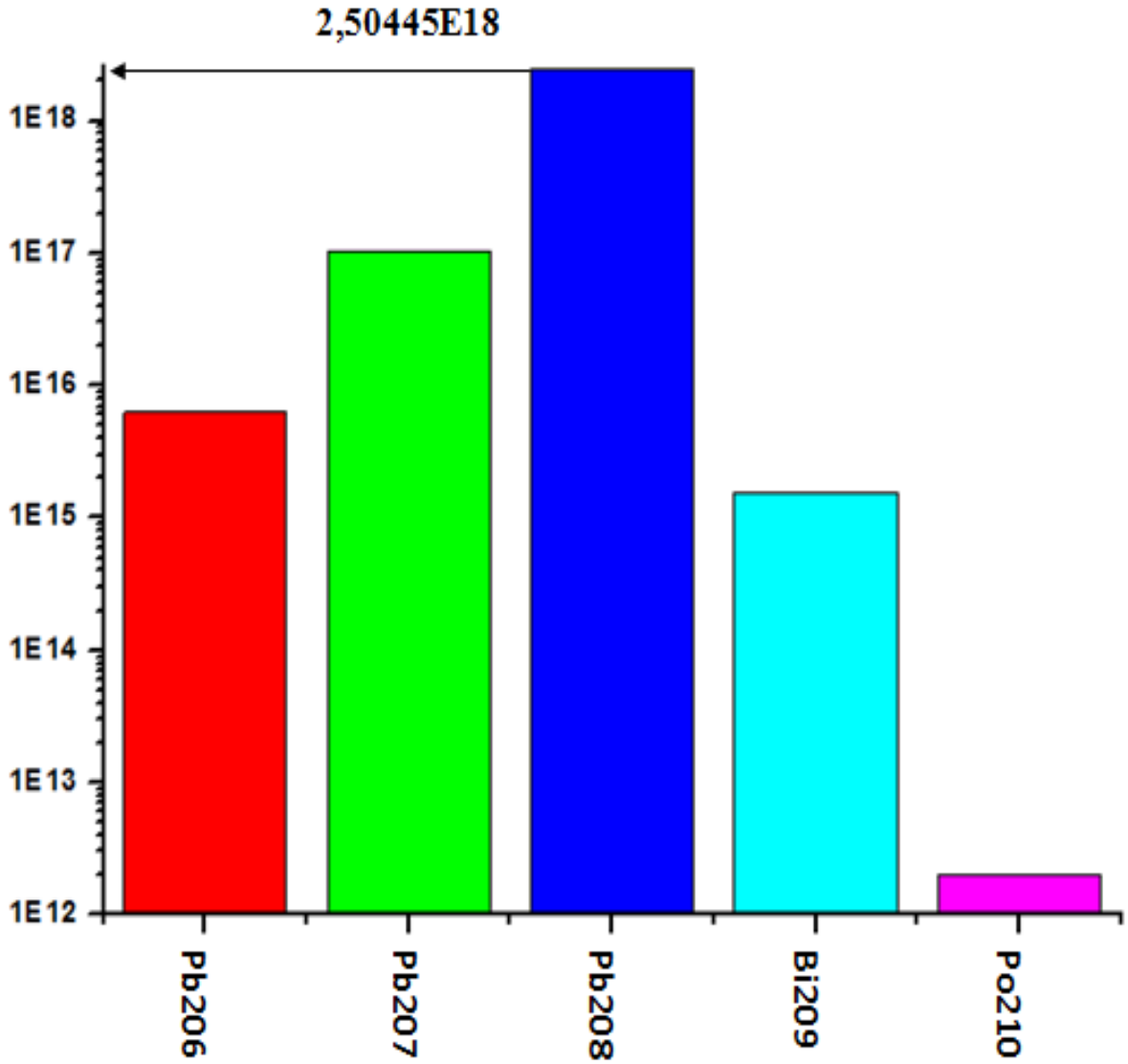

Figure 16 – The intensity of gamma rays of (n,g) reaction at the equilibrium stage for neutron flux 10^{15} neutron/cm^2.

Due to the difficulties associated with determining the exact concentration of neutrons in an accreted substance on the surface of NS, we calculated the amounts of gamma quanta emitted by the cyclic Pb-Bi reaction as a function of the neutron flux. The result of which is shown in figure 17.

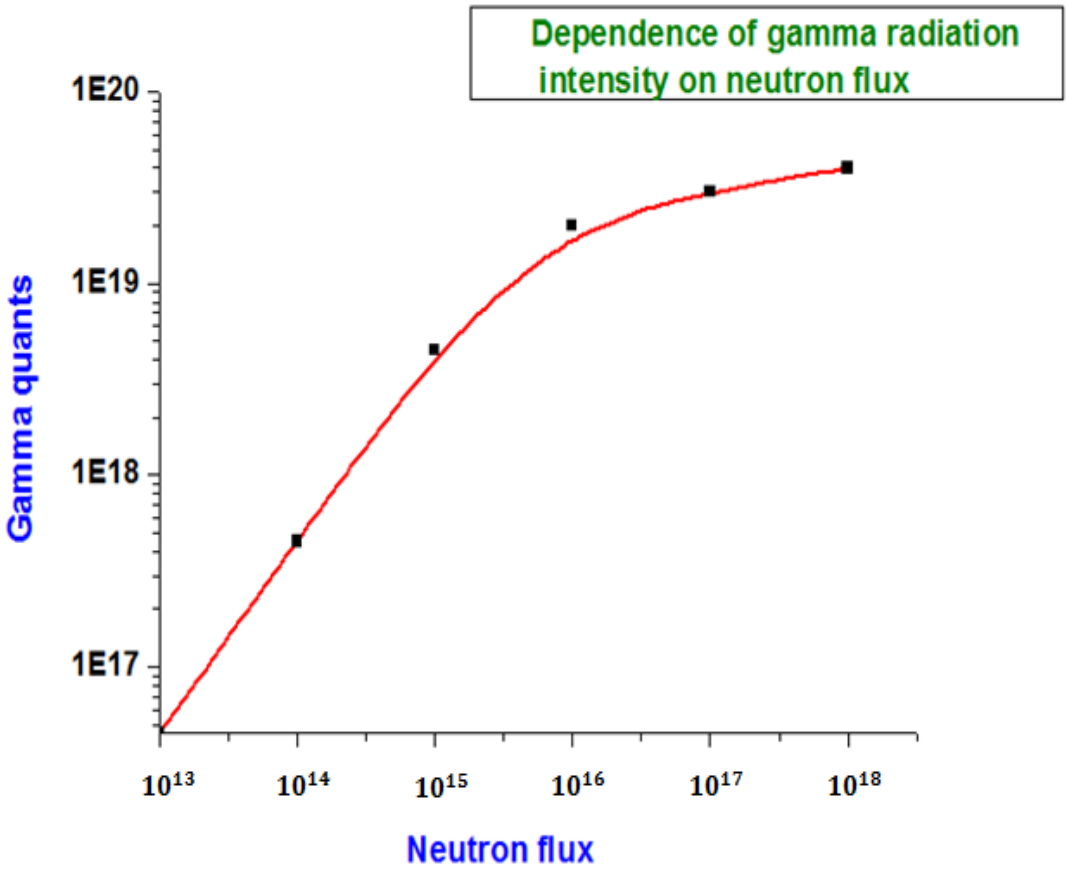

Figure 17 – The intensity of gamma rays released by Pb-Bi cycle depending on neutron flux.

The results of the work show that with an increase in the neutron flux up to 10^{18} the number of gamma quanta cycles reaches its upper value and a further increase in the neutron flux does not lead to an increase in gamma quanta [45].

2 THE PROPAGATION OF GAMMA RADIATION IN THE MAGNETOSPHERE OF NEUTRON STARS

2.1 On measurements of the polarization of gamma radiation of astrophysical objects.

Although about several hundred pulsars were detected in hard X-ray and gamma radiation, and their temporal and spectral parameters were considered with enough good accuracy, there is not complete data on the polarization properties of these astrophysical objects. Very few space experiments have been performed to study polarizations in hard radiation. Very few space experiments have been performed to study polarizations in hard radiation. Mostly, solar flares were observed, such as polarization measurements on the InterCosmos [105] and Coronas-F [106] and RHESSI satellites, a space observatory that makes it possible in principle to polarize the detection of solar flare gamma rays and cosmic gamma-ray bursts[107].

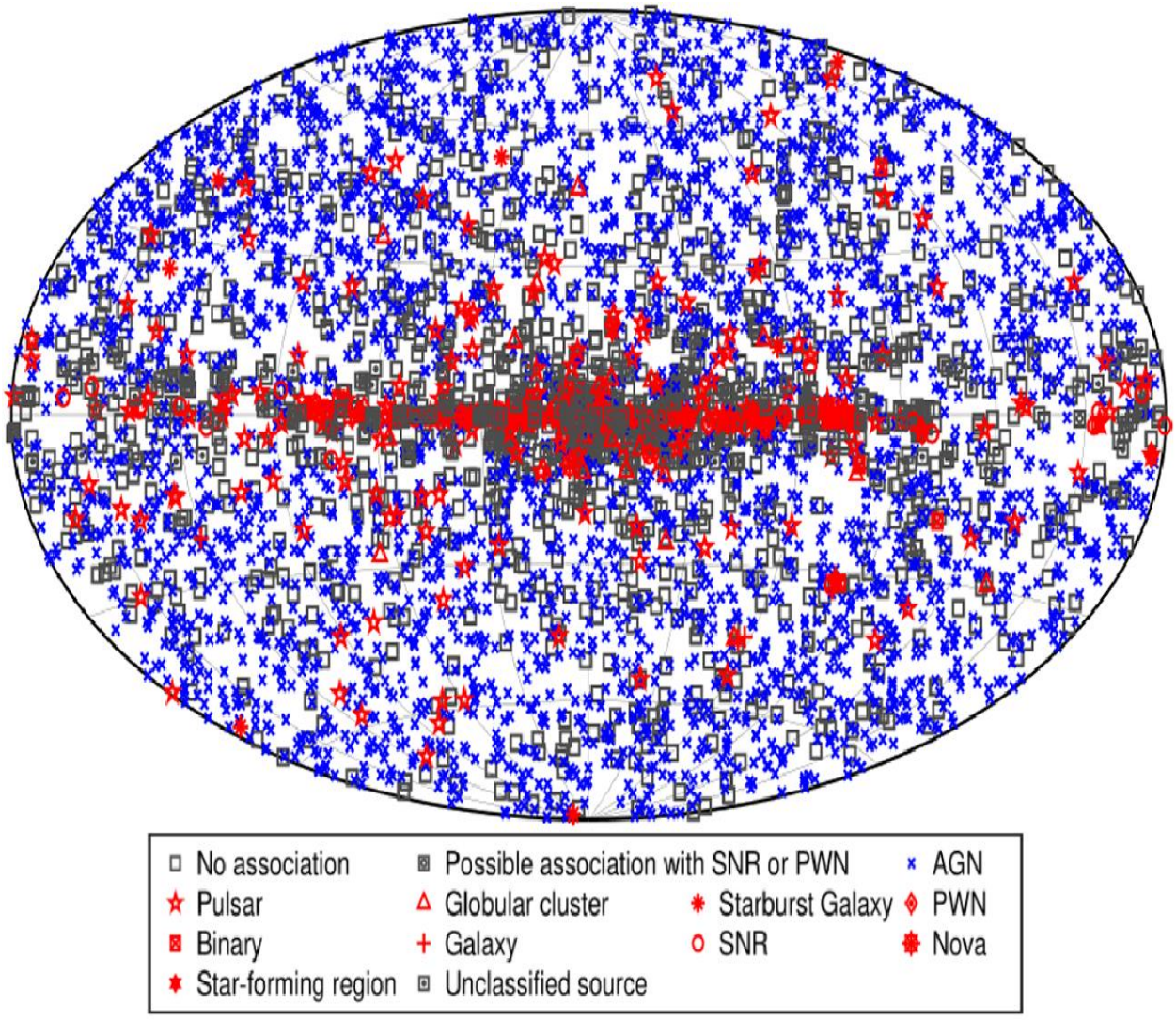

Figure 18 – Distribution in the sky of all point sources discovered by the 2018 LAT[107].

Polarimetry can diagnose specific phenomena in cosmic sources in the ranges of radio waves and optical energies, though very paucity results are accessible for high energy photons. To date, the only essential observation in the X-ray energy range is the measurement of the linear fraction of polarization P = 19 + 1% of the radiation of the Crab nebula with an energy of 2.6 keV using the Bragg polarimeter on board the OSO-8. At higher energies, telescopes with hard X-ray and soft gamma radiation that flew into space in the past (for example, COMPTEL CGRO,) not suitable for measuring polarimetry, since they do not have sufficient sensitivity to polarization. However, with the active mission of INTEGRAL IBIS and SPI, some improvement was achieved. The measurements of P = 28 + 6% (from 130 to 440 keV) and P = 47 + 19-13% (from 200 to 800 keV) were achieved for the Crab Nebula [86].

A number of Compton telescope polarimeter designs have been developed, with a variety of recording technologies such as such as scintillator arrays POGO, GRAPE, POLAR, Si or Ge microstrip detectors MEGA, ASTROGAM or combinations of those (Si + $LaBr_3$ for GRIPS, Si + CsI(Tl) for TIGRE, semiconductor pixel detectors CIPHER, liquid xenon LXeGRIT and gas mixture CF4 at 3 atm) time projection chambers (TPC)[86].

It is assumed that the hard radiation of astrophysical sources contains highly magnetized neutron stars, which should be more or less polarized. This can be caused by the geometry of the emitting regions, i.e., by the accretion disk (in the case of a neutron star in a binary system) or by the configuration of the magnetic field and also by the high anisotropy of the primary electron beams. Another reason is related to the influence of certain physical conditions in the magnetosphere of a neutron star on x-ray and gamma radiation.

Effects where polarization of gamma radiation is observed can also occur in other physical processes. In particular, this is due to the influence of sufficiently strong electromagnetic fields on gamma radiation. The supreme value is so called Schwinger field $B_q = m^2c^3/(e\hbar) = 4.41 \cdot 10^{13} G$, which the non-linear electrodynamic effects in vacuum is important. However, in terrestrial conditions, we encounter difficulties associated with the inability to obtain such strong magnetic fields for testing by nonlinear electrodynamics. But in space such fields are not so rare.

Most gamma-ray pulsars, according to theoretical calculations, have magnetic fields comparable with the Bq value, but for magnetars it will be even higher and reach about 10^{15} G. Thus, in the most suitable astrophysical objects, which has favorable conditions for nonlinear electrodynamic effects, are magnetars. According to theoretical calculations, such effects as birefringence in vacuum can be observed in its vicinity [62, 82, 108].This effect may have different manifestations. One is the dramatically increases the linear polarization of the thermal radiation of the isolated neutron stars [109], from a level of a few per cent up to even 100 per cent, depending on the viewing geometry and the surface emission mechanism. Currently, this vacuum non-linear electrodynamics prediction can be tested by measurement of a polarization degree of isolated neutron star thermal emission. First observations [110] of optical polarization from a thermally emitting isolated neutron star RX

J1856.5-3754 shown that a linear polarization degree of this star thermal emission is 16.43+5.26 per cent.

It is arguing in [110] that, independently on how thermal photons are produced, such a high value of linear polarization in the signal is extremely unlikely to be reproduced by models in which QED vacuum polarization effects are not accounted for[86].

In the next three paragraphes we will show how to take in account quantum electrodynamics effect for vacuum polarization.

2.2 Nonlinear vacuum electrodynamics.

It is well known that Maxwell's electrodynamics in vacuum is a linear theory and it's predictions on a wide range of issues that do not affect the subatomic level are constantly confirmed with increasing accuracy[49]. It is known that one of the most reliable physical theories capable of describing various processes occurring in atoms is quantum electrodynamics. Quantum electrodynamics, in turn, is based on Maxwell's electrodynamics

However, some of fundamental physical considerations indicate that it is only the first approximation of the more general nonlinear theory of electrodynamics of vacuum.

At present, there are two nonlinear generalizations of Maxwell's equations and both of them are best known in the scientific literature. One of them was proposed by Born and Infeld [50]. The Born-Infeld's nonlinear electrodynamics is based on a classical theory and uses Lagrangian:

$$L = -\frac{1}{4\pi a^2}[\sqrt{1+a^2(\mathbf{B}^2-\mathbf{E}^2)-\mathrm{a}^4(\mathbf{B}\mathbf{E})^2}-1] \qquad (2.1)$$

Where a- is a constant, which has a dimension inverse to the dimensions of the magnetic field induction.

Born and Infeld determined this constant by the supposing that the rest energy of electron $\mathcal{E}_0$ has electromagnetic origin. From this supposing the value of the constant is $1/a = 9.8\,10^{15}$G. However, from the standpoint of modern theoretical physics, it is quite obvious that it is impossible to represent all the interactions of nature as a single nonlinear electromagnetic interaction.

The main part of the electron's rest energy is the energy of the spinor field, so the energy $\mathcal{E}_e$ of its electric field, at least, does not exceed half of the rest energy: $\mathcal{E}_e \leq \mathcal{E}_0/2$. It follows that $1/a < 2\cdot 10^{15}$G. We will use this assessment further.

Thus, although the Born- Infeld's theory has a determined Lagrangian, largely it is phenomenological. Therefore, it needs a measurement the value of the parameter a in the experiment or at least estimate its limit from the above[75].

In nonlinear electrodynamics of Born-Infeld the vectors **D** and **H** are the functions of following vectors **B** and **E**:

$$\mathbf{D} = \frac{\mathbf{E} + \alpha^2(\mathbf{BE})\mathbf{B}}{\sqrt{1+\alpha^2(\mathbf{B}^2-\mathbf{E}^2)-\alpha^4(\mathbf{BE})^2}}$$
$$\mathbf{H} = \frac{\mathbf{B} - \alpha^2(\mathbf{BE})\mathbf{E}}{\sqrt{1+\alpha^2(\mathbf{B}^2-\mathbf{E}^2)-\alpha^4(\mathbf{BE})^2}} \quad (2.2)$$

It should be especially emphasized that at present there is no any experiment that would reject this theory.

In laboratory conditions, the values $a^2\boldsymbol{E^2}$ and $a^2\boldsymbol{B^2}$ are significantly less than one. In this case, the Lagrangian (2.1) can be expanded in small parameters $a^2\boldsymbol{E^2} \ll \mathbf{1}$ and $a^2\boldsymbol{B^2} \ll 1$.

$$L = -\frac{1}{8\pi}(\mathbf{B}^2 - \mathbf{E}^2) + \frac{a^2}{32\pi}[(\mathbf{B}^2 - \mathbf{E}^2)^2 + 4(\mathbf{BE})^2] \quad (2.3)$$

The first part of this expansion is the Lagrangian of Maxwell electrodynamics, and the rest of expression is a correction according to the indicated small parameters.

From the effect of polarization of electron-positron vacuum by electromagnetic fields follows another non-linear generalization of vacuum electrodynamics. According to quantum electrodynamics [51], Maxwell's linear electrodynamics is only the first approximation of more general nonlinear electrodynamics (in vacuum),which is applicable in the case when the magnitude of the electromagnetic fields B and significantly less than the characteristic E is quantum-electrodynamics' value[76].

$$B_q = m^2c^3 / e\hbar = 4.41 \cdot 10^{13} B_q = m^2c^2 \quad (2.4)$$

where m is the electron mass, e is its charge modulus, $\hbar$ is the Planck constant.

In this theory, the exact form of the Lagrangian is not yet determined; however, for “small” electromagnetic fields, the corrections to Maxwell Lagrangian in the first order of the perturbation theory of quantum electrodynamics have a strictly defined form. As [52–56] calculations show, for weak electromagnetic fields $B \ll B_q, E \ll B_q$ the first two terms of the expansion in small parameters of a nonlinear Lagrangian which describes electromagnetic field in vacuum $(\boldsymbol{B^2} - \boldsymbol{E^2})/B_q^2$ and $(\boldsymbol{BE})/B_q^2$, should have the form:

$$L = -\frac{1}{8\pi}(\mathbf{B}^2 - \mathbf{E}^2) + \frac{\alpha^2}{360\pi^2 B_q^2}[(\mathbf{B}^2 - \mathbf{E}^2)^2 + 7(\mathbf{BE})^2] \quad (2.5)$$

where $\alpha = e^2/\hbar c \approx 1/137 -$ is the fine structure constant.

Comparing expressions (2.3) and (2.5), it is easy to notice that even in the approximation of the "weak" electromagnetic field these theories are different, since there is no choice to reduce these expressions to one another by the choice of constant.

If we consider only those theoretical models in which the equations of electromagnetic fields must be obtained from the general covariant Lagrangian, then the equations of the electromagnetic field in nonlinear vacuum electrodynamics are similar to the equations of macroscopic electrodynamics:

$$\begin{aligned} \text{rot}\,\mathbf{H} &= \frac{1}{c}\frac{\partial \mathrm{D}}{\partial t} + \frac{4\pi}{c}\mathrm{j}\,, \quad \text{div}\,\mathbf{D} = \mathbf{4}\pi\rho \\ \text{rot}\,\mathbf{E} &= -\frac{1}{c}\frac{\partial \mathrm{B}}{\partial \mathrm{t}}\,, \quad \text{div}\,\mathbf{B} = 0 \end{aligned} \tag{2.6}$$

However, the form of the equations $\boldsymbol{D} = \boldsymbol{D}(\boldsymbol{B}, \boldsymbol{E})$ and $\boldsymbol{H} = \boldsymbol{H}(\boldsymbol{B}, \boldsymbol{E})$ in different Lagrangian models is different and is entirely determined by the specific type of Lagrangian $L = L(\boldsymbol{B}, \boldsymbol{E})$:

$$\mathbf{D} = 4\pi\frac{\partial \mathrm{L}}{\partial \mathbf{E}} \qquad \mathbf{H} = -4\pi\frac{\partial \mathrm{L}}{\partial \mathbf{B}} \tag{2.7}$$

Other field models of nonlinear vacuum electrodynamics are also considered in field theory. It is quite obvious that in other theoretical models of nonlinear electrodynamics, the coefficients at the terms $(\boldsymbol{B}^2 - \boldsymbol{E}^2)^2$ and $(\boldsymbol{BE})$ in the expansion of the Lagrangian can be completely arbitrary.

Therefore, to choose nonlinear electrodynamics that is most adequate to nature, it is necessary to calculate nonlinear effects in various theories and compare their predictions with the results of the corresponding experiments.

To simplify the calculations in the weak electromagnetic field approximation, we will use the parameterized post-Maxwell formalism developed in [57-59], which is very similar to the parameterized post-Newtonian formalism widely used in the theory of gravity [60].

According to the post-Maxwell formalism, the generalized Lagrangian of nonlinear vacuum electrodynamics in the case of weak fields can be written [59, 61-63] in a parameterized form:

$$\begin{aligned} L = -\frac{\sqrt{-g}}{32\pi}\{2J_2 + \xi[(\eta_1 - 2\eta_2)J_2^2 + 4\eta_2 J_4] + \xi^2[4(\eta_1\eta_2 - 2\eta_2^2 - \eta_4)J_2 J_4 + \\ + \frac{1}{3}(6\eta_4 - 6\eta_1\eta_2 + 12\eta_2^2 + \eta_1^2 - \eta_3)J_2^3 + O(\xi^3 J_4^2)]\} \end{aligned} \tag{2.8}$$

where $J_2 = F_{ik}F^{ki}$ $J_4 = F_{ik}F^{km}F_{ml}F^{li}$ - are invariants of the electromagnetic field tensor, $g -$ determinant of the metric tensor g_{ik}, $\xi = 1/B_q^2$, and the value of the dimensionless post-Maxwell parameters $\eta_1, \eta_2, \eta_3, \eta_4$ depends on the choice of model of nonlinear electrodynamics of vacuum[75].

In particular, in non-linear electrodynamics of Heisenberg-Euler [64], which is a consequence of quantum electrodynamics, the parameters η_1, η_2, η_3 and η_4 have specific values

$$\eta_1 = \frac{a}{45\pi} = -5.1\cdot 10^{-5}, \eta_2 = \frac{7a}{180\pi} = 9.0\cdot 10^{-5}$$

$$\eta_3 = \frac{2\alpha}{105\pi} + \frac{\alpha^2}{2025\pi^2} = -4.4\cdot 10^{-5} \quad , \quad \eta_4 = -\frac{13\,\alpha}{1260\pi} - \frac{7\alpha^2}{3240\pi^2} = -2.3\cdot 10^{-5} \tag{2.9}$$

while in the Born-Infeld's theory[50] they are expressed in terms of the same unknown constant $a^2 : \eta_1 = \eta_2 = a^2 B_q^2/4,\ \eta_3 = \eta_4 = -a^4 B_q^4/8.$

With this approach, each nonlinear electrodynamics will correspond to a well-defined set of post-Maxwell parameters η_1 and η_2. From the point of view of experiments performed in a weak electromagnetic field, one nonlinear electrodynamics will differ from another only by the values of these parameters.

Substituting expressions (2.8) into expression (2.7), we find the vectors **D** and **H** of the parameterized nonlinear vacuum electrodynamics:

$$\begin{aligned}\mathbf{D} = \mathbf{E} + 2\xi\{&\eta_1(\mathbf{E}^2 - \mathbf{B}^2)\mathbf{E} + 2\eta_2(\mathbf{B}\mathbf{E})\mathbf{B}\} + \\ &+2\xi^2\{(6\eta_4 - 6\eta_1\eta_2 + 12\eta_2^2 + \eta_1^2 - \eta_3)(\mathbf{E}^2 - \mathbf{B}^2)\mathbf{E} + \\ &+(\eta_1\eta_2 - 2\eta_2^2 - \eta_4)[6(\mathbf{E}^2 - \mathbf{B}^2)^2\mathbf{E} + 4(\mathbf{E}\mathbf{B})^2\mathbf{E} + \\ &+4(\mathbf{E}^2 - \mathbf{B}^2)(\mathbf{E}\mathbf{B})\mathbf{B}]\}.\end{aligned} \tag{2.10}$$

$$\begin{aligned}\mathbf{H} = \mathbf{B} + 2\xi\{&\eta_1(\mathbf{E}^2 - \mathbf{B}^2)\mathbf{B} + 2\eta_2(\mathbf{B}\mathbf{E})\mathbf{E}\} \\ &+ 2\xi^2\{(6\eta_4 - 6\eta_1\eta_2 + 12\eta_2^2 + \eta_1^2 - \eta_3)(\mathbf{E}^2 - \mathbf{B}^2)^2\mathbf{B} \\ &+ (\eta_1\eta_2 - 2\eta_2^2 - \eta_4)[6(\mathbf{E}^2 - \mathbf{B}^2)^2\mathbf{B} + 4(\mathbf{E}\mathbf{B})^2\mathbf{B} \\ &+ 4(\mathbf{E}^2 - \mathbf{B}^2)(\mathbf{E}\mathbf{B})\mathbf{E}]\}\end{aligned}$$

Thus, post-Maxwellian formalism, abstracting from the details of one or another nonlinear electrodynamics, from its equations, hypotheses and postulates, from everything that constitutes its complete theoretical scheme, takes only the final result: an expansion of the Lagrangian, which, according to this theory, is fair in the approximation of a weak electromagnetic field. Further analysis of the theories and finding out whether their predictions are consistent with the results of experiments is of a general nature and boils down to answering two

questions: what values of post-Maxwell parameters has the theory under the study and what are these parameters equal to according to the results of the experiments[75].

Therefore, one of the tasks facing mathematical physics is the calculation of "weakly" nonlinear electrodynamics' effects irrespective of any nonlinear theory: the task of theory and experiment in this case should not be only the search for one effect or another that will disprove one or another nonlinear electrodynamics, but also systematic calculation and formulation of experiments to determine with the required accuracy the values of all post-Maxwell parameters[75].

As is well known, the nonlinear electrodynamics of vacuum for a long time did not have experimental confirmation and therefore was perceived by many people as an abstract theoretical model. The experiments posed recently and described in Ref. [48] related to the inelastic scattering of laser photons by gamma radiation confirm the nonlinearity of theories of vacuum electrodynamics. However, as was said, there are various models [50, 51] of nonlinear electrodynamics of vacuum. Due to the fact that there are also predictions [65, 66] of these theories that can be tested in an experiment on the nonlinear electrodynamics of vacuum, it requires serious attention from scientists.

Nonlinear effects in vacuum, according to theoretical calculations, should manifest themselves with a characteristic magnetic field induction $B_q = \frac{m^2c^2}{e\hbar} \sim 4.41 \cdot 10^{13}$ G .

Thus, at magnetic fields $B \sim 10^5$G , obtainable under earthly conditions, nonlinear electrodynamics' effects are so small [27,33,37-39] that it is very problematic to observe them in the near future. However, under terrestrial conditions, one experiment has already been done [48], which showed that vacuum electrodynamics is indeed a nonlinear theory.

In this experiment, laser radiation with a wavelength of 527 nm was subjected to backscattering by an electron beam with an energy of 46.6 GeV at the Stanford Electron-Positron Linear Collider (SLC), generating gamma rays with an energy of 29.2 GeV. According to the energy of the process, if vacuum electrodynamics is a nonlinear theory, then the scattering of four or more laser photons on a gamma quantum can lead to the production of an electron-positron pair. In the experiment, 106 ± 4 positrons were observed. Thus, the authors claim about the first observation of inelastic scattering of light by light[48].

However, in quantitative terms, the results of this experiment do not allow one to distinguish one nonlinear model of electrodynamics from another. It should also be noted that the production of an electron-positron pair in this experiment is also possible with other reaction channels, for example, when five or more laser photons are scattered by an electron beam with an energy of 46.6 GeV.

Therefore, it is necessary to continue the development of methods of mathematical physics to study the effects of nonlinear vacuum electrodynamics on purpose to identify its basic laws.

2.3 Magnetars.

Such vacuum principles can be studied using the strong electromagnetic fields of astrophysical objects [70-72]: pulsars and magnetars, which have magnetic dipole fields of $B \sim 10^{13}$G, unattainable in laboratory conditions.

In the present work we consider the problems of nonlinear electrodynamics of vacuum with such sources of an external electromagnetic field[76].

Modern observational data from astrophysics show that neutron stars are distinguished by the extremely characteristics of matter: enormous densities of matter, comparable to the density of matter in atomic nuclei, super strong gravitational and magnetic fields. Therefore, the study of neutron stars and the processes occurring around their surfaces allows us to investigate the properties of matter in unusual states which are unattainable in terrestrial conditions.

For the study of nonlinear electrodynamics' effects occurring in astrophysical conditions, the main interest is not only pulsars, but also is magnetars. Therefore, let's describe the main characteristics of these astrophysical objects.

Neutron stars consist mainly of neutron matter with a density of $\rho \sim 10^{14} - 10^{15}$ g/cm^3. From the observational data it follows that the mass of a typical neutron star is comparable to the mass of the Sun, and its radius R_0 is concluded [73,74] in the range from 7 km to 200 km. Therefore, the dimensionless gravitational potential $r_g/R_o = 2GM/(c^2 R_0)$ on the surface of neutron stars lies in the range: $0.1 > r_g/R_o > 0.001$.

Many neutron stars have a dipole magnetic field:

$$\mathbf{B} = \frac{3(\mathrm{m\,r})\mathrm{r} - \mathrm{r}^2 m}{r^5} \tag{2.11}$$

where $\vec{m}$ is the magnetic dipole moment.

Outside of a neutron star, due to the presence of a super strong magnetic field, the magnetosphere is formed, the radius of which can reach several star radii.
This magnetosphere is, as a rule, transparent for the low-frequency part of the electromagnetic spectrum. It can only be guaranteed that the magnetospheres of neutron stars are transparent in the region of x-ray and gamma radiation.

The gravitational field of a neutron star is created by its substance, as well as a magnetic dipole field with charged particles in the magnetosphere. Since the energy density of the substance of compact neutron stars ~ 10^{36}erg/cm^3 is more than six orders of magnitude greater than the maximum energy density of the magnetic field, even in the case of a magnetar, the star matter makes the main contribution to the gravitational field. Assuming that it is spherically symmetric distributed, the Schwarzschild metric(see chapter 2.4) can be used as the metric tensor of pseudo-Riemannian space-time [73]:

$$g_{00} = 1 - \frac{r_g}{r}\ ,\ g_{rr} = -\frac{r}{r - r_g}\ ,\ g_{\theta\theta} = -r^2,\quad g_{\varphi\varphi} = -r^2 \sin^2\theta, \tag{2.12}$$

where r_g is the gravitational radius of a neutron star.

Pulsars and magnetars rotate around the axes, which often do not coincide with the vector of the dipole magnetic moment.

There are two possible scenarios for the accretion of matter onto a neutron star: the first is by capturing matter from the stellar wind of the companion, the second is by flowing out of a donor star through a Roche lobe. The accreted flux of matter is strongly ionized near the neutron star due to the strong magnetic field and moves along the lines of force of the magnetic field and then falls on the poles of the neutron star. To date, two mechanisms for the emission of electromagnetic radiation in the x-ray and gamma spectrum are known for neutron stars. The first mechanism is associated with the effect of accretions that occur in close binary systems. The second mechanism occurs in single pulsars and is associated with the rotation and strong magnetic field of a neutron star.

The number of pulsars emitting electromagnetic radiation in the gamma spectrum to date has been discovered about ten.

It is assumed that gamma pulsars are magnetic neutron stars whose field on their surface is characterized by values of $\sim 10^{12}\ Gs$.

In the past few years, a special class of so-called anomalous or six-second pulsars (magnetars) has been established, whose properties differ significantly from the properties of conventional accreting pulsars that are part of binary systems with a massive optical companion [74-76]. Magnetars are objects containing neutron stars with a super strong ($\sim 10^{15} G$) magnetic field. Nowadays, six magnetars are known [77].

Thus, pulsars and magnetars have magnetic fields of $B \sim 10^{11} - 10^{15}$ Gs, unattainable in laboratory conditions, and fields of such intensity extend over considerable distances L ~ 10–100 km.

Therefore, surroundings of the pulsars and magnetars are the most convenient natural laboratory for studying the effects of nonlinear vacuum electrodynamics[75].

2.4 Magnetar external field metric.

Let us consider the movement of masses with island distribution. With the island distribution of masses, the gravitational field at infinity tends to zero. Where there is no gravitational field, the space-time geometry should be pseudo-Euclidean, therefore, the limiting values of $g_{\mu\nu}$ at infinity:

$$\left(g_{00}\right)_\infty = 1;\ \left(g_{0i}\right)_\infty = 0;\ \left(g_{ij}\right)_\infty = -\delta_{ij};\quad (i, j = 1, 2, 3) \tag{2.13}$$

The corresponding limit values for the contravariant components of the metric tensor will be equal

$$\left(g^{00}\right)_\infty = 1;\ \left(g^{0i}\right)_\infty = 0;\ \left(g^{ij}\right)_\infty = -\delta_{ij}; \tag{2.14}$$

These conditions must be supplemented by others characterizing the asymptotic behavior of the differences $g_{\mu\nu}$ - $(g_{\mu\nu})_\infty$ at a large distance from the masses:

$$\lim_{(r\to\infty)}\left(\frac{\partial\left(r\left(g_{\mu\nu}-\left(g_{\mu\nu}\right)_\infty\right)\right)}{\partial r}+\frac{1}{c}\frac{\partial\left(r\left(g_{\mu\nu}-\left(g_{\mu\nu}\right)_\infty\right)\right)}{\partial t}\right)=0. \tag{2.15}$$

To find the metric

$$ds^2=g_{\mu\nu}dx^\mu dx^\nu, \tag{2.16}$$

we need to define the expressions for the metric tensor $g_{\mu\nu}$. System of equations will be

$$R^{\mu\nu}-\frac{1}{2}g^{\mu\nu}R=-\chi T^{\mu\nu}, \tag{2.17}$$

$$.\frac{\partial}{\partial x^\nu}\left(\sqrt{g}\,g^{\mu\nu}\right)=0,\quad \mu,\nu=0,1,2,3, \tag{2.18}$$

where (2.17) - Einstein's equation, (2.18) - the condition of harmony, taking into account the above assumptions, can be reduced to

$$\frac{1}{2}\left(\Delta-\frac{1}{c^2}\frac{\partial^2}{\partial t^2}\right)g^{\mu\nu}=-\chi\left(T^{\mu\nu}-\frac{1}{2}g^{\mu\nu}T\right), \tag{2.19}$$

which are solved by the method of successive approximations. Thus, the components of the metric tensor and the momentum energy tensor are successively found, and the constant χ is also determined. With the right degree of accuracy

$$\begin{aligned} g_{00}&=1-\frac{2U}{c^2}+\frac{2}{c^4}\left(U^2-\frac{\partial^2 W}{\partial t^2}-c^2\tilde{U}\right)+\ldots,\\ g_{0i}&=\frac{4U_i}{c^3}+\ldots,\\ g_{ij}&=-\left(1+\frac{2U}{c^2}\right)\delta_{ij}+\ldots \end{aligned} \tag{2.20}$$

Hence

$$g^{00} = 1 + \frac{2U}{c^2} + \frac{2}{c^4}\left(U^2 + \frac{\partial^2 W}{\partial t^2} + c^2 \widetilde{U} \right) + \ldots,$$
$$g^{0i} = \frac{4U_i}{c^3} + \ldots,$$
$$g^{ij} = -\left(1 - \frac{2U}{c^2}\right)\delta_{ij} + \ldots \tag{2.21}$$

and

$$g = -\left(1 + \frac{4U}{c^2} + \ldots\right). \tag{2.22}$$

Accordingly, the energy-momentum tensor of macroscopic bodies has the form

$$T^{00} = \rho\left[1 + \frac{1}{c^2}\left(\frac{1}{2}v^2 + \Pi - U\right)\right] + \ldots,$$
$$cT^{0i} = \rho v_i\left[1 + \frac{1}{c^2}\left(\frac{1}{2}v^2 + \Pi - U\right)\right] + \frac{1}{c^2}pv_i + \ldots,$$
$$c^2 T^{ij} = \rho v_i v_j + p\delta_{ij} + \ldots \tag{2.23}$$

where p - isotropic pressure, Π - elastic energy of unit mass. Here U - newtons potential, U_i - vector- potential, W, $\widetilde{U}$ - secondary functions. We need to find these expressions with the right degree of accuracy. Они удовлетворяют They satisfy the relations

$$\Delta U = -4\pi\gamma\rho, \tag{2.24}$$

$$\Delta U_i = -4\pi\gamma\rho v_i, \tag{2.25}$$

$$\Delta W = U, \tag{2.26}$$

$$\Delta\widetilde{U} = -4\pi\gamma(\sigma - \rho), \tag{2.27}$$

where ρ - body mass density, $\sigma = T^{\mu\mu}$ or

$$\sigma = \rho + \frac{1}{c^2}\rho\left(\frac{3}{2}v^2 - U + \Pi\right) + \frac{3p}{c^2}, \tag{2.28}$$

In each of the functions U, U_i, W, $\widetilde{U}$ can be distinguished the inner part due to the body under consideration and the external part due to the action of the other bodies

$$\begin{aligned} U &= u^{(a)} + U^{(a)}, \\ U_i &= u_i^{(a)} + U_i^{(a)}, \\ W &= w^{(a)} + W^{(a)}, \\ \widetilde{U}^{(a)} &= \widetilde{u}^{(a)} + \widetilde{U}^{(a)}. \end{aligned} \tag{2.29}$$

The internal parts will be defined by expressions

$$\begin{aligned} u^{(a)} &= \gamma \int_{(a)} \frac{\rho' (dx')^3}{|\mathbf{r} - \mathbf{r}'|}, & u_i^{(a)} &= \gamma \int_{(a)} \frac{\rho' v_i (dx')^3}{|\mathbf{r} - \mathbf{r}'|}, \\ w^{(a)} &= \frac{1}{2} \gamma \int_{(a)} \rho' |\mathbf{r} - \mathbf{r}'| (dx')^3, & \widetilde{u}^{(a)} &= \gamma \int_{(a)} \frac{(\sigma' - \rho')(dx')^3}{|\mathbf{r} - \mathbf{r}'|}. \end{aligned} \tag{2.30}$$

The mass of the body under consideration, the coordinates and velocity components of the center of inertia are expressed by the integrals

$$M_a = \int_{(a)} \rho (dx)^3, \tag{2.31}$$

$$M_a a_i = \int_{(a)} \rho\, x_i (dx)^3, \tag{2.32}$$

$$M_a \dot{a}_i = \int_{(a)} \rho\, v_i (dx)^3. \tag{2.33}$$

We will assume that the velocity distribution inside the body has the form

$$v_i = \dot{a}_i + \omega_{ki}^{(a)} (x_k - a_k), \tag{2.34}$$

where ω_{ij} - antisymmetric angular velocity tensor with components

$$(\omega_{ij}) = \begin{pmatrix} 0 & \omega_3 & -\omega_2 \\ -\omega_3 & 0 & \omega_1 \\ \omega_2 & -\omega_1 & 0 \end{pmatrix}. \tag{2.35}$$

The values

$$I^{(a)}_{i_1,i_2\ldots i_n} = \int\limits_{(a)} \rho\left(x_{i_1} - a_{i_1}\right)\left(x_{i_2} - a_{i_2}\right)\ldots\left(x_{i_n} - a_{i_n}\right)(dx)^3 \tag{2.36}$$

determine the moments of inertia of order n (n = 2, 3, ...). Their time derivatives satisfy the kinematic relations

$$\dot{I}^{(a)}_{i_1,i_2\ldots i_n} = \omega_{ki_1} I^{(a)}_{k,i_2\ldots i_n} + \omega_{ki_2} I^{(a)}_{i_1,k\ldots i_n} + \ldots + \omega_{ki_n} I^{(a)}_{i_1,i_2\ldots k}. \tag{2.37}$$

If we denote the potential of centrifugal forces by $\Omega^{(a)}$

$$\Omega^{(a)} = \frac{1}{2}\omega^{(a)}_{km}\,\omega^{(a)}_{km}\left(x_k - a_k\right)\left(x_l - a_l\right), \tag{2.38}$$

then the kinetic energy of rotation and moments of the first and second orders will be

$$\begin{aligned}
T^{(a)} &= \int\limits_{(a)} \rho\Omega^{(a)}(dx)^3 = \frac{1}{2}\omega^{(a)}_{km}\,\omega^{(a)}_{km} I^{(a)}_{kl},\\
T^{(a)}_i &= \int\limits_{(a)} \rho\Omega^{(a)}\left(x_i - a_i\right)(dx)^3 = \frac{1}{2}\omega^{(a)}_{km}\,\omega^{(a)}_{lm} I^{(a)}_{ikl},\\
T^{(a)}_{ij} &= \int\limits_{(a)} \rho\Omega^{(a)}\left(x_i - a_i\right)\left(x_j - a_j\right)(dx)^3 = \frac{1}{2}\omega^{(a)}_{km}\,\omega^{(a)}_{lm} I^{(a)}_{ijkl}.
\end{aligned} \tag{2.39}$$

When calculating the integrals of the internal parts of the integrands, we need auxiliary integrals that depend only on the internal structure of the body:

$$\begin{aligned}
B^{(a)}_{kl} &= \frac{1}{2}\gamma \int\limits_{(a)(a)}\int \rho\rho' \frac{\left(x_k - x'_k\right)\left(x_l - x'_l\right)}{\left|\mathbf{r} - \mathbf{r}'\right|^3}(dx)^3\left(dx'\right)^3,\\
B^{(a)}_{ikl} &= \frac{1}{2}\gamma \int\limits_{(a)(a)}\int \rho\rho' \frac{\left(x_k - x'_k\right)\left(x_l - x'_l\right)}{\left|\mathbf{r} - \mathbf{r}'\right|^3}\left(x_i - a_i\right)(dx)^3\left(dx'\right)^3,\\
B^{(a)}_{ijkl} &= \frac{1}{2}\gamma \int\limits_{(a)(a)}\int \rho\rho' \frac{\left(x_k - x'_k\right)\left(x_l - x'_l\right)}{\left|\mathbf{r} - \mathbf{r}'\right|^3}\left(x_i - a_i\right)\left(x_j - a_j\right)(dx)^3\left(dx'\right)^3.
\end{aligned} \tag{2.40}$$

Using these integrals we find

$$\varepsilon^{(a)} = \frac{1}{2}\int_{(a)} \rho u^{(a)} (dx)^3 = B_{kk}^{(a)},$$
$$\varepsilon_i^{(a)} = \frac{1}{2}\int_{(a)} \rho u^{(a)} (x_i - a_i)(dx)^3 = B_{ikk}^{(a)},$$
$$\varepsilon_{ij}^{(a)} = \frac{1}{2}\int_{(a)} \rho u^{(a)} (x_i - a_i)(x_j - a_j)(dx)^3 = B_{ijkk}^{(a)} \qquad (2.41)$$

and

$$\varphi_{kl}^{(a)} = \frac{1}{2}\int_{(a)} \rho \frac{\partial^2 w^{(a)}}{\partial x_k \partial x_l}(dx)^3 = \varepsilon^{(a)}\delta_{kl} - B_{kl}^{(a)},$$
$$\varphi_{ikl}^{(a)} = \frac{1}{2}\int_{(a)} \rho \frac{\partial^2 w^{(a)}}{\partial x_k \partial x_l}(x_i - a_i)(dx)^3 = \varepsilon_i^{(a)}\delta_{kl} - B_{ikl}^{(a)},$$
$$\varphi_{ijkl}^{(a)} = \frac{1}{2}\int_{(a)} \rho \frac{\partial^2 w^{(a)}}{\partial x_k \partial x_l}(x_i - a_i)(x_j - a_j)(dx)^3 = \varepsilon_{ij}^{(a)}\delta_{kl} - B_{ijkl}^{(a)}. \qquad (2.42)$$

We introduce two more groups of integrals, which also depend only on the internal structure of the body

$$\xi^{(a)} = \int_{(a)} (-\rho u^{(a)} + \rho\Pi + 3p)(dx)^3,$$
$$\xi_i^{(a)} = \int_{(a)} (-\rho u^{(a)} + \rho\Pi + 3p)(x_i - a_i)(dx)^3,$$
$$\xi_{ij}^{(a)} = \int_{(a)} (-\rho u^{(a)} + \rho\Pi + 3p)(x_i - a_i)(x_j - a_j)(dx)^3 \qquad (2.43)$$

or

$$\eta^{(a)} = \int_{(a)} (-\rho u^{(a)} + \rho\Pi + p)(dx)^3,$$
$$\eta_i^{(a)} = \int_{(a)} (-\rho u^{(a)} + \rho\Pi + p)(x_i - a_i)(dx)^3,$$
$$\eta_{ij}^{(a)} = \int_{(a)} (-\rho u^{(a)} + \rho\Pi + p)(x_i - a_i)(x_j - a_j)(dx)^3. \qquad (2.44)$$

The integrals of the outer parts are calculated by expanding the functions of $|\mathbf{r} - \mathbf{r}'|$ in the vicinity of the corresponding body

$$U^{(a)}(\mathbf{r})=\sum_{b}{}^{(a)}\gamma\int_{(b)}\frac{\rho'(dx')^3}{|\mathbf{r}-\mathbf{r}'|}=\gamma\sum_{b}{}^{(a)}\left\{\frac{M_b}{|\mathbf{r}-\mathbf{b}|}+\frac{1}{2}I^{(b)}_{kl}\frac{\partial^2}{\partial x_k\partial x_l}\frac{1}{|\mathbf{r}-\mathbf{b}|}-\right.$$
$$\left.-\frac{1}{6}I^{(b)}_{klm}\frac{\partial^3}{\partial x_k\partial x_l\partial x_m}\frac{1}{|\mathbf{r}-\mathbf{b}|}+\frac{1}{24}I^{(b)}_{klmn}\frac{\partial^4}{\partial x_k\partial x_l\partial x_m\partial x_n}\frac{1}{|\mathbf{r}-\mathbf{b}|}+\ldots\right\},\tag{2.45}$$

$$U^{(a)}_i(\mathbf{r})=\sum_{b}{}^{(a)}\gamma\int_{(b)}\frac{\rho'v'_i(dx')^3}{|\mathbf{r}-\mathbf{r}'|}=\gamma\sum_{b}{}^{(a)}\left\{\frac{M_b\dot{b}_i}{|\mathbf{r}-\mathbf{b}|}-\omega^{(b)}_{li}I^{(b)}_{kl}\frac{\partial}{\partial x_k}\frac{1}{|\mathbf{r}-\mathbf{b}|}+\right.$$
$$\left.+\frac{1}{2}\left(\dot{b}_iI^{(b)}_{kl}+\omega^{(b)}_{mi}I^{(b)}_{klm}\right)\frac{\partial^2}{\partial x_k\partial x_l}\frac{1}{|\mathbf{r}-\mathbf{b}|}+\ldots\right\},\tag{2.46}$$

$$W^{(a)}(\mathbf{r})=\sum_{b}{}^{(a)}\frac{1}{2}\gamma\int_{(b)}\rho'|\mathbf{r}-\mathbf{r}'|(dx')^3=\frac{1}{2}\gamma\sum_{b}{}^{(a)}\left\{M_b|\mathbf{r}-\mathbf{b}|+\frac{1}{2}I^{(b)}_{kl}\frac{\partial^2}{\partial x_k\partial x_l}|\mathbf{r}-\mathbf{b}|-\right.$$
$$\left.-\frac{1}{6}I^{(b)}_{klm}\frac{\partial^3}{\partial x_k\partial x_l\partial x_m}|\mathbf{r}-\mathbf{b}|+\frac{1}{24}I^{(b)}_{klmn}\frac{\partial^4}{\partial x_k\partial x_l\partial x_m\partial x_n}|\mathbf{r}-\mathbf{b}|+\ldots\right\},\tag{2.47}$$

$$\frac{\partial W^{(a)}(\mathbf{r})}{\partial t}=\frac{1}{2}\gamma\sum_{b}{}^{(a)}\left\{-M_b\dot{b}_k\frac{\partial}{\partial x_k}|\mathbf{r}-\mathbf{b}|+\frac{1}{2}\dot{I}^{(b)}_{kl}\frac{\partial^2}{\partial x_k\partial x_l}|\mathbf{r}-\mathbf{b}|-\right.$$
$$-\frac{1}{2}\left(I^{(b)}_{kl}\dot{b}_m+\frac{1}{3}\dot{I}^{(b)}_{klm}\right)\frac{\partial^3}{\partial x_k\partial x_l\partial x_m}|\mathbf{r}-\mathbf{b}|+\frac{1}{6}\left(I^{(b)}_{klm}\dot{b}_n+\frac{1}{4}\dot{I}^{(b)}_{klmn}\right)\times$$
$$\left.\times\frac{\partial^4}{\partial x_k\partial x_l\partial x_m\partial x_n}|\mathbf{r}-\mathbf{b}|+\ldots\right\},$$

$$\frac{\partial^2 W^{(a)}(\mathbf{r})}{\partial t^2}=\frac{1}{2}\gamma\sum_{b}{}^{(a)}\left\{M_b\dot{b}_k\dot{b}_l\frac{\partial^2}{\partial x_k\partial x_l}|\mathbf{r}-\mathbf{b}|+\right.$$
$$+M_b\gamma\sum_{c}{}^{(b)}\frac{M_c(b_k-c_k)}{|\mathbf{b}-\mathbf{c}|}\frac{\partial}{\partial x_k}|\mathbf{r}-\mathbf{b}|-$$
$$\left.-\left(\dot{I}^{(b)}_{kl}\dot{b}_m-\frac{1}{2}I^{(b)}_{kl}\gamma\sum_{c}{}^{(b)}\frac{M_c(b_m-c_m)}{|\mathbf{b}-\mathbf{c}|}\right)\frac{\partial^3}{\partial x_k\partial x_l\partial x_m}|\mathbf{r}-\mathbf{b}|+\ldots\right\},\tag{2.48}$$

$$\tilde{U}^{(a)}(\mathbf{r}) = \sum_{b}{}^{(a)} \gamma \int_{(b)} \frac{(\sigma' - \rho')(dx')^3}{|\mathbf{r} - \mathbf{r}'|} = \frac{\gamma}{c^2} \times$$

$$\times \sum_{b}{}^{(a)} \left\{ \left(\frac{3}{2} M_b \dot{b}_k^2 - M_b U^{(b)}(\mathbf{b}) + 3T^{(b)} + \xi^{(b)} \right) \frac{1}{|\mathbf{r} - \mathbf{b}|} - \right.$$

$$- \left(3\dot{b}_m \omega_{lm}^{(b)} I_{kl}^{(b)} + 3T_k^{(b)} + \xi_k^{(b)} \right) \frac{\partial}{\partial x_k} \frac{1}{|\mathbf{r} - \mathbf{b}|} +$$

$$+ \frac{1}{2} \left(\frac{3}{2} \dot{b}_m^2 I_{kl}^{(b)} - I_{kl}^{(b)} U^{(b)}(\mathbf{b}) + 3\dot{b}_n \omega_{mn}^{(b)} I_{klm}^{(b)} + \right.$$

$$+ 3T_{kl}^{(b)} + \xi_{kl}^{(b)} \Big) \frac{\partial^2}{\partial x_k \partial x_l} \frac{1}{|\mathbf{r} - \mathbf{b}|} + \frac{1}{6} I_{kl}^{(b)} \left(\frac{\partial U^{(b)}}{\partial x_l} \right)_b \times$$

$$\left. \left. \times \frac{\partial}{\partial x_k} \frac{1}{|\mathbf{r} - \mathbf{b}|} - \frac{1}{2} I_{kl}^{(b)} \left(\frac{\partial^2 U^{(b)}}{\partial x_k \partial x_l} \right)_b \frac{1}{|\mathbf{r} - \mathbf{b}|} + \ldots \right\} \right. . \tag{2.49}$$

We rewrite the last expression in the form

$$\tilde{U}^{(a)}(\mathbf{r}) = \frac{\gamma}{c^2} \sum_{b}{}^{(a)} \left\{ \frac{1}{|\mathbf{r} - \mathbf{b}|} \left(\frac{3}{2} M_b \dot{b}_k^2 - M_b \sum_{c}{}^{(b)} \frac{\gamma M_c}{|\mathbf{b} - \mathbf{c}|} + 3T^{(b)} + \xi^{(b)} \right) - \right.$$

$$- \left(3\dot{b}_m \omega_{lm}^{(b)} I_{kl}^{(b)} + 3T_k^{(b)} + \xi_k^{(b)} \right) \frac{\partial}{\partial x_k} \frac{1}{|\mathbf{r} - \mathbf{b}|} + \frac{1}{2} \left(\frac{3}{2} \dot{b}_m^2 I_{kl}^{(b)} - I_{kl}^{(b)} \sum_{c}{}^{(b)} \frac{\gamma M_c}{|\mathbf{b} - \mathbf{c}|} + \right.$$

$$3\dot{b}_n \omega_{mn}^{(b)} I_{klm}^{(b)} + + 3T_{kl}^{(b)} + \xi_{kl}^{(b)} \Big) \frac{\partial^2}{\partial x_k \partial x_l} \frac{1}{|\mathbf{r} - \mathbf{b}|} + \frac{1}{6} I_{kl}^{(b)} \frac{\partial}{\partial x_k} \frac{1}{|\mathbf{r} - \mathbf{b}|} \sum_{c}{}^{(b)} \gamma M_c \times$$

$$\left. \left. \times \frac{\partial}{\partial b_l} \frac{1}{|\mathbf{b} - \mathbf{c}|} - \frac{1}{2} \frac{1}{|\mathbf{r} - \mathbf{b}|} \sum_{c}{}^{(b)} \gamma \left(M_b I_{kl}^{(c)} + M_c I_{kl}^{(cb)} \right) \frac{\partial^2}{\partial b_k \partial b_l} \frac{1}{|\mathbf{b} - \mathbf{c}|} + \ldots \right\} \right. . \tag{2.50}$$

Substituting the results obtained in (2.20) and (2.21), we obtain expressions for the components of the metric tensor

$$g_{00}=1-\frac{2\gamma}{c^2}\sum_b{}^{(a)}\left\{\frac{M_b}{|\mathbf{r}-\mathbf{b}|}+\frac{1}{2}I^{(b)}_{kl}\frac{\partial^2}{\partial x_k\partial x_l}\frac{1}{|\mathbf{r}-\mathbf{b}|}-\frac{1}{6}I^{(b)}_{klm}\frac{\partial^3}{\partial x_k\partial x_l\partial x_m}\frac{1}{|\mathbf{r}-\mathbf{b}|}+\right.$$

$$\left.+\frac{1}{24}I^{(b)}_{klmn}\frac{\partial^4}{\partial x_k\partial x_l\partial x_m\partial x_n}\frac{1}{|\mathbf{r}-\mathbf{b}|}\right\}+\frac{2\gamma^2}{c^4}\left(\sum_b{}^{(a)}\left(\frac{M_b}{|\mathbf{r}-\mathbf{b}|^2}+\frac{1}{2}I^{(b)}_{kl}\frac{\partial^2}{\partial x_k\partial x_l}\frac{1}{|\mathbf{r}-\mathbf{b}|}\right)\right)^2+$$

$$+\frac{2}{c^4}\left\{\frac{1}{2}\gamma\sum_b{}^{(a)}\left\{M_b\dot{b}_k\dot{b}_l\frac{\partial^2}{\partial x_k\partial x_l}|\mathbf{r}-\mathbf{b}|+M_b\gamma\sum_c{}^{(b)}\frac{M_c(b_k-c_k)}{|\mathbf{b}-\mathbf{c}|}\times\right.\right.$$

$$\left.\left.\times\frac{\partial}{\partial x_k}|\mathbf{r}-\mathbf{b}|-\left(\dot{I}^{(b)}_{kl}\dot{b}_m-\frac{1}{2}I^{(b)}_{kl}\gamma\sum_c{}^{(b)}\frac{M_c(b_m-c_m)}{|\mathbf{b}-\mathbf{c}|}\right)\frac{\partial^3}{\partial x_k\partial x_l\partial x_m}|\mathbf{r}-\mathbf{b}|\right\}-\right.$$

$$-\gamma\sum_b{}^{(a)}\left\{\frac{1}{|\mathbf{r}-\mathbf{b}|}\left(\frac{3}{2}M_b\dot{b}_k^2-M_b\sum_c{}^{(b)}\frac{\gamma M_c}{|\mathbf{b}-\mathbf{c}|}+3T^{(b)}+\xi^{(b)}\right)-\right.$$

$$-\left(3\dot{b}_m\omega^{(b)}_{lm}I^{(b)}_{kl}+3T^{(b)}_k+\xi^{(b)}_k\right)\frac{\partial}{\partial x_k}\frac{1}{|\mathbf{r}-\mathbf{b}|}+\frac{1}{2}\left(\frac{3}{2}\dot{b}_m^2I^{(b)}_{kl}-I^{(b)}_{kl}\sum_c{}^{(b)}\frac{\gamma M_c}{|\mathbf{b}-\mathbf{c}|}+\right.$$

$$+3\dot{b}_n\omega^{(b)}_{mn}I^{(b)}_{klm}++3T^{(b)}_{kl}+\xi^{(b)}_{kl}\Big)\frac{\partial^2}{\partial x_k\partial x_l}\frac{1}{|\mathbf{r}-\mathbf{b}|}+\frac{1}{6}I^{(b)}_{kl}\frac{\partial}{\partial x_k}\frac{1}{|\mathbf{r}-\mathbf{b}|}\sum_c{}^{(b)}\gamma M_c\times$$

$$\left.\left.\left.\times\frac{\partial}{\partial b_l}\frac{1}{|\mathbf{b}-\mathbf{c}|}-\frac{1}{2}\frac{1}{|\mathbf{r}-\mathbf{b}|}\sum_c{}^{(b)}\gamma\left(M_bI^{(c)}_{kl}+M_cI^{(cb)}_{kl}\right)\frac{\partial^2}{\partial b_k\partial b_l}\frac{1}{|\mathbf{b}-\mathbf{c}|}\right\}\right\}+\ldots \tag{2.51}$$

$$g_{0i}=\frac{4\gamma}{c^3}\sum_b{}^{(a)}\left\{\frac{M_b\dot{b}_i}{|\mathbf{r}-\mathbf{b}|}-\omega^{(b)}_{li}I^{(b)}_{kl}\frac{\partial}{\partial x_k}\frac{1}{|\mathbf{r}-\mathbf{b}|}+\right.$$

$$\left.+\frac{1}{2}\left(\dot{b}_iI^{(b)}_{kl}+\omega^{(b)}_{mi}I^{(b)}_{klm}\right)\frac{\partial^2}{\partial x_k\partial x_l}\frac{1}{|\mathbf{r}-\mathbf{b}|}\right\}+\ldots, \tag{2.52}$$

$$g_{ij}=-\left(1+\frac{2\gamma}{c^2}\sum_b{}^{(a)}\left\{\frac{M_b}{|\mathbf{r}-\mathbf{b}|}+\frac{1}{2}I^{(b)}_{kl}\frac{\partial^2}{\partial x_k\partial x_l}\frac{1}{|\mathbf{r}-\mathbf{b}|}\right\}\right)\delta_{ij}+\ldots, \tag{2.53}$$

contravariant components of the metric tensor

$$g^{00}=1+\frac{2\gamma}{c^2}\sum_b{}^{(a)}\left\{\frac{M_b}{|\mathbf{r}-\mathbf{b}|}+\frac{1}{2}I^{(b)}_{kl}\frac{\partial^2}{\partial x_k\partial x_l}\frac{1}{|\mathbf{r}-\mathbf{b}|}-\frac{1}{6}I^{(b)}_{klm}\frac{\partial^3}{\partial x_k\partial x_l\partial x_m}\frac{1}{|\mathbf{r}-\mathbf{b}|}+\right.$$

$$\left.+\frac{1}{24}I^{(b)}_{klmn}\frac{\partial^4}{\partial x_k\partial x_l\partial x_m\partial x_n}\frac{1}{|\mathbf{r}-\mathbf{b}|}\right\}+\frac{2\gamma^2}{c^4}\left(\sum_b{}^{(a)}\left(\frac{M_b}{|\mathbf{r}-\mathbf{b}|^2}+\frac{1}{2}I^{(b)}_{kl}\frac{\partial^2}{\partial x_k\partial x_l}\frac{1}{|\mathbf{r}-\mathbf{b}|}\right)\right)^2+$$

$$+\frac{2}{c^4}\left\{\frac{1}{2}\gamma\sum_b{}^{(a)}\left\{M_b\dot b_k\dot b_l\frac{\partial^2}{\partial x_k\partial x_l}|\mathbf{r}-\mathbf{b}|+M_b\gamma\sum_c{}^{(b)}\frac{M_c(b_k-c_k)}{|\mathbf{b}-\mathbf{c}|^3}\times\right.\right.$$

$$\left.\left.\times\frac{\partial}{\partial x_k}|\mathbf{r}-\mathbf{b}|-\left(\dot I^{(b)}_{kl}\dot b_m-\frac{1}{2}I^{(b)}_{kl}\gamma\sum_c{}^{(b)}\frac{M_c(b_m-c_m)}{|\mathbf{b}-\mathbf{c}|^3}\right)\frac{\partial^3}{\partial x_k\partial x_l\partial x_m}|\mathbf{r}-\mathbf{b}|\right\}+\right.$$

$$+\gamma\sum_b{}^{(a)}\left\{\frac{1}{|\mathbf{r}-\mathbf{b}|}\left(\frac{3}{2}M_b\dot b_k^2-M_b\sum_c{}^{(b)}\frac{\gamma M_c}{|\mathbf{b}-\mathbf{c}|}+3T^{(b)}+\xi^{(b)}\right)-\right.$$

$$-\left(3\dot b_m\omega^{(b)}_{lm}I^{(b)}_{kl}+3T^{(b)}_k+\xi^{(b)}_k\right)\frac{\partial}{\partial x_k}\frac{1}{|\mathbf{r}-\mathbf{b}|}+\frac{1}{2}\left(\frac{3}{2}\dot b_m^2I^{(b)}_{kl}-I^{(b)}_{kl}\sum_c{}^{(b)}\frac{\gamma M_c}{|\mathbf{b}-\mathbf{c}|}+\right.$$

$$+3\dot b_n\omega^{(b)}_{mn}I^{(b)}_{klm}++3T^{(b)}_{kl}+\xi^{(b)}_{kl}\Big)\frac{\partial^2}{\partial x_k\partial x_l}\frac{1}{|\mathbf{r}-\mathbf{b}|}+\frac{1}{6}I^{(b)}_{kl}\frac{\partial}{\partial x_k}\frac{1}{|\mathbf{r}-\mathbf{b}|}\sum_c{}^{(b)}\gamma M_c\times$$

$$\left.\left.\left.\times\frac{\partial}{\partial b_l}\frac{1}{|\mathbf{b}-\mathbf{c}|}-\frac{1}{2}\frac{1}{|\mathbf{r}-\mathbf{b}|}\sum_c{}^{(b)}\gamma\left(M_bI^{(c)}_{kl}+M_cI^{(cb)}_{kl}\right)\frac{\partial^2}{\partial b_k\partial b_l}\frac{1}{|\mathbf{b}-\mathbf{c}|}\right\}\right\}+\ldots \tag{2.54}$$

$$g^{0i}=\frac{4\gamma}{c^3}\sum_b{}^{(a)}\left\{\frac{M_b\dot b_i}{|\mathbf{r}-\mathbf{b}|}-\omega^{(b)}_{li}I^{(b)}_{kl}\frac{\partial}{\partial x_k}\frac{1}{|\mathbf{r}-\mathbf{b}|}+\right.$$

$$\left.+\frac{1}{2}\left(\dot b_iI^{(b)}_{kl}+\omega^{(b)}_{mi}I^{(b)}_{klm}\right)\frac{\partial^2}{\partial x_k\partial x_l}\frac{1}{|\mathbf{r}-\mathbf{b}|}\right\}+\ldots, \tag{2.55}$$

$$g^{ij}=-\left(1-\frac{2\gamma}{c^2}\sum_b{}^{(a)}\left\{\frac{M_b}{|\mathbf{r}-\mathbf{b}|}+\frac{1}{2}I^{(b)}_{kl}\frac{\partial^2}{\partial x_k\partial x_l}\frac{1}{|\mathbf{r}-\mathbf{b}|}\right\}\right)\delta_{ij}+\ldots, \tag{2.56}$$

In the case of spherically symmetric bodies, all of the above formulas are greatly simplified. Integrals that depend on the internal structure take on values

$$B^{(a)}_{kl}=\frac{1}{3}\delta_{kl}B^{(a)}_{mm},\quad B^{(a)}_{ikl}=0,\quad B^{(a)}_{ijkl}=\frac{1}{9}\delta_{ij}\delta_{kl}B^{(a)}_{mmnn}. \tag{2.57}$$

The quantities $\varepsilon_i^{(a)}$, $\eta_i^{(a)}$, $\xi_i^{(a)}$ vanish, and the quantities $\varepsilon_{ij}^{(a)}$, $\eta_{ij}^{(a)}$, $\xi_{ij}^{(a)}$ become proportional to δ_{ij}. Further,

$$I_{kl}^{(a)} = \delta_{kl} I_a, \quad I_{klm}^{(a)} = 0,$$
$$I_{klmn}^{(a)} = \left(\delta_{kl}\delta_{mn} + \delta_{km}\delta_{ln} + \delta_{kn}\delta_{lm}\right) I'_a. \tag{2.58}$$

therefore

$$T^{(a)} = \boldsymbol{\omega}_a^2 I_a, \quad T_i^{(a)} = 0, \quad T_{ij}^{(a)} = \left(2\boldsymbol{\omega}_a^2 \delta_{ij} - \omega_i^{(a)}\omega_j^{(a)}\right) I'_a, \tag{2.59}$$

where $\boldsymbol{\omega}_a$ means a three-dimensional vector of angular velocity with components ω_1, ω_2, ω_3. Moreover, for a homogeneous body of radius R_a

$$I_a = \frac{1}{5} M_a R_a^2, \quad I'_a = \frac{1}{35} M_a R_a^4. \tag{2.60}$$

For spherical bodies, formulas (2.45), (2.46), (2.48) and (2.49) give

$$U^{(a)}(\mathbf{r}) = \sum_b{}^{(a)} \gamma \int_{(b)} \frac{\rho'(dx')^3}{|\mathbf{r} - \mathbf{r}'|} = \gamma \sum_b{}^{(a)} \frac{M_b}{|\mathbf{r} - \mathbf{b}|}, \tag{2.61}$$

$$U_i^{(a)}(\mathbf{r}) = \gamma \sum_b{}^{(a)} \left\{ \frac{M_b \dot{b}_i}{|\mathbf{r} - \mathbf{b}|} - {}_{li}^{(b)} I_{kl}^{(b)} \frac{I_b}{|\mathbf{r} - \mathbf{b}|^3} [\boldsymbol{\omega}_b \times (\mathbf{r} - \mathbf{b})]_i \right\}, \tag{2.62}$$

$$W^{(a)}(\mathbf{r}) = \frac{1}{2} \gamma \sum_b{}^{(a)} M_b |\mathbf{r} - \mathbf{b}| + \ldots, \tag{2.63}$$

$$\tilde{U}^{(a)}(\mathbf{r}) = \frac{\gamma}{c^2} \sum_b{}^{(a)} \left\{ \frac{1}{|\mathbf{r} - \mathbf{b}|} \left(\frac{3}{2} M_b \dot{\mathbf{b}}^2 - M_b \sum_c{}^{(b)} \frac{\gamma M_c}{|\mathbf{b} - \mathbf{c}|} + 3\boldsymbol{\omega}_b^2 I_b + \xi^{(b)} \right) + \right.$$
$$\left. + \frac{3 I_b}{|\mathbf{r} - \mathbf{b}|^3} \left(\boldsymbol{\omega}_b [(\mathbf{r} - \mathbf{b}) \times \dot{\mathbf{b}}]\right) + \ldots \right\}. \tag{2.64}$$

Introducing effective mass

$$m_a = M_a + \frac{1}{c^2} \xi^{(a)} \tag{2.65}$$

and determining the potentials $g_{\mu\nu}$ by formulas (2.20), we find the metric of the external gravitational field N of rotating spherically symmetric bodies in harmonic coordinates

$$ds^2 = \left\{1 - \frac{2\gamma}{c^2}\sum_a \frac{m_a}{|\mathbf{r}-\mathbf{a}|} + \frac{2\gamma^2}{c^4}\left(\sum_a \frac{m_a}{|\mathbf{r}-\mathbf{a}|}\right)^2 - \frac{\gamma}{c^4}\frac{\partial^2}{\partial t^2}\sum_a m_a|\mathbf{r}-\mathbf{a}| - \right.$$

$$- \frac{3\gamma}{c^4}\sum_a \frac{m_a}{|\mathbf{r}-\mathbf{a}|}\dot{\mathbf{a}}^2 + \frac{2\gamma^2}{c^4}\sum_a \frac{m_a}{|\mathbf{r}-\mathbf{a}|}\sum_b{}^{(a)} \frac{m_b}{|\mathbf{a}-\mathbf{b}|} - \frac{6\gamma}{c^4}\sum_a \frac{I_a}{|\mathbf{r}-\mathbf{a}|^3} \times$$

$$\left. \times (\boldsymbol{\omega}_a[(\mathbf{r}-\mathbf{a})\times\dot{\mathbf{a}}]) - \frac{6\gamma}{c^4}\sum_a \frac{I_a}{|\mathbf{r}-\mathbf{a}|}\boldsymbol{\omega}_a^2 \right\} c^2 dt^2 + \frac{8\gamma}{c^3}\sum_a \left\{ \frac{m_a}{|\mathbf{r}-\mathbf{a}|}\dot{\mathbf{a}}_i + \right.$$

$$\left. + \frac{I_a}{|\mathbf{r}-\mathbf{a}|^3}[\boldsymbol{\omega}_a \times (\mathbf{r}-\mathbf{a})]_i \right\} c\, dt\, dx_i - \left(1 + \frac{2\gamma}{c^2}\sum_a \frac{m_a}{|\mathbf{r}-\mathbf{a}|}\right) d\mathbf{r}^2. \tag{2.66}$$

2.4 Propagation of gamma radiation in a quadruple magnetic field.

According to the ideas of modern theoretical astrophysics[94], neutron stars have magnetic dipole field, which on their surface reaches the values comparable with quantum electrodynamic induction $B_q = 4.41 \cdot 10^{13}\mathrm{G}$. In a such field, the nonlinearity of electrodynamics in a vacuum must appear, leading to the appearance of various physical effects[75, 81, 82, 88, 89]. Theoretical studies of such nonlinear electrodynamic processes use the post-Maxwellian approximation [95].

In this approximation, the Lagrangian of the nonlinear electrodynamics of vacuum is written in the parameterized form:

$$L = \frac{1}{32\pi}\{2J_2 + \xi[(\eta_1 - 2\eta_2)J_2^2 + 4\eta_2 J_4]\} - \frac{1}{c}J^m A_m \tag{2.67}$$

where $J_2 = F_{nk}F^{kn}$ and $J_4 = F_{nk}F^{km}F_{mi}F^{in}$ –are invariants of the electromagnetic field tensor F_{kn}, $\xi = 1/B_q^2$, $n_{1,2}-$ are post-Maxwellian parameters whose magnitude varies in different theoretical models of nonlinear electrodynamics of vacuum[80].

In the Heisenberg-Euler theory, which is a consequence of quantum electrodynamics, the numerical values of the parameters η_1 and η_2 are not equal to each other: $\eta_1 = e^2/45\pi\hbar c = 5.1 \cdot 10^{-5}$, $\eta_2 = 7e^2/(180\pi\hbar c) = 9.0 \cdot 10^{-5}$.

In the nonlinear Born-Infeld electrodynamics the parameters η_1 and η_2 coincide: $\eta_1 = \eta_2 = aB_q/4$. M. Born and L. Infeld have obtained an estimation $1/a = 9.18 \cdot 10^{15}$ Gauss for the constant a. Then in the nonlinear Born-Infeld electrodynamics $\eta_1 = \eta_2 = 5.8 \cdot 10^{-6}$.

The equations of the electromagnetic field with the Lagrangian (2.67) have the form:

$$\frac{\partial^2}{\partial x^n}\{[1 + \xi(\eta_1 - 2\eta_2)J_2]F^{mn} + 4\xi\eta_2 F^{mk}F_{kp}F^{pn}\} = -\frac{4\pi}{c}j^m \tag{2.68}$$

The second pair of equations of the electromagnetic field coincides with the corresponding equations of Maxwell's theory:

$$\frac{dF_{kn}}{dx^m}+\frac{dF_{nm}}{dx^k}+\frac{dF_{mk}}{dx^n}=0 \tag{2.69}$$

When studying the laws of propagation for weak electromagnetic waves in a strong external field F_{ik} the Eikonal equation was used. This equation was obtained in a number of previously published papers [86,96]). Calculations have shown that the propagation of a weak electromagnetic wave according to the laws of nonlinear electrodynamics (2.68) in space-time with a metric tensor g_{nk} and in the presence of an external electromagnetic field occurs by geodesic of some elective pseudo-Riemannian space-time. The metric tensor of this space-time G_{nk} depends on the metric tensor g_{nk}; the quadratic combination of the electromagnetic field tensor $F_{ni}g^{im}F_{mk}$ and at $\eta_1 \neq \eta_2$ it is different for waves of different polarization (nonlinear electrodynamic birefringence). While for the first normal wave the tensor G_{nk} has the form

$$G^{(1)}_{nk}=g_{nk}-4\eta_1\xi F_{ni}g^{im}F_{mk} \tag{2.70}$$

for the second normal wave, having orthogonal polarization to the polarization of the first wave, the tensor differs by the second term coefficient:

$$G^{(2)}_{nk}=g_{nk}-4\eta_2\xi F_{ni}g^{im}F_{mk} \tag{2.71}$$

According to the Lagrange-Charpit theorem, this means that in order to find the trajectories along which the pulse of a weak electromagnetic wave propagates in the external field and determine the laws of its motion along these trajectories, we need to solve the equations of isotropic geodesic motion in the effective space-time with the metric tensor $G^{(1,2)}_{nk}$:

$$\frac{dK^i}{d\sum}+\Gamma^i_{mn}K^mK^n=0\ ,\ G^{(1,2)}_{mn}K^nK^m=0\ , \tag{2.72}$$

where $\Gamma^i_{mn}-$ are Christopher symbols of the space-time with a metric tensor $G^{(1)}_{nk}$ or $G^{(2)}_{nk}$, depending on the mode being studied, $\Sigma-$is affine parameter, $K^i=dx^i/d\Sigma-$ is a four-vector tangent to the corresponding isotropic geodesic.

Affine parameter $\Sigma-$ is not related to curvilinear abscissa "s" in space-time, because for isotropic geodesic motion we have: $ds=0$ but $d\Sigma\neq 0$.

This method has been successfully used to study various nonlinear processes occurring in magnetic dipole fields of pulsars and magnetars [82], as well as in an electric dipole field [89]. Calculations have shown that in this case the rays of electromagnetic waves are bent, and the electromagnetic wave itself splits at $\eta_1 \neq \eta_2$ into two normal modes with mutually perpendicular polarization. These modes propagate along different rays at different speeds. At the present time another polarization effect of nonlinear electrodynamics of vacuum is observed [99, 84]: polarized thermal emission from X-ray dim isolated neutron stars (the case of RX J1856.5-3754).

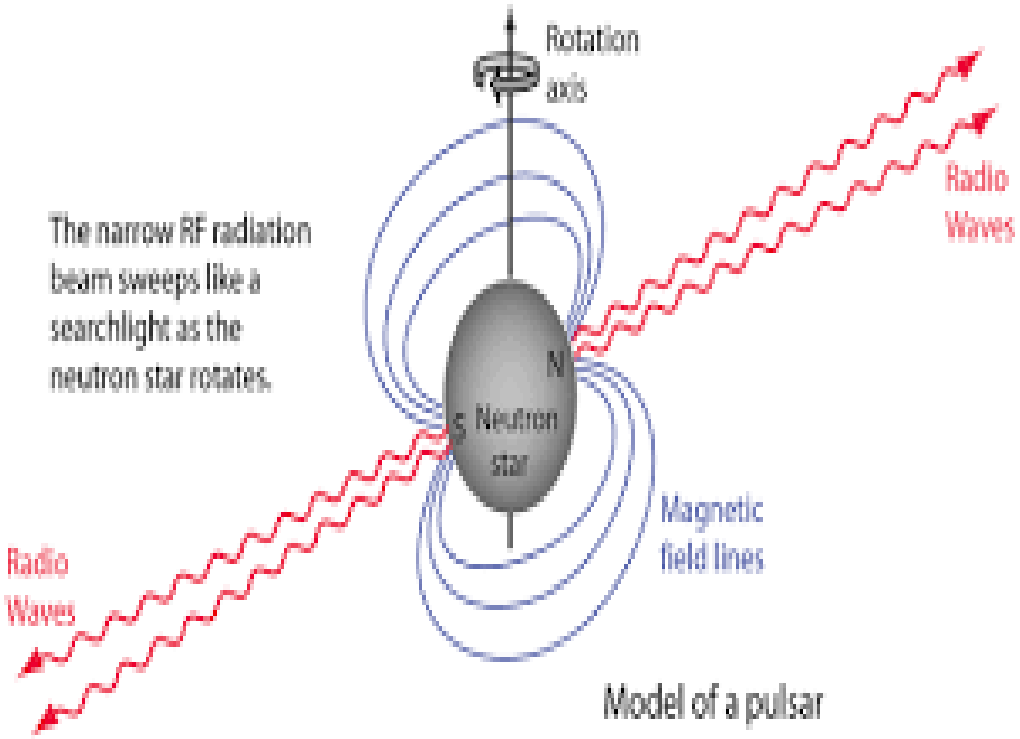

Figure 19 – Model of a pulsar as a rotating neutron star with an inclined magnetic field [104].

Recent papers [97] assume that neutron stars can also have quadruple magnetic field, the intensity of which can reach the intensity of dipole fields [78,79,80].

To the date, there was not any study of the nonlinear-electrodynamic effect of the magnetic quadruple field on the propagation of pulses of electromagnetic radiation. Therefore, the purpose of this article is to calculate the non-linear effect of the magnetic dipole and quadruple fields on the propagation of electromagnetic waves.

We place the origin of the Cartesian coordinate system at the point where the pulsar or magnetar is located. Then, the vector of magnetic induction **B** will have the form:

$$\mathbf{B} = \mathbf{B}_1 + \mathbf{B}_2 \tag{2.73}$$

where $\mathbf{B_1}$ is the vector of the dipole magnetic induction, $\mathbf{B_2}$ is the vector of the quadruple magnetic induction.

In the Maxwellian approximation we have:

$$\mathbf{B}_1(\mathbf{r}) = \frac{3(\mathrm{mr})\,\mathrm{r} - \mathrm{r}^2\, m}{r^5} \tag{2.74}$$

where **m** is the magnetic dipole moment of the pulsar or magnetar.

The components of the quadruple magnetic induction vector $\mathbf{B_2}$ in a spherical coordinate system r, θ, φ as shown in [97], will have the form:

$$B_r = -\frac{BR_S^4}{r^4}\{[\frac{1}{2}\sqrt{\frac{5}{2}}(1+3\cos 2\theta)]\cos\chi_1 - [3\sqrt{\frac{5}{6}}\sin 2\theta\cos\varphi]\sin\chi_1\cos\chi_2 +$$

$$[3\sqrt{\frac{5}{6}}\sin^2\theta\cos 2\varphi]\sin\chi_1\sin\chi_2\},$$

$$B_\theta = -\frac{BR_S^4}{r^4}\{[\sqrt{\frac{5}{2}}\sin 2\theta]\cos\chi_1 + [10\sqrt{\frac{1}{30}}\cos 2\theta\cos\varphi]\sin\chi_1\cos\chi_2 -$$

$$[\sqrt{\frac{5}{6}}\sin 2\theta\cos 2\varphi]\sin\chi_1\sin\chi_2\},$$

$$B_\varphi = \frac{BR_S^4}{r^4}\{5\sqrt{\frac{2}{15}}\cos\theta\sin\varphi\sin\chi_1\cos\chi_2 - \sqrt{\frac{10}{3}}\sin\theta\sin 2\varphi\sin\chi_1\sin\chi_2\}, \tag{2.75}$$

where R_S is the neutron star radius, B is a constant having a dimension of magnetic induction, $\chi_1 \in [0,\pi]$ and $\chi_2 \in [0,2\pi]$ are two angles specifying the particular geometry of the quadruple magnetic field [78].

However, for further calculations it is more convenient for us to use a rectangular Cartesian coordinate system. Re-designating the constants B, χ_1 and χ_2 in accordance with relations

$$B_0 = B\sqrt{1+2\cos^2\chi_1}$$

$$\cos\xi = \frac{\sqrt{3}\cos\chi_1}{\sqrt{1+2\cos^2\chi_1}} \quad , \quad \sin\xi = \frac{\sin\chi_1}{\sqrt{1+2\cos^2\chi_1}} \tag{2.76}$$

from the expressions (2.75) we obtain:

$$B_{2x} = \sqrt{\frac{5}{6}} \frac{B_0 R_S^4}{r^7} \{x[r^2 - 5z^2] f_1 + 2z[5x^2 - r^2] f_2 + x[5z^2 - 3r^2 + 10y^2] f_3\},$$

$$B_{2y} = \sqrt{\frac{5}{6}} \frac{B_0 R_S^4 y}{r^7} \{[r^2 - 5z^2] f_1 + 10xz f_2 + [3r^2 - 10x^2 - 5z^2] f_3\}, \quad (2.77)$$

$$B_{2z} = \sqrt{\frac{5}{6}} \frac{B_0 R_S^4}{r^7} \{z[3r^2 - 5z^2] f_1 + 2x[5z^2 - r^2] f_2 - 5z[x^2 - y^2] f_3\},$$

where the notations were introduced: $f_1 = cos\xi, f_2 = sin\xi cos\chi_2$ at that $f_1^2 + f_2^2 + f_3^2 = 1$. The B_0 constant can be expressed in terms of the magnetic induction of a quadruple B_N at a point $\theta = \frac{\pi}{2}, \varphi = \frac{\pi}{4}$ on the surface of a neutron star:

$$B_{.0} = B_N \sqrt{\frac{6}{5(1 + (1 + 2\sin^2 \chi_1)\sin^2 \xi)}} \quad (2.78)$$

Suppose that an electromagnetic pulse is emitted from a certain point $\mathbf{r} = \mathbf{r}_s = \{x_s, y_s, z_s\}$ at time $t = t_s$. We assume that at the point $\mathbf{r} = \mathbf{r}_d = \{x_d, y_d, z_d\}$ there is an electromagnetic radiation detector. We orient the axes of the Cartesian coordinate system so that the source and the electromagnetic radiation detector lie in the XOZ; plane, and the Z axis is directed so that the following conditions are fulfilled: $x_s = x_d, y_s = y_d = 0$. Then $\mathbf{r}_s = \{x_s, 0, z_s\}$ and $\mathbf{r}_d = \{x_s, 0, z_d\}$. (see figure 20).

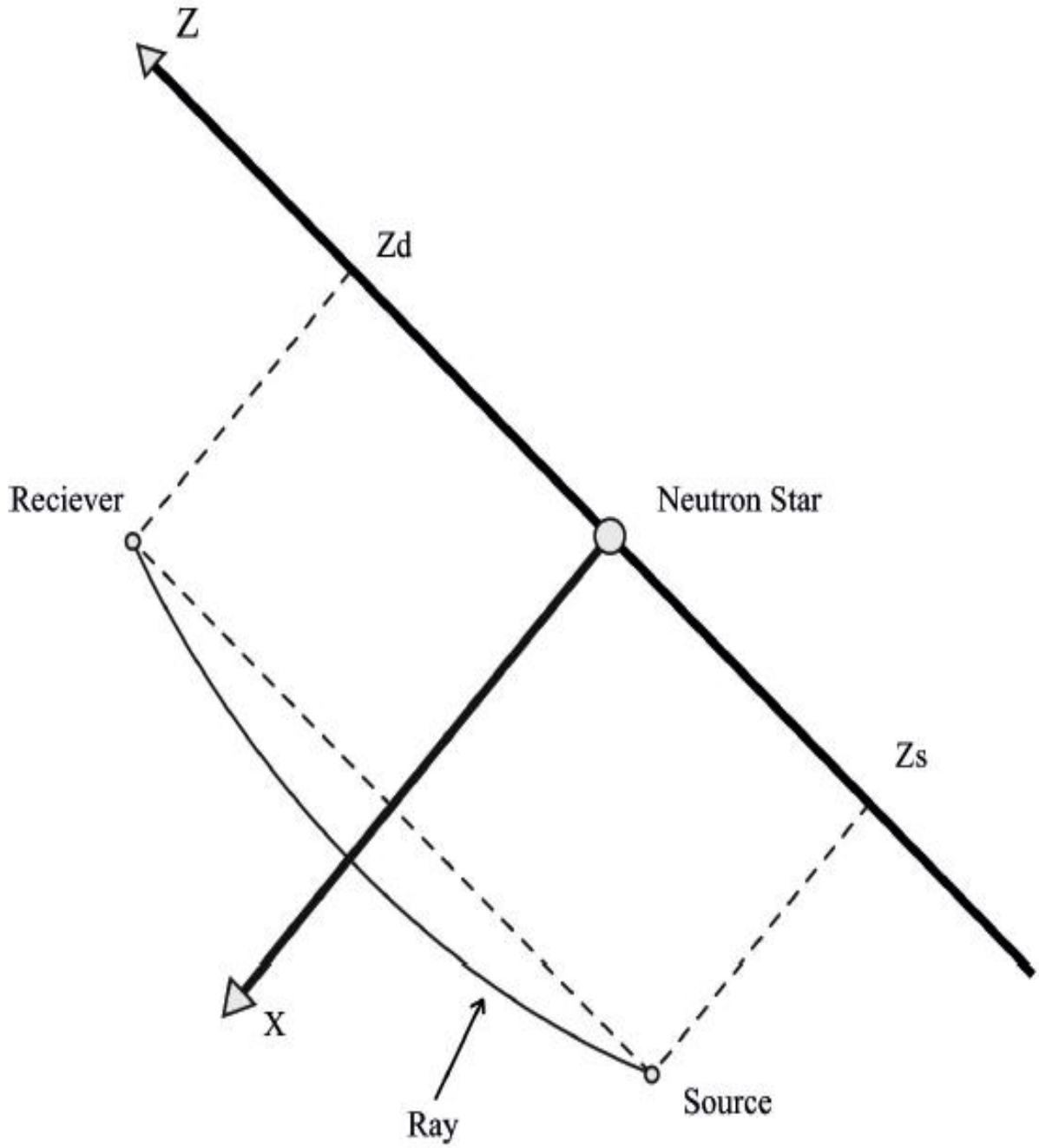

Figure 20 – The orientation of the coordinate axes and the location of the source and receiver of hard radiation.

As in [89], we will consider the propagation of pulses of only X-ray and gamma frequencies, for which the influence of the magnetosphere of a pulsar and a magnetar can be neglected. Let us find out by which rays the electromagnetic pulses will propagate from the point $\mathbf{r}_d$ to the point rd, and also determine the laws of motion of electromagnetic pulses along these rays [79].

Pulsars and magnetars have a gravitational field, which can to impact on the propagation of X-ray and gamma pulses. To study the post-Newtonian motion of photons components of the metric tensor g_{ik} to be written in a linear approximation on the gravitational potential $\psi = r_g/r,$ where r_g is star's gravitational radius.

The components of the metric tensor g_{ik} with the required accuracy, take the form

$$g_{00} = 1 - \frac{r_g}{r} \quad , \quad g_{11} = g_{22} = g_{33} = -[1 + \frac{r_g}{r}], \tag{2.79}$$

The remaining components of the tensor g_{ik} are zero.

Using expressions (2.79), we find the components of metric tensors $G_{nk}^{(1,2)}$ of the effective pseudo-Riemannian space-time (2.70) - (2.71) for the problem under consideration:

$$G_{00}^{(1,2)} = 1 - \frac{r_g}{r}$$

$$G_{\alpha\beta}^{(1,2)} = -\delta_{\alpha\beta}[1 + \frac{r_g}{r} + 4\eta_{1,2}\mathbf{B}^2(\mathbf{r})] + 4\eta_{1,2}\xi B_\alpha(\mathbf{r})\mathrm{B}_\beta(\mathbf{r}) \tag{2.80}$$

Thus, we have two small dimensionless parameters: r_g/r and $\eta_{1,2}\xi\mathbf{B}^2(r)$, differently depending on the distance r. The main part of gravitational and nonlinear electrodynamics influence on the X-ray and gamma pulses are felt near the neutron star $r \sim R_s$, where should satisfy the relation $(r_g/R_s)^2 \sim \eta_{1,2}\xi B^2(R_s) < 10^{-4}$. Therefore for further calculations we must hold in the linear approximation on $\eta_{1,2}\xi B^2(R_s)$ and quadratic approximation in the small parameter (r_g/R_s). The propagation of electromagnetic waves in the gravitational field has been considered repeatedly in the scientific literature[87]. As shown in these papers, there is no birefringence in the gravitational field, as a result of which the law of propagation of an electromagnetic wave does not depend on its polarization. Rays of any wave in approximation $(r_g/R_s)^2$ are bent by the angle $\delta\psi \sim 2r_g/R_s \sim 10^{-5}$ rad. The nonlinear-electrodynamic action of $\sim\eta_{1,2}\xi B^2(R_s)$ on the propagation of electromagnetic waves in the problem under consideration has the form of an additive correction and does not depend on (r_g/R_s). Therefore, in this paper we will not consider the well-studied effect of the gravitational field, but focus our attention on the additive correction $\sim\eta_{1,2}\xi B^2(R_s)$. This means that as background metric g_{ik} we will use the Minkowski metric.

To calculate the effects in the linear approximation in the small parameter $\eta_{1,2}\xi B^2(R_s)$, the vector **B** in the expression (2.73) must be taken in Maxwell's approach.

The equations of geodesics (2.72) in space-time (2.70) - (2.71), following [96], can be written by differentiating not with respect to the parameter Σ, but in the coordinate z in accordance with expression $d/d\Sigma = \mathrm{K}^3 d/dz$: As a result, we get:

$$\frac{d^2ct}{dz^2}-\{\Gamma^0_{mp}-\frac{dct}{dz}\Gamma^3_{mp}\}\frac{dx^p}{dz}\frac{dx^m}{dz}$$

$$\frac{d^2x}{dz^2}=-\{\Gamma^1_{mp}-\frac{dx}{dz}\Gamma^3_{mp}\}\frac{dx^p}{dz}\frac{dx^m}{dz} \qquad (2.81)$$

$$\frac{d^2y}{dz^2}=-\{\Gamma^2_{mp}-\frac{dy}{dz}\Gamma^3_{mp}\}\frac{dx^p}{dz}\frac{dx^m}{dz}$$

System of equations (2.81) has the first integral:

$$\frac{dx^n}{dz}\frac{dx^p}{dz}G^{(1,2)}_{np}=0 \qquad (2.82)$$

From the system of equations (2.81) - (2.82) one can find the equations for rays $x = x(z), y = y(z)$ and the law of motion of electromagnetic pulses along these rays $t = t(z)$ in a parametric form, where the coordinate *z* plays the role of the parameter [78].

From the source of hard electromagnetic radiation located at $r_s = \{x_s, 0, z_s\}$, the electromagnetic radiation propagates along the rays in different directions. From this beam of rays we are only interested in the ray passing through the detector located at the point $r_d = \{x_d, 0, z_d\}$. To isolate this ray in the general solution we shall use not the initial but the boundary conditions for equations (2.81):

$$x(z_s)=x(z_d)=x_s, y(z_s)=y(z_d)=0, t(z_s)=t_s \qquad (2.83)$$

Equations (2.81) and (2.82) are nonlinear, for which the usual methods of integration [92, 101,102] are not applicable. However, they contain a small parameter $\eta_{1,2}\xi B^2(r) \le \eta_{1,2}\xi B^2(R_s) \ll 1$, Therefore, as in [96], we represent expressions $x = x_{1,2}(z),\ y = y_{1,2}(z), t = t_{1,2}(z)$ in the form of expansions with respect to this small parameter:

$$t_{1,2}(z) = t_0(z) + \eta_{1,2}\xi[t(z) - t(z_s)],$$

$$x_{1,2}(z) = x_0(z) + \eta_{1,2}\xi[X(z) - X(z_s) + \frac{(z-z_s)[X(z_s)-X(z_d)]}{(z_d-z_s)}], \qquad (2.84)$$

$$y_{1,2}(z) = y_0(z) + \eta_{1,2}\xi[Y(z) - Y(z_s) + \frac{(z-z_s)[Y(z_s)-Y(z_d)]}{(z_d-z_s)}].$$

Functions $t_{1,2}(z), x_{1,2}(z)$ and $y_{1,2}(z)$, by virtue of the boundary conditions (2.83),

describe the propagation of the electromagnetic pulse from $z = z_S$ to $z = z_d$. If z changes sign as a result of the transformation $z \to -z$, then in the expressions $x = x(z), y = y(z)$ and $t = t(z)$, we need to change the sign of z_S and z_d also.

We now substitute the expressions (2.84) into equations (2.81) - (2.82) and expand them according to the available small parameter. Then in the Maxwellian approximation we will have:

$$c\frac{d^2t_0(\mathrm{z})}{dz^2} = \frac{d^2x(\mathrm{z})}{dz^2} = \frac{d^2y_0(\mathrm{z})}{dz^2} = 0$$

$$c^2\left(\frac{dt_0(\mathrm{z})}{dz}\right)^2 - \left(\frac{dx_0(\mathrm{z})}{dz}\right)^2 - \left(\frac{dy_0(\mathrm{z})}{dz}\right)^2 = 1 \qquad (2.85)$$

From these equations, taking into account conditions (2.83), it follows that:

$$t_0(\mathrm{z}) = \mathrm{t}_s + \frac{z - z_0}{c},\ x_0(\mathrm{z}) = x_s, y_0(\mathrm{z}) = 0 \qquad (2.86)$$

According to these expressions, in the absence of the influence of the magnetic field on the propagation of the electromagnetic pulse, it moves along the straight line $x_0(z) = x_S, y_0(z) = 0$ and has the law of motion $Z = z_S + c(t - t_S)$.

Substituting expressions (2.84) and (2.85) into equations (2.81)-(2.82), we can obtain equations for the next approximation. From the first integral (2.82) in this case we have:

$$c\frac{dt(\mathrm{z})}{dz} = 2\left\{B_x^2 + B_y^2\right\} =$$

$$= \frac{18x_s^3}{r^{10}}\left[x_s(\mathrm{m}_x^2 - \mathrm{m}_z^2) + 2\mathrm{m}_x m_z z\right] + \frac{6x_s}{r^8}\left[x_s(3\mathrm{m}_z^2 - 2\mathrm{m}_x^2) - 2\mathrm{m}_x m_z z\right]$$

$$+ \frac{2}{r^6}\left(m_x^2 + m_y^2\right)$$

$$+ \frac{2\sqrt{30}B_0R^4}{3}\{\frac{15x_s^4}{r^{12}}[x_s(f_1\mathrm{m}_x - 2f_2\mathrm{m}_z - f_3\mathrm{m}_x)$$

$$+ z(f_1\mathrm{m}_z + 2f_2\mathrm{m}_x - 3f_3\mathrm{m}_z)$$

$$+ \frac{x_s^2}{r^{10}}[x_s(36f_2m_z - 17f_1m_x + 11f_3m_x)$$

$$+ z(6f_3\mathrm{m}_z - 12f_1\mathrm{m}_z - 16f_2\mathrm{m}_x)$$

$$+ \frac{2}{r^8}[x_s(2f_1\mathrm{m}_x - 3f_2\mathrm{m}_z - f_3\mathrm{m}_x) + zf_2m_x]\} +$$

$$+\frac{5B_0^2R_s^8}{3}\left\{\frac{25x_s^5}{r^{14}}\left[4zf_2(f_1-f_2)+x_s(1-2f_1f_3-5f_2^2)\right]\right\}+$$
$$+\frac{20x_s^3}{r^{12}}[zf_2(3f_3-5f_1)+x_s(f_3^2+9f_2^2+3f_1f_3-2)]+$$
$$+\frac{4f_2^2}{r^8}+\frac{4x_s}{r^{10}}[2z\,f_2(2f_1-f_3)+x_s(4-4f_1f_3-15f_2^2-3f_3^3)]\ ,$$

(2.87)

where m_x, m_y, m_z are corresponding components of the magnetic dipole moment of the pulsar or magnetar m and in the approximation under consideration $r = \sqrt{z^2+x_s^2}$.

Integrating this equation, we find the dependence of $t(z)$:

$$ct(z)=\{\frac{1}{8r^6}\left[z\left(3m_z^2+5m_x^2\right)+16x_sm_zm_x\right]-$$
$$-\frac{9x_s^2}{4r^8}\left[z\left(m_z^2-m_x^2\right)+2x_sm_zm_x\right]+\left[\frac{z}{32r^4x_s^2}-\frac{3z}{64r^2x_s^2}+\frac{3}{64x_s^5}a\tan\left(\frac{z}{x_s}\right)\right]\times$$
$$\times\left[16\mathbf{m}^2-m_z^2+25m_x^2\right]\}+\frac{5B_0^2R_s^8}{6}\{\frac{50x_s^5}{3r^{12}}f_2(f_3-f_1)+\frac{4x_s^3}{r^{10}f_2}(5f_1-3f_3)+$$
$$+\frac{x_s}{r^8}f_2\left(2f_3-4f_1\right)-\frac{8f_2^2z}{7r^8}+\frac{25x_s^4z}{6r^{12}}(1-5f_2^2-2f_1f_3)-$$
$$-\frac{x_s^2z}{12r^{10}}(41-48f_3^2-157f_2^2-34f_1f_3)+\frac{5}{512}[a\tan\left(\frac{z}{x}\right)+$$
$$+\frac{zx_s}{r^2}+\frac{2zx_s^3}{3r^4}+\frac{8zx_s^5}{15r^6}+\frac{16zx_s^7}{35r^8}]\left[35-182f_1f_3+193f_2^2+336f_3^2\right]\}+$$
$$+\sqrt{30}B_0R_s^4\{\frac{(15f_1m_x+30f_2m_z-67f_3m_x)}{1152x_s^6}\times$$
$$\times\left[a\tan\left(\frac{z}{x_s}\right)+\frac{15zx_s^3}{r^4}+\frac{8zx_s^5}{r^6}\right]-\frac{2f_2m_x}{9r^6}-$$
$$-\frac{x_s}{24r^8}[z(7f_1m_x-8f_2m_z+5f_3m_x)+4x_s(3f_3m_z-$$
$$8f_2m_x-6f_1m_z)]-\frac{x_s^3}{r^{10}}[z(f_3m_x+2f_2m_z-f_1m_x)+$$
$$x_s(2f_2m_x+f_1m_z-f_3m_z)]\}$$

(2.88)

For the function $X(z)$ entering into the expressions (2.84), we obtain the following equation:

$$\frac{d^2X(z)}{dz^2}=\frac{180x_s^4}{r^{12}}\left[x_s(m_x^2-m_z^2)+2zm_x m_z\right]+$$

$$+\frac{12x_s^2}{r^{10}}\left[x_s\left(25m_z^2-21m_x^2\right)-31zm_x m_z\right]+$$

$$+\frac{12}{r^8}\left[x_s\left(4m_x^2-m_y^2-11m_z^2\right)+3zm_x m_z\right]+$$

$$+\frac{1750B_0^2R_s^8x_s^4}{3r^{16}}\{4zf_2(f_1-f_3)+x_s(1-2f_1f_3-5f_2^2+f_3^2)\}+$$

$$+\frac{100B_0^2R_s^8}{3r^{10}}\{z(43f_1-13f_3)f_2+x_s(25-28f_1f_3-101f_2^2+20f_3^2)+$$

$$\frac{40B_0^2R_s^8}{3r^{10}}\{x_s(15f_3^2+5f_1f_3-14+35f_2^2)-z(6f_1+f_3)f_2\}+$$

$$+\frac{2\sqrt{30}B_0R_s^4}{3r^8}\{\frac{180x_s^5}{r^6}[x_s(f_1m_x-f_3m_x-2f_2m_z)+$$

$$+z(f_1m_z+2f_2m_x-f_3m_z)]+$$

$$+\frac{5x_s^3}{r^4}[x_s(51f_3m_x-63f_1m_x+130f_2m_z)+z(38f_3m_z-50f_1m_z-$$

$$-84f_2m_x)]+\frac{2x_s}{r^2}[x_s(70f_1m_x-25f_3m_x163f_3m_z)+$$

$$+z(44f_1m_z+32f_2m_x-10f_3m_z)]+2[11f_2m_z-5f_1m_x-f_3m_x]\}.$$

Integrating this equation, we find:

$$X(z)=\frac{3}{64x_s^6}[52x_sm_xm_z-5z(41m_x^2+16m_y^2+15m_z^2)\operatorname{atan}\left(\frac{z}{x_s}\right)-$$

$$-\frac{9x_s^2}{4r^8}[x_s(m_x^2-m_z^2)+2zm_xm_z]+\frac{1}{8r^6}[20zm_xm_z+x_s(15m_x^2-23m_z^2)]+$$

$$+\frac{1}{32x_s^2r^4}[x_s(41\mathrm{m}_x^2+16\mathrm{m}_y^2+15\mathrm{m}_z^2)+52\mathrm{z}m_x m_z]+$$

$$+\frac{1}{64x_s^4r^2}[156zm_x m_z+5x_s(41\mathrm{m}_x^2+16\mathrm{m}_y^2+15\mathrm{m}_z^2)]+$$

$$+\frac{25B_0^2R_s^8}{3072x_s^8}\{z(1274f_1f_3-1596f_2^2-245f_1^2-$$

$$-2597f_3^2)-64x_s(f_1+13f_3)f_2)\}\mathrm{atan}\left(\frac{z}{x_s}\right)+$$

$$+\frac{125B_0^2R_s^8x_s^4}{36r^{12}}\{4z(f_3-f_1)f_2-x_s(f_1^2-2f_1f_3-4f_2^2+f_3^2)\}+$$

$$+\frac{5B_0^2R_s^8x_s^2}{72r^{10}}\{16z(13f_1-7f_3)f_2-x_s(83f_1^2-118f_1f_3-284f_2^2+36f_3^2)\}+$$

$$+\frac{5B_0^2R_s^8}{576r^8}\{x_s(145f_3^2+524f_2^2+46f_1f_3-287f_1^2)-$$

$$-192z(f_1+2f_3)f_2\}+\frac{5B_0^2R_s^8}{1152x_s^2r^6}\{x_s(35f_1^2+228f_2^2-182f_1f_3+$$

$$+371f_3^2)-64z(f_1+13f_3)f_2\}+\frac{5B_0^2R_s^8}{4608x_s^4r^4}\{x_s(245f_1^2-$$

$$-1274f_1f_3+1596f_2^2+2597f_3^2)-320z(f_1+13f_3)f_2\}+$$

$$+\frac{25B_0^2R_s^8}{9216x_s^6r^2}\{x_s(245f_1^2-1274f_1f_3+1596f_2^2+2597f_3^2)-$$

$$-192z(f_1+13f_3)f_2\}+$$

$$+\sqrt{30}B_0R_s^4\{\frac{15}{1152x_s^7}a\tan\left(\frac{z}{x_s}\right)[x_s(82f_2m_x-15f_1m_z-$$

$$-37f_3m_z)+6z(67f_3m_x-30f_2m_z-15f_1m_x)]+$$

$$+\frac{15}{1152x_s^5r^2}[z(82f_2m_x-15f_1m_z-37f_3m_z)+2x_s(15f_1m_x+$$

$$+30f_2m_z-67f_3m_x)]+\frac{1}{576x_s^3r^4}[5z(82f_2m_x-37f_3m_z-$$

$$-15f_1m_z)+6x_s(30f_2m_z+15f_1m_x-67f_3m_x)]+$$

$$+\frac{1}{144x_sr^6}[z(82f_2m_x-37f_3m_z-15f_1m_z)+2x_s(38f_2m_z-$$

$$-5f_1m_x-31f_3m_x)]+\frac{x_s}{24r^8}[z(30f_2m_x+23f_1m_z-11f_3m_z)+$$

$$2x_s(15f_1m_x-32f_2m_z-9f_3m_x)]+\frac{x_s^3}{r^{10}}[z(f_3m_z-2f_2m_x-$$
$$-f_1m_z)+x_s(f_3m_x+2f_2m_z-f_1m_x)] \tag{2.89}$$

The function $Y(z)$ satisfies the equation:

$$\frac{d^2Y(z)}{dz^2}=\frac{12m_y}{r^8}\left[(5x_sm_x+3zm_z)-\frac{5x_s^2(x_sm_x+zm_z)}{r^2}\right]+$$

$$\frac{2\sqrt{30}m_yB_0R_s^4}{3r^8}\{\frac{35x_s^3}{r^4}[x_s(f_3-f_1)-2zf_2]+\frac{2x_s}{r^2}[x_s(22f_1-17f_3)+24zf_2]+2f_3-10f_1 \tag{2.90}$$

The solution of this equation has the form:

$$Y(z)=\frac{m_yB_0R_s^4\sqrt{30}}{1152x_s^7}\{(15(15f_1z+2f_2x_s-3f_3z)a\tan\left(\frac{z}{x_s}\right)+$$
$$+\frac{15x_s^2}{r^2}[f_3x_s+2f_2z-5f_1x_s]-\frac{2x_s^4}{r^4}[15f_1x_s-10f_2z-3f_3x_s]-$$

$$-\frac{8x_s^6}{r^6}[25f_1x_s-2f_2z-5f_3x_s]+\frac{336x_s^8}{r^8}[f_1x_s+2f_2z-f_3x_s]\}-$$

$$-\frac{5m_y}{4r^6}[zm_z + x_s m_x] + \frac{m_y}{16r^4 x_s^2}[zm_z - 5x_s m_x] +$$

$$+\frac{m_y}{64r^2 s_s^4}[3zm_z - 25x_s m_x] + \frac{3m_y}{32x_s^6} arctg\left(\frac{z}{x_s}\right)[x_s m_z + 25zm_x]. \quad (2.91)$$

Relations (2.84) and (2.87)-(2.91) completely determine the equations for rays, according to the post-Maxwellian electrodynamics of vacuum, and also the law of motion of electromagnetic pulses along these rays.

Let us consider the effects of the nonlinear electrodynamic action of the magnetic dipole and quadruple fields on the electromagnetic wave. Let us first find the magnitude of the angle of curvature of rays due to the nonlinearity of electrodynamics in vacuum. For this we introduce the vector $N(z) = d\boldsymbol{r}/dz$; tangent to the ray at an arbitrary point z: Using the expressions (8.84), we have

$$N(z) = \eta_{1,2}\xi\left\{\left[\frac{dX(z)}{dz} + \frac{X(z_s) - X(z_d)}{z_d - z_s}\right]\mathbf{e}_x + \left[\frac{dY(z)}{dz} + \frac{Y(z_s) - Y(z_d)}{z_d - z_s}\right]\mathbf{e}_y\right\} + \mathbf{e}_z \quad (2.92)$$

Taking into account that in the post-Maxwellian approximation $|\mathbf{N}| = 1$; angle β of the curvature of the ray in the XOZ plane can be determined by examining the expression for the vector product $[\mathbf{N}(z_s), \mathbf{N}(z_d)]$:

$$\sin\beta = \left|\left[\mathbf{N}(z_s), \mathbf{N}(z_d)\right]\right|_y = \eta_{1,2}\xi\left[\frac{dX(z)}{dz}_{|z=z_s} - \frac{dX(z)}{dz}_{|z=z_d}\right]. \quad (2.93)$$

The angle ψ of the curvature of the ray in the YOZ plane can be determined by examining the expression for the vector product $[\mathbf{N}(z_s), \mathbf{N}(z_d)]$:

$$\sin\psi = \left|\left[\mathbf{N}(z_s), \mathbf{N}(z_d)\right]\right|_x = \eta_{1,2}\xi\left[\frac{dY(z)}{dz}_{|z=z_s} - \frac{dY(z)}{dz}_{|z=z_d}\right]. \quad (2.94)$$

The expressions (2.93) and (2.94) take the simplest form in the case when the pulsar or magnetar is at an equal distance from the emitter and the receiver of electromagnetic waves ($z_d = -z_s$) and $z_d >> x_s$: In this case, the sine of the angle of curvature of the ray in the XOZ plane is equal to:

$$\sin\beta = -\eta_{1,2}\xi\{\frac{15\pi}{64x_s^6}\left[41m_x^2 + 16m_y^2 + 15m_z^2\right] +$$

$$+\frac{175\pi B_0^2 R_s^8}{3072 x_s^8}[35-182 f_1 f_3+193 f_2^{\,2}+336 f_3^{\,2}]+$$

$$+\frac{5\pi\sqrt{30}B_0 R_s^4}{64 x_s^7}[15 f_1 m_x+30 f_2 m_z-67 f_3 m_x]\}. \qquad (2.95)$$

The sine of the angle of curvature of the ray in the YOZ plane is equal to:

$$\sin\psi=\eta_{1,2}\xi\left\{\frac{75\pi m_x m_y}{32 x_s^6}+\frac{5\pi\sqrt{30}B_0 R_s^4 m_y}{128 x_s^7}\left[5 f_1-f_3\right]\right\}. \qquad (2.96)$$

Estimates show that when $|\mathbf{B}|\sim 10^{13}$ G the angles β and ψ can reach several arc seconds.

Further, for $\eta_1 \neq \eta_2$ because of the nonlinear electrodynamic birefringence, each electromagnetic pulse emitted at the point $\mathbf{r}_0=\{x_s,0,z_s\}$, splits into two pulses, one of which is carried by the first normal wave and the other by the second normal wave having orthogonal polarization. These pulses move to the receiver along different rays, spending on this way different time. Let us calculate in the case, when $z_d=-z_s \gg x_s$, the delay time of the electromagnetic pulse carried by the first normal wave, in comparison with the propagation of the pulse carried by the second normal wave. Using expressions (2.84) and (2.87), we have:

$$\Delta t=t_2\left(z_d\right)-t_1\left(z_d\right)=$$

$$\frac{\pi\left(\eta_2-\eta_1\right)\xi}{64 c x_s^5}\{3\left[41 m_x^2+16 m_y^2+15 m_z^2\right]+$$

$$\frac{25 B_0^2 R_s^8}{48 x_s^2}[35-128 f_1 f_3+193 f_2+336 f_3^{\,2}]+$$

$$\frac{5\sqrt{30}B_0 R_s^4}{6 x_s}\left[\left(15 f_1-67 f_3\right)m_x+30 f_2 m_z\right]\} \qquad (2.97)$$

The presence of a non-zero value of Δt leads to the appearance of unusual polarization properties for an electromagnetic pulse. These properties are a consequence of the different magnitude of the propagation velocity of two modes in an external magnetic field. Indeed, suppose that a pulse of an arbitrarily polarized hard radiation has finite duration T. Because of the birefringence of the vacuum, it splits into two modes, polarized in mutually perpendicular planes, with the leading

edges of these modes coinciding at the initial instant of time. The leading edge of the faster mode will arrive at the hard radiation detector earlier than the leading edge of the slow mode, which for some time is equal to Δt. Therefore, during the time Δt only the faster normal pulse mode will pass through the detector and the detector will detect the linear polarization of this part of the electromagnetic pulse.

After the time Δt; the front of the pulse transferred by another normal mode, the phase of which differs from the phase of the faster mode on $\omega\Delta t$, where $\omega -$ is the frequency of the wave. The addition of these orthogonally polarized normal modes in the subsequent time will create in the detector radiation with elliptical polarization that will pass through the detector for a time $T - \Delta t$.

Quite analogously, the trailing edge of the faster mode will leave the detector before the trailing edge of the slow mode. Therefore, at the back of the pulse duration Δt, the polarization will also be linear, but orthogonal to the linear polarization of the faster mode. Thus, the detection of the above-mentioned polarization properties of hard pulses coming from pulsars makes it possible not only to assert the manifestation of nonlinear electrodynamics of vacuum, but also to estimate the magnitude of the induction of the magnetic field on the surface of the pulsar from the value of Δt[78, 79, 80].

CONCLUSION

The study of the expanded composition of thallium, lead, bismuth, and polonium isotopes made it possible to determine the main isotopic composition involved in cyclic reaction Pb-Bi. Based on the calculation of energy release, the intensity of gamma radiation from each neutron capture reactions was determined. The simulation has been done for different values of the neutron flux, i.e. $10^{13}, 10^{14}, 10^{15}, 10^{16}, 10^{17}, 10^{18}$. The results of the work show that with an increase in the neutron flux up to 10^{20} the number of gamma quanta cycles reaches its upper value and a further increase in the neutron flux does not lead to an increase in gamma quanta.

Analysis of the obtained expressions (2.31) and (2.32) shows that in the plane in which the neutron star, the source and receiver of hard radiation are located, the field of the magnetic dipole acts on the rays as a collecting lens. The deviation of the rays caused by the magnetic quadruple field and its superposition with dipole field is not sign-definite and depends on the orientation of the vector **m**, relative to the principal axes of the magnetic quadruple, so can serve both as a collecting lens and a scattering lens. Further, it follows from expression (2.33) that in the magnetic dipole field the second normal mode propagates slower than the first normal mode for any orientation of the vector **m**. The rest of the expression (3.33) is not sign-definite and depends on the orientation of the vector **m** relative to the principal axes of the magnetic quadruple. Therefore, the joint action of the dipole field and the magnetic quadruple field can lead to a decrease in the value of Δt, compared with the value Δt, created only by magnetic dipole field.

The calculation showed that, according to the equations of nonlinear electrodynamics of vacuum, the magnetic dipole and quadruple fields bends the rays of electromagnetic waves and the magnitude of the angle of this curvature depends on the orientation of the dipole and quadruple moments with respect to the direction of propagation of the electromagnetic wave.

The propagation velocities of electromagnetic pulses at $\eta_1 \neq \eta_2$ depend on the polarization of the electromagnetic wave. If a short pulse is emitted from the electromagnetic radiation source, then in the general case it will propagate in the magnetic dipole and quadruple fields in the form of two normal waves having mutually perpendicular polarization.

In the receiver these pulses will arrive along different rays and at different instants, as a result of which the recorded total pulse will have an unusual polarization: the front and back parts of each pulse of length $c\Delta t$ will be linearly polarized in mutually perpendicular planes, and the rest part of pulse will be elliptically polarized. A simple analysis shows that at $x_s \sim R_s \sim 10$ km and $|\boldsymbol{B}| \sim 10^{13}\ G$ the value of (2.33), with a favorable orientation of the dipole and quadruple relative to the z axis of the Cartesian coordinate system chosen by us, can reach several tens of nanoseconds.

This effect can be detected after the creation of space-based polarimeters, such as wide-field gamma ray ($0.02 - 3.0$ MeV) telescope GAMMASCOPE[96], which is

elaborated now at Moscow State University as a part of Russian space program, such as the XIPE (X-ray Imaging Polarimetry Explorer) project [98] being developed by ESA and the Imaging X-ray Polarimetry Explorer (IXPE) [100] being developed by the NASA / Italian Space Agency[78,79,80,81,82].

REFERENCES

1. David H., Staelin C., Edward C., Reifenstein I. Pulsating Radio Sources near the Crab Nebula // Science New Series. –1968. –Vol. 162. –P. 1481–1483.
2. Sandberg A., Sollerman J. Optical and infrared observations of the Crab Pulsar and its nearby knot // Astronomy and Astrophysics. –2009. –Vol. 504. –P. 525–530.
3. Wang Z., Chakrabarty D., Kaplan D. L. A debris disk around an isolated young neutron star // Nature. –2006. –Vol. 440. –P. 772–775.
4. D. L. Kaplan, D. 4. Chakrabarty, Z. Wang, S. Wachter. A Mid-Infrared Counterpart to the Magnetar IE 2259+586 // Astrophysical Journal. –2009. –Vol. 700. –P. 149–154.
5. Kazuo Makishima. X-ray studies of neutron stars and their magnetic fields // Proceedings of the Japan Academy, Series B Physical and Biological Science. –2016. –Vol. 92. –P. 135–155.
6. Robert Kirshner. Supernovae, an accelerating universe and the cosmological constant // Proc. Natl. Acad. Sci USA. –1999. –Vol. 96. –P. 4224–4227.
7. Pruzhinskaya M. V., Krushinsky V. V., Lipunova G. V. Optical polarization observations with the MASTER robotic net // New Astronomy. –2014. –Vol. 29. –P. 65–74.
8. Потехин А. Ю. Физика нейтронных звёзд // *УФН.* –2010. –Том. 180. –Ст. 1279–1304.
9. Nicolas Chamel., Pawel Haensel. Physics of Neutron Star Crusts // Living Rev Relativ. –2008. –Vol. 11. –P. 10–182.
10. Cheng Z., Mendez M., Diaz-Trigo M., Costantini E. The cooling, mass and radius of the neutron star in EXO 0748-676 in quiescence with XMM-Newton // Monthly Notices of the Royal Astronomical Society. –2017. –Vol. 471. –P. 2605–2615.
11. Degenaar N., Ootes L. S., Page D., Wijnands R., Parikh A. S., Homan J., Cackett E. M., Miller J. M., Altamirano D., Linares M. Crust cooling of the neutron star in Aql X-1: different depth and magnitude of shallow heating during similar accretion outbursts // Monthly Notices of the Royal Astronomical Society. –2019. –Vol. 488. –P. 4477–4486.
12. А. Ю. Потехин. Физика нейтронных звезд // Успехи физических наук. –2010. –Том. 180. –Ст. 12–79.
13. В. Л. Гинзбург. "Пульсары (Теоретические представления)" // УФН. –1971. –Том. 103. –Ст. 393–429.
14. C. J. Pethick., D.G. Ravenhall. Matter at large neutron excess and the physics of neutron-star crusts // Anmi. Rev. Nuc. Pan. Sci. –1995. –Vol. 45. –P. 429.
15. I. Chugunov., P. Haensel. Thermal conductivity of ions in a neutron star envelope // Monthly Notices of the Royal Astronomical Society. –2007. –Vol. 381. –P. 1143–1153.

16. D. N. Aguilera., et al. Superfluid Heat Conduction and the Cooling of Magnetized Neutron Stars // Physical Review Letters. –2009. –Vol. 102. –P. 1–4.

17. Pethick C. J., Potekhin A. Y. Liquid crystals in the mantles of neutron stars // Phys. Lett. B. –1998. –Vol. 427. –P. 7–12.

18. Y. Potekhin., G. Chabrier. Equation of state of fully ionized electron-ion plasma // Physical Review. E. –2000. –Vol. 62. –P. 1–11.

19. D. Lai. Matter in strong magnetic fields // Rev. Mod. Phys. –2001. –Vol. 73. –P. 629–662.

20. S. Dall'Osso., S.N. Shore., L. Stella. Early evolution of newly born magnetars with a strong toroidal field // Monthly Notices of the Royal Astronomical Society. –2009. –Vol. 398. –P. 1869–1885.

21. Chandrasekhar S., Fermi E. Problems of Gravitational Stability in the Presence of a Magnetic Field // Astrophysical Journal. –1953. –Vol. 118. –P. 116.

22. Lai. Dong., Shapiro E.E. Cold equation of state in a strong magnetic field–Effects of inverse beta-decay // Astrophysical Journal. –1991. –Vol. 383. –P. 745–751.

23. Thompson Christopher., Duncan R. C. Neutron star dynamos and the origins of pulsar magnetism // Astrophysical Journal. –1993. –Vol. 408. –P.194–217.

24. Larry Niven. Neutron Star // Del Rey. –1986. –P. 113.

25. S. Zane., R. Turolla., L. Zampieri., M. Colpi., A. Treves. Old isolated accreting neutron stars: Contribution to the soft x-ray background in the 0.5–2 Kev band // Astrophysical Journal. –1995. –Vol. 451. –P. 739.

26. S. Fabrika., Y. Ueda., A. Vinokurov., O. Sholukhova., M. Shidatsu. Supercritical accretion disks in ultraluminous X-ray sources and SS 433 // Nature Physics. –2015. –Vol. 11. –P. 551–553.

27. F. Hoyle., R. A. Lyttleton. The effect of interstellar matter on climatic variation // Proceedings of the Cambridge Philosophical Society. –1939. –Vol. 35. –P. 405.

28. V. G. Shvartsman. Ionization Zones around Neutron Stars: Hα Emission, Heating of the Interstellar Medium, and the Influence on Accretion // Astronomicheskii Zhurnal. –1970. –Vol. 47. –P. 824.

29. Treves A., Colpi M., Lipunov V. M. Old isolated neutron stars – Fire burns and cauldron bubbles // Astronomy and Astrophysics. –1993. –Vol. 269. –P. 319–324.

30. Bondi H. On spherically symmetrical accretion // Monthly Notices of the Royal Astronomical Society. –1952. –Vol. 112. –P. 195.

31. S. B. Popov., M. Colpi., M. E. Prokhorov., A. Treves., R. Turolla. The log N-log S distributions of accreting and cooling isolated neutron stars // The Astrophysical Journal Letters. –2000. –Vol. 544. –P. L53.

32. Бисноватый-Коган Г. С. Физические вопросы теории звездной эволюции // М.: Наука. –1989. Ст. 488.

33. O. D. Toropina., M. M. Romanova., Yu. M. Toropin., R. V. E. Lovelace. Magnetic Inhibition of Accretion and Observability of Isolated Old Neutron Stars // R.V.E. –2003. –Vol. 593. –P. 472–480.

34. Shapiro S. L., Teukolsky S. A. Black holes, white dwarfs, and neutron stars: The physics of compact objects // Cornell University, Ithaca, New York. –1983.

35. M. Y. Fujimoto., T. Hanawa., I. Jr. Iben., M. B. Richardson. Thermal evolution of accreting neutron stars // Astrophysical Journal. –1984. –Vol.278. –P. 813–824.

36. Burrows A., Lattimer J. M. The birth of neutron stars // ApJ. –1986. –Vol. 307. –P. 178–196.

37. H. Schatz., A. Aprahamian., J. Goerres., et al. rp-Process Nucleosynthesis at Extreme Temperature and Density Conditions // Phys. Rep. –1998. –Vol. 294. –P. 167–264.

38. Wallace R. K., Woosley S. E. Explosive hydrogen burning // ApJS. –1981. –Vol. 45. –P. 389–420.

39. M. A. Ruderman. Crystallization and Torsional Oscillations of Superdense Stars // Nature –1968. –Vol. 218. –P. 1128–1129.

40. Бисноватый-Коган Г.С., Чечеткин В.М. Неравновесные оболочки нейтронных звезд, их роль в поддержании рентгеновского излучения и нуклеосинтез // Успехи физических наук. –1979. –Том. 127. –Ст. 263–292.

41. Clayton D. D., Rassbach M. E. Termination of the *s*-process // The Astrophysical Journal. –1967. –Vol. 148. –P. 69–85.

42. Chamel Nicolas., Haensel Pawel. Physics of Neutron Star Crusts // Living Reviews in Relativity. –2008. –Vol. 11. –P. 182.

43. Абишев М.Е., Хасанов М.К., Утепова Д.С., Айтасов Т. Моделирование взаимодействия тепловых нейтронов с каталитическим составом (Pb, Bi, Po) с безграничной среде // Reports of National Academy of Science RK. –2016. –Vol. 3. –P. 5–9.

44. Абишев М.Е., Хасанов М.К. Расчет количества тепла испускаемая каталитическим составом (Pb, Bi, Po) в программном комплексе "IBUS" // News of the Reports of National Academy of Science of the RK, physico-mathematical series. –2017. –Vol. 3. –P. 53–56.

45. Хасанов М.К., Айтасов Т., Джанибеков А. Моделирование взаимодействия тепловых нейтронов с каталитическим составом (Pb, Bi, Po) в безграничной среде // International Scientific Conference of Students and Young Scientists «Farabi alemi». –Almaty. –2016. –P. 85.

46. Хасанов М.К. О программном комплексе "IBUS" // International Scientific Conference of Students and Young Scientists «Farabi alemi». –Almaty. –2017. –P. 111.

47. H. Bateman. Solution of a System of Differential Equations Occurring in the Theory of Radio-active Transformations // Proc. Cambridge Phil.Soc.IS. –1910. –Vol. 423. –P.12–19.

48. Burke D. L., et al. Positron Production in Multiphoton Light-by-Light Scattering // Phys. Rev. Lett. –1997. –Vol. 79. –P. 1626–1629.

49. Терлецкий Я. П., Рыбаков Ю. П. Электродинамика. –М.: Высшая школа. –1980. –Ст. 335.

50. Born M., Infeld L. Foundation of the new field theory // ProC. Roy. SoC. – 1934. –Vol. 144. –P. 425–430.

51. Heisenberg W., Euler H. Consequences of Dirac Theory of the Positron // Z.Phys. –1936. –Vol. 98. –P.714–732.

52. Александров Е.В., Ансельм А.А., Москалев А. Н. Двойное преломление вакуума в области интенсивного лазерного излучения. Журнал Экспериментальной и Теоретической Физики. – 1985. – Т. 89. – Ст. 1181–1189.

53. Bakalov D., Brandia F., Cantatorec G., et al. Experimental method to detect the magnetic birefringence of vacuum // Quantum Semiclass. Opt. –1998. –Vol. 10. – P. 239–250.

54. Гальцев Д. В., Никитина Н. С. Макроскопические эффекты вакуума в неоднородных и нестационарных электромагнитных полях // Журнал Экспериментальной и Теоретической Физики. – 1983. – Том. 84. – С. 1227–1224.

55. Родионов В.Н. Поляризация электрон-позитронного вакуума сильным магнитным полем с учетом аномального магнитного момента частиц // Журнал Экспериментальной и Теоретической Физики. – 2004. – Том. 125. – С. 453–461.

56. Денисов В.И., Денисова И.П., Кривченков И.В. Эффект нелинейно-электродинамического запаздывания электромагнитного сигнала в поле магнитного диполя // Журнал Экспериментальной и Теоретической Физики. – 2002. –Том. 122. –С. 227–232.

57. Денисов В.И., Денисова И.П. Проверяемый пост-максвелловский эффект нелинейной электродинамики в вакууме // Оптика и спектроскопия. – 2001. –Том. 90. –С. 329–335.

58. Денисов В.И., Денисова И.П. Уравнения эйконала в параметризованной нелинейной электродинамике вакуума // Доклады Российской Академий Наук. –2001. –Том. 378. –С. 463–465.

59. Денисов В.И., Исследование эффективного пространства-времени нелинейной электродинамики вакуума в поле магнитного диполя // Теоретическая и математическая физика. –2002. –Том. 132. –С. 211–221.

60. Уилл К. Теория и эксперимент в гравитационной физике. –М.: Энергоатомиздат. –1985. –С. 293.

61. Denisov V.I., Krivchenkov I.V., Kravtsov N.V. The experiment for measuring of the post-Maxwellian parameters of nonlinear electrodynamics of vacuum with laser-interferometer techniques // Physical Review, D. –2004. –Vol. 69. –P. 211–221.

62. V. I. Denisov., S. I. Svertilov. Nonlinear electrodynamic and gravitational actions of the neutron star fields on the propagation of the electromagnetic waves // Physical Review, D. –2005. –Vol. 71. –P. 063002.

63. V. I. Denisov. New effect in nonlinear Born-Infeld electrodynamics // Physical Review D. –2000. –Vol. 61. –P. 036004.

64. Adler S. L. Photon splitting and dispersion in a strong magnetic field // Annals of Physics (N.Y.). –1971. –Vol. 67. –P. 599.

65. Тернов И.М., Халилов В.Р., Родионов В.Н. Взаимодействие заряженных частиц с сильным электромагнитным полем. –М.: МГУ. –1982. –Ст. 304.

66. Гриб А. А., Мамаев С. Г., Мостепанеико В. М. Вакуумные квантовые эффекты в сильных полях. –М.: Энергоатомиздат. –1988.

67. Denisov V.I., Denisov M.I. Verification of Einstein's principle of equivalence using a laser gyroscope in terrestrial conditions // Physical Review D. –1999. –Vol. 60. –P. 047301.

68. Розанов Н.Н. Четырех волновое взаимодействие интенсивного излучения в вакууме. ЖЭТФ. –1993. –Том. 103. –С. 1996–2007.

69. Denisov V.I. Nonlinear effect of quantum electrodynamics for experiments with a ring laser // Journal of Optics A. –2000. –Vol. 2. –P. 372–379.

70. A. K. Harding., A. Muslimov. High-Altitude Particle Acceleration and Radiation in Pulsar Slot Gaps // Astrophysical Journal. –2003. –Vol. 508. –P. 328–335.

71. Thomson C., Duncan R.C. The Soft Gamma Repeaters as Very Strongly Magnetized Stars. Astrophysical Journal. –1996. –Vol. 473. –P. 322.

72. R. Wijnands M., Van Der Klis. A millisecond pulsar in an X-ray binary system // Nature. –1998. –Vol. –394. –P. 344.

73. Чандрасекар С. Математическая теория черных дыр. –М.: Мир. –1986. –Ст. –276.

74. Mereghetti S. ProC. NATO ASI «The Neutron Star - Black Hole Connection». –1999. Astro-ph. –9911252.

75. P.A. Vshivtseva., M.M. Denisov. Mathematical Modeling of Electromagnetic Wave Propagation in Nonlinear Electrodynamics // Computational Mathematics and Mathematical Physics. –2009. –Vol. 49. –No. 12. –P. 2092–2102.

76. Денисов В. И. Лекции по электродинамике. –М.: УНЦ ДО. –2005. –Ст. 271.

77. Mereghetti S. Workshop «Frontier Objects in Astrophysics and Particle Physics» // Astro-ph. –2000. –P0102017.

78. Abishev M.E., Toktarbay S., Beissen N.A., Belissarova F.B., Khassanov M.K., Kudussov A.S., Abylayeva A.Zh. Effect of nonlinear electrodynamics of vacuum in the magnetic quadruple field of a pulsar // Materials of the International Scientific Conference dedicated to the 80th anniversary of Academician of the NAS RK Abdildin M.M. Abdildin readings: Actual Problems of Modern Physics. –Almaty. –2018. –P. 73–79.

79. Abishev M.E., Toktarbay S., Amankhan T., Abylayeva A.Zh., Khassanov M.K. Effects Of Nonlinear Electrodynamics Of Vacuum In The Strong Magnetic Field Of A NS // Proceedings of the Fourteenth Marcel Grossmann Meeting on Recent Developments in Theoretical and Experimental General Relativity, Astrophysics, and Relativistic Field Theories. –Singapore: World Scientific Publishing. –2018. –P. 4379–4384.

80. Abishev M.E., Toktarbay S., Beissen N.A., Belissarova F.B., Khassanov M.K., Kudussov A.S., Abylayeva A.Zh. Effect of nonlinear electrodynamics of

vacuum in the magnetic quadruple field of a pulsar // Monthly Notices of the Royal Astronomical Society. –2018. –Vol. 481. –Issue. 1. –P. 36–43.

81. Abishev M.E., Toktarbay S., Khassanov M.K., Abylayeva A.Zh. Propagation of a electromagnetic radiation in the strong magnetic quadrupole and gravitational field // Recent Contributions to Physics(Rec. Contr. Phys.). –2018. –Vol. 66. –No. 3. –P. 4–11.

82. Medeu Abishev, Yerlan Aimuratov, Yermek Aldabergenov, Nurzada Beissen, Zhami Bakytzhan, Meruert Takibayeva. Some astrophysical effects of nonlinear vacuum electrodynamics in the magnetosphere of a pulsar // Astroparticle Physics. –2016. –Vol. 73. –P. 8–13.

83. Kaspi V.M., Lackey J.R., Mattox J., Manchester R.N., Bailes M., Pace R. High-energy gamma-ray observations of two young, energetic radio pulsars // Astrophysical Journal. –2000. –Vol. 528. –P. 445.

84. Caniulef D.G., Zane S., Taverna R., Turolla R., Wu K. Evidence of vacuum birefringence from the polarization of the optical emission from an Isolated Neutron Star // Monthly Notices of the Royal Astronomical Society. –2016. –Vol. 459. –P. 3585.

85. Denisov V.I., Sokolov V.A. Analysis of regularizing properties of nonlinear electrodynamics in the Einstein-Born-Infeld theory // Journal of Experimental and Theoretical Physics. –2011. –Vol. 113. –P. 926–933.

86. Denisov V.I., Sokolov V.A., Svertilov S.I. Vacuum non-linear electrodynamic polarization effects in hard emission of pulsars and magnetars // JCAP. –2017. –Vol. 9. –P.004.

87. Epstein R., Shapiro I.I. Post-post-Newtonian deflection of light by the Sun // Phys. Rev. D. –1980. –Vol. 22. –P.2947.

88. Landau L.D., Lifshitz E.M. The Classical Theory of Fields. Pergamum Press, Oxford Manchester –1971.

89. Denisov V.I., Sokolov V.A., Vasili'ev M.I. Nonlinear vacuum electrodynamics birefringence effect in a pulsar's strong magnetic field // Physical Review. D. –2014. –Vol. 90. –P.023011.

90. Denisov V.I., Denisova I.P., Pimenov A.B., Sokolov V. Rapidly rotating pulsar radiation in vacuum nonlinear electrodynamics // Eur. Phys. J. C. –2016. –Vol. 76. –P. 612.

91. Manchester R.N., Hobbs G. B., Teoh A., Hobbs M. // Freeman W.H. and Company, San Francisco. –2005.

92. Mathews L.D., Walker R.L. Mathematical Methods of Physics // New York.: W.A. Benjamin. –1970.

93. Mignani R. P., Testa V., Caniulef D. G., Taverna R., Turolla R., Zane S., Wu K. The Physics and Astrophysics of Neutron Stars // Monthly Notices of the Royal Astronomical Society. –2017. –Vol. 465. –P. 492.

94. Olausen S.A., Kaspi V.M. The Mc GILL magnetar catalog // ApJS. –2014. –Vol. 212. –P. 1-22.

95. Denisov V.I., Shvilkin B.N., Sokolov V.A., Vasili'ev M.I. Pulsar radiation in post-Maxwellian vacuum nonlinear electrodynamics // Physical Review. D. –2016. –Vol. 94. –P.045021.

96. Denisov V. I., Dolgaya E.E., Sokolov V.A. Nonperturbative QED vacuum birefringence // JHEP. –2017. –Vol. 105. –P. 1.

97. P´etri J. Multipolar electromagnetic fields around neutron stars: exact vacuum solutions and related properties // Monthly Notices of the Royal Astronomical Society. –2015. –Vol. 450. –P. 714–742.

98. Soffitta P. et al. XIPE: the X-ray imaging polarimetry explorer // Exp. Astron. –2013. –Vol. 36. –P. 523–567.

99. Taverna R., Muleri F., Turolla R., Soffitta P., Fabiani S., Nobili L. Probing magnetar magnetosphere through X-ray polarization measurements // Monthly Notices of the Royal Astronomical Society. –2014. –Vol. 438. –P.1686–1697.

100. Weisskopf M. C., Willem den Herder A., Tadayuki T., Marshall B., et al. Ultraviolet to Gamma Ray // Proc. SPIE Conf. Ser. Bellingham. –2016. –P. 990517.

101. Zhukovsky K.V. Solving evolutionary-type differential equations and physical problems using the operator method // Theoretical and Mathematical Physics. –2017. –Vol. 190. –P. 52–68.

102. Zhukovsky K.V. Operational solution for some types of second order differential equations and for relevant physical problems // J. Math. Anal. Appl. –2017. –Vol. 446. –P. 628–647.

103. Newton W. G. A taste of pasta? // Nature Physics. –2013. –Vol. 9. –Issue. 7. –P. 396–397.

104. Акимов В.В., Бисноватый-Коган Г.С., Лебков Н.С. Цилиндрический гамма-монитор CYGUM. Новая концепция гамма-телескопов высоких энергий. // Информационный буклет. Москва. –2005.

105. I. P. Tindo., V. D. Ivanov., S. L. Mandel'stam., A. I. Shuryghin. New measurements of the polarization of X-ray solar flares // Solar Physics. –1972. –Vol. 24. –P. 429–433.

106. Денисов Ю.И., Кузнецов С.Н., Логачев Ю.И., Морозов О.В., Мягкова И.Н., Свертилов С.И., Игнатьев А.П., Опарин С.Н., Перцов А.А., Лисин Д.В., Степанов А.И., Тиндо И.П., Житник И.А. Жесткое рентгеновское излучение солнечных вспышек во второй половине 2001 г.: Предварительные результаты эксперимента с прибором СПР-Н на станции «Коронас-Ф» // Астрономический вестник. –2003. –Vol. 37. –Iss. 2. –P. 127–136.

107. http://hesperia.gsfc.nasa.gov/hessi/.

108. Denisov D.M. Effects of nonlinear electrodynamics in the magnetic field of a pulsar // Canadian Journal of Physics. –2014. –Vol. 92. –P. 1453.

109. Heyl, J.S., Shaviv N.J. Polarization evolution in strong magnetic fields // Monthly Notices of the Royal Astronomical Society. –2000. –Vol. 311. –P. 555.

110. Mignani R. P., et. al. Evidence for vacuum birefringence from the first optical polarimetry measurement of the isolated neutron star RX J1856.5-3754 // Monthly Notices of the Royal Astronomical Society. –2017. –Vol. 465. –P. 492.

111. Klebesadel R. W., Strong I. B., Olson R.A. Observations of Gamma-Ray Bursts of Cosmic Origin // Astrophysical Journal Letters. – 1973. – Vol. 182. – P. L85.

112. Prilutsky O.P., Usov V. V. О природе всплесков γ-излучения // Astrophys. Space Sci. –1975. –Vol. 34. –P. 387.

113. Berezinsky V. S., Prilutsky O. F. Neutrino-antineutrino annihilation around a collapsar // Astron. Astrophys. –1987. –Vol. 175. –P. 309.

114. G.S. Bisnovatyi-Kogan., V. S. Imshennik., D. K. Nadyozhin., V. M. Chechetkin. Pulsed gamma-ray emission from neutron and collapsing stars and supernovae // Astrophys.Space Sci. –1975. –Vol. 35. –P. 23.

115. Г.С. Бисноватый-Коган. Всплески космического гамма-излучения: наблюдения и моделирование // Физика элементарных частиц и атомного ядра. –2006. –Том. 37. –С. 1235–1281.

116. Coburn W., Boggs S. E. Polarization of the prompt gamma ray emission from the gamma ray burst of 6 December 2002 (RHESSI) // Nature. –2003. –Vol. 423. –P. 415.

117. Rutledge R. E., Fox D. B. Re-analysis of polarization in the γ-ray flux of GRB 021206 // Monthly Notices of the Royal Astronomical Society. –2004. –Vol. 350. –P. 1288.

118. Mazets E. P., et al. A Giant Flare from a Soft Gamma Repeater in the Andromeda Galaxy (M31) // Astrophysical Journal Letters. –1999. –Vol. 519. –P. L151.

119. P. Haensel., J. L. Zdunik., J. Dobaczewski. Composition and equation of state of cold catalyzed matter below neutron drip // Astron. Astrophys. –1989. –Vol. 222. –P. 353–357.

120. B. G. Todd-Rutel., J. Piekarewicz. Neutron-rich nuclei and neutron stars: A new accurately calibrated interaction for the study of neutron-rich matter. matter. Phys. Rev. Lett –2005. –Vol. 95. –P. 122501.

121. Raditya Utama. A Study of Nuclear Structure and Neutron Stars with a Bayesian Neural Network Approach // Florida State University Libraries. –2016. –P. 63.

122. R.M. Neal. Bayesian Learning of Neural Network // Springer, New York. –1996.

123. D. M. Titterington. Bayesian methods for neural networks and related models // Statist. Sci. –2004. –Vol. 19. –P. 128–139.

124. James V. Stone. Bayes' Rule: A Tutorial Introduction to Bayesian Analysis // Sebtel Press, Sheffield, UK, first edition. 2013.

125. X. Roca-Maza., J. Piekarewicz. Impact of the symmetry energy on the outer crust of nonaccreting neutron stars. Phys. Rev. –2008. –Vol. 78. –P. 025807.

126. Walter de Gruyter., H. AMANN, Ordinary Differential Equations, An Introduction to Nonlinear Analysis // Berlin. –1990.

127. Maria Pusa., Jaakko Leppänen. Computing the Matrix Exponential in Burnup Calculations // NUCLEAR SCIENCE AND ENGINEERING. –2010. –Vol. 164. –P. 140–150.

128. C. Moler., C. Van Loan. Nineteen Dubious Ways to Compute the Exponential of a Matrix, Twenty-Five Years Later // SIAM Rev. –2003. –Vol. 45. –P. 3–46.

129. W.J. Cody., G. Meinardus., R.S. Varga. Chebyshev Rational Approximations and Applications to Heat-Conduction Problems // J. Approx. Theory. –1969. –Vol. 2. –P. 50.

130. A. A. Gonchar., E. A. Rakhmanov. Equilibrium Distributions and Degree of Rational Approximation of Analytic Functions // Mat. Sb. –1987. –Vol. 134. –P. 306.

131. E. Gallopoulos., Y. Saad. Efficient Solution of Parabolic Equations by Krylov Approximation Methods // SIAM J. Sci. Stat. Comput. –1992. –Vol. 13. –P. 12–36.

132. John J. Cowan., Friedrich-Karl Thielemann. R-Process Nucleosynthesis in Supernovae // Physics Today. –2004. –Vol. 57. –Iss. 10. –P. 47.

133. Amy Bartlett., Joachim Görres., Grant J. Mathews., Kaori Otsuki., Michael Wiescher., Dieter Frekers., Alberto Mengoni., Jeffrey Tostevin. Two-neutron capture reactions and the r-process // Physical Review C. – 2006. – Vol. 74. – P. 015802.

134. Maria Pusa. Rational Approximations to the Matrix Exponential in Burnup Calculations // Nuclear Science and Engineering. –2011. –Vol. 169. –Iss. 2. –P. 155–167.

135. I. Bartos., S.A. Marka. A nearby neutron-star merger explains the actinide abundances in the early Solar System. // Nature. –2019. –Vol. 569. –P. 85–88.

136. Абишева М.Е. «Исследование проблемы однозначности релятивистских уравнений движения в общей теории относительности». Диссертация на соискание ученой степени доктора наук. // Алматы. –2009. –P. 193.

137. Daniel Kasen., Brian Metzger., Jennifer Barnes., Eliot Quataert., Enrico Ramirez-Ruiz. Origin of the heavy elements in binary neutron-star mergers from a gravitational-wave event // Nature. –2017. –Vol. 551. –P. 76–78.

138. David. Eichler., Mario Livio., Tsvi Piran., David Schramm. Nucleosynthesis, neutrino bursts and gamma rays from coalescing neutron stars // Nature. –1989. –Vol. 340. –P. 126–128.

139. B. Cote., Ch. L. Fryer., K. Belczynski., O. Korobkin., M. Chruślińska., N. Vassh., M. R. Mumpower., J. Lippuner., T. Sprouse., R. Surman., R. Wollaeger. The origin of r-process elements in the Milky Way // The American Astronomical Society. –2018. –Vol. 855. –P. 9.

140. N. Zh. Takibayev., M. N. Takibayeva., V. O. Kurmangaliyeva., D. M. Nassirova. Physical processes in crystals of super dense neutron stars in the crusts // News of the Reports of National Academy of Science of the RK, physico-mathematical series. –2015. –Vol. 2. –P. 129–135.

141. S. Van Eck., S. Goriely., A. Jorissen., B. Plez. Discovery of three lead-rich stars // Nature. –2001. –Vol. 412. –P. 793–795.

142. Takibavev N.J., Kato R., Nasirova D., Exited nuclei in Neutron Star Crust // Adv. Studies Theor. Phys. –2013. –Vol. –7. –P. 151–161.

143. Walter R., Ferrigno C. Handbook of Supernovae // Springer Internationa; Publishing, Cham. –2017. –P. 1385–1399.

144. Jing Wang. Physical Environment of Accreting Neutron Stars // Hindawi Publishing Corporation Advances in Astronomy. – 2019. – Vol. – 2016. – P. 1–15.

145. Tananbaum H., Gursky H., Kellogg E. M., Levinson R., Schreier E., Giacconi, R. Discovery of a Periodic Pulsating Binary X-Ray Source in Hercules from UHURU // Astrophysical Journal. – 1972. – Vol. 174. – P. L143.

146. D. Bhattacharya., E.P. Jvan den Heuvel. Formation and evolution of binary and millisecond radio pulsars // Physics Reports. – 1991. – Vol. 203. – Iss. 1–2. –P. 1-124.

147. Davidson K., Ostriker J. P. Neutron-Star Accretion in a Stellar Wind: Model for a Pulsed X-Ray Source. // Astrophysical Journal. –1973. –Vol. 179. –P. 585-598.

148. Jing Wang. H.K. Chang. Retrograde wind accretion – an alternative mechanism for long spin period of SFXTs. // Astronomy and Astrophysics. – 2012. – Vol. 547. – P. 1–5.

149. Konstantin A. Postnov., Lev R. Yungelson. The Evolution of Compact Binary Star Systems. // Living Rev Relativ. – 2014; – Vol. 17. – P.3– 22.

THANKS.

The author expresses sincere gratitude to its scientific consultants: Professor Abishev Medeu Erzhanovich (Al-Farabi KazNU, Almaty, Kazakhstan), whose immense support and assistance in carrying out all stages of preparation for the research from beginning to completion.

Also author expresses sincere gratitude to Claudio Spitaleri (University of Catania, Italy)–for highly qualified scientific advice and for organizing scientific trip to Catania university and INFN, also for assistance in preparation of my dissertation.

The author also expressed deep gratitude to everyone who helped in the preparation and conduct of research on the topic of the dissertation, as well as in the discussion of its results.